THE UNIVERSITY OF ALBERTA

FATIGUE OF REINFORCING BARS

BY

(C) ISHWAR C. JHAMB

A THESIS
SUBMITTED TO THE FACULTY OF GRADUATE STUDIES AND RESEARCH
IN PARTIAL FULFILLMENT OF THE REQUIREMENTS FOR DEGREE
OF DOCTOR OF PHILOSOPHY

DEPARTMENT OF CIVIL ENGINEERING

EDMONTON, ALBERTA

SPRING, 1972

ABSTRACT

A comprehensive investigation was undertaken to study the fatigue of hot rolled reinforcing bars. The investigation included fatigue tests, metallographical observations and stress concentration analyses. The fatigue test results were analysed statistically and the findings were compared with previous results. The fatigue behavior of reinforcing bars were explained on the basis of metallographical observations and stress concentration analyses.

The main objectives of this project were to study the effect of deformations, decarburization of the bar surface, rust and mill scale, grade of steel, minimum stress level and bar size on the fatigue of reinforcing bars.

In all, thirteen types of plain and deformed bars with three nominal yield strengths and three sizes were tested. Seventy-two concrete beams containing a single straight bar as a main reinforcement were tested under repeated flexural loads. Eighty-eight deformed or plain bar specimens and thirty-two specimens machined from the reinforcing bars were tested in air under cyclic tension stresses.

Metallographical observations and observations of the fatigue failure phenomenon were carried out.

Strain measurements and finite element stress analyses were used to determine the influence of various geometrical parameters of

the deformations on the stress concentrations caused by the deformations. The analyses indicated that the stress concentration factor K_T increased as the ratio of the lug base radius to the lug height was decreased below a value of 1.25. Other variables were less significant.

The test results suggest there is a significant decrease in the fatigue strength due to the deformations and the decarburization of the bar surface. However, no influence of rust or mill scale was observed. The grade of steel had no influence on fatigue strength of deformed bars, while machined polished specimens showed a linear increase in fatigue strength with grade. The effect of grade on plain as-rolled bars was between that for deformed and machined polished specimens. The test data at various minimum stress levels from this and other projects may be represented by a Modified Goodman Law. No appreciable influence of size was observed on the fatigue strength. Finally, the fatigue strength of bars in concrete beams was 2 ksi higher than for bars tested in air.

An engineering method has been suggested for the estimation of fatigue strength of reinforcing bars. This method was used to analyse previously published fatigue data on deformed reinforcing bars. To improve the fatigue strength of deformed bars, a proposal is made for the inclusion of an additional clause in the deformation specifications. Finally, a design specification for the permissible stresses under repeated loading for commercially available North American bars is also suggested.

ACKNOWLEDGEMENTS

TABLE OF CONTENTS

TABLE OF CONTENTS (continued)

TABLE OF CONTENTS (continued)

viii

TABLE OF CONTENTS (continued)

ix

TABLE OF CONTENTS (continued)

LIST OF TABLES

LIST OF TABLES (continued)

xii

LIST OF FIGURES

LIST OF FIGURES (continued)

xv

LIST OF FIGURES (continued)

xvi

LIST OF FIGURES (continued)

LIST OF SYMBOLS

A	regression coefficient
B	regression coefficient
D	bar diameter
D_{nom}	nominal bar diameter
DF	degrees of freedom
f_y	yield stress
f_u	ultimate tensile stress
g	grain size, number of grains at 100 magnificiation
G	specified minimum yield strength according to ASTM specification
h	height of deformation lug
K_f	strength reduction factor
K_T	theoretical stress concentration factor
log N	logarithm of fatigue life, to the base 10
MS	mean square
N	fatigue life, number of cycles at which 50 percent of a group of specimens would be expected to have failed or the number of cycles causing failure in a given specimen
p	percent survival
q	notch sensitivity factor
r	minimum radius at base of deformation lug

LIST OF SYMBOLS (continued)

R   surface roughness, CLA values (40)

R^2 multiple correlation coefficient

s   standard deviation

S   stress, tensile stress positive

S_{max} maximum stress in the cycle, tensile stress positive, ksi

S_{min} minimum stress in the cycle, tensile stress positive, ksi

S_r stress range, i.e., algebraic difference between the maximum and minimum stress in one cycle, $S_{max} - S_{min}$, ksi

S_{CR} computed fatigue limit of deformed reinforcing bar in concrete beam at the specified minimum stress level, ksi

S_{Df} computed fatigue limit of deformed bar in air at $S_{min} = 0$, ksi

S_{mf} computed fatigue limit of machined polish specimen at $S_{min} = 0$, ksi

S_{Rf} computed fatigue limit of plain as-rolled bars at $S_{min} = 0$, ksi

w   half width of deformation lug

θ face angle of deformation lug

CHAPTER I

INTRODUCTION

The use of hot rolled deformed high strength* bars as concrete reinforcement has been increasing for the past two decades and a similar trend is expected in the nineteen seventies (1)**. These bars show a definite economic advantage over conventional mild steel reinforcing bars in many circumstances. Their increased use has prompted extensive investigations of their behavior in concrete members. Accordingly, the study of fatigue performance of high strength reinforcing bars has received considerable attention since poor fatigue properties have been a major drawback of high strength steels (2). Several major investigations of this problem have been reported from Germany, U.S.A., Canada, Japan and Sweden.

The majority of reinforcing bars are manufactured by two manufacturing processes; hot rolling alone, and cold working combined with aging after rolling. Because this investigation was restricted to hot rolled bars and because most of the reinforcing bars produced in North America belong to this type, this report will be limited to a discussion of hot rolled reinforcing bars.

---

*Bars having yield strength greater than 50 ksi are referred to as high strength bars.
**Number in parentheses designate references.

1

Hot rolled bars are available in various parts of the world with numerous deformation patterns and with yield strengths ranging from 60 to 90 ksi. The various codes (3-7) on deformed bars generally specify proof yield and ultimate strengths, deformation details and requirements for elongation and bendability. Some European codes (4,5) also specify fatigue strength and weldability requirements. For example, the German code (4) requires the reinforcing bar manufacturer to supply fatigue strength data if the bars are to be used for structures predominantly subjected to repeated loads. The American Society for Testing and Materials (ASTM) Standard (A615-68)(3) on deformed billet steel bars specifies minimum requirements for Grade 40, 60 and 75 concrete reinforcing steel bars. These requirements do not include clauses on fatigue strength. The permissible stresses for these bars for highway bridge structures are governed by the AASHO Code (8), which does not permit higher stresses in fatigue for higher grades of steels due to the lack of supporting data. This code provision has led to a lower demand for higher grade steels for concrete bridges than for other concrete building structures.

On the basis of the extensive literature on metal fatigue and the fatigue strength of reinforcing bars, the factors which may effect the fatigue behavior of reinforcing bars are as follows:

Group I Manufacturing Process
         Deformation Details
         Bar Grade and Size

Group II Stress Range

Expected Life

Minimum Stress

Stress Gradient across bar in service

Group III Weldability

Bends

The above parameters are divided into three groups on the basis of variables controlled by the bar manufacturer, the designer, and the usage of the bar. An investigation of all three groups would be necessary to establish rational design code specifications for the fatigue strengths of reinforcing bars and/or for the development of bars of improved fatigue strength. Investigation of the first two factors in group I requires close cooperation between the investigators and the reinforcing bar manufacturers. The remaining parameters have been investigated extensively and a large amount of test data is available; however, due to non-uniformity of the variables controlled by the manufacturers, it is difficult to correlate this data. The specially rolled bars produced by the Steel Company of Canada for this investigation made it possible to study in some depth one particular set of variables controlled by the manufacturer.

1.1 Previous Researches

German research on fatigue strength of deformed bars reported by Rehm (9) in 1960 led to the development of a laboratory fatigue

specimen to test straight and bent reinforcing bars in concrete beams. In later years Soretz (10), and Wascheidt (11) attempted to simplify the fatigue specimen by testing reinforcing bars in air. These tests have provided initial data on the effect of concrete encasement on the fatigue strength of reinforcing bars.

In 1964, a major investigation on the fatigue strength of hot rolled deformed bars manufactured in North America was reported by the Portland Cement Association (PCA) (12). This was followed by several other reports (13,14,15,16). These investigations are the biggest source of information on the fatigue behavior of American deformed reinforcing bars. The influence of such variables as bar grade, bar size, deformation type, minimum stress level, bar bends, tack welding and nominal depth of bar in concrete beam was investigated.

Tests on bars of different grades have been reported by Lash (17). Wascheidt (10), Kokubu and Okamura (18), and Grönqvist (19,20) carried out fatigue tests on bars of different grades, sizes and deformation patterns. Fatigue tests on welded reinforcing bars have been reported by the University of Illinois (21,22). A number of other references (23-27) provide significant data from several other test series.

The findings from the test series mentioned above will be compared and discussed in Chapter VII along with the findings from this project.

1.2 Research Objectives and Approach

The objectives of this project were to investigate the influence of bar grade, bar surface characteristics, bar size and minimum stress in the stress cycle on the fatigue strength* of one type of commercially available deformed reinforcing bars. The fatigue studies were made in two phases. In the first phase, previously reported in the authors M.Sc. thesis (29), the influence of bar grade, bar size and minimum stress level were investigated. The second phase was primarily devoted to a study of the influence of bar surface characteristics such as deformation shape, decarburization of the rolled surface and rust and mill scale.

The tests in the first phase were initiated in 1967. The test program consisted of flexure fatigue tests on 72 reinforced concrete beams containing Grade 40, 60 and 75 reinforcement of bar sizes Nos. 5, 8 and 10. The minimum stresses in the cycles were set at 10 and 40 percent of the yield strength in the tests of No. 8 bars and 10 percent of the yield strength in the tests of No. 5 and No. 10 bars. In order to isolate the variables under investigation, the beam size and concrete strength were kept approximately constant for each bar diameter. The beam dimensions were varied in proportion to the bar diameter so that the steel percentage was approximately equal for

---

*Terminology and notation in this report follows, insofar as possible, the recommendations of ASTM Committee E-9 on fatigue (28). The fatigue strength of a bar is a hypothetical value of stress corresponding to failure at exactly N cycles as determined from an S-N diagram. Throughout this report, the hypothetical value of S referred to will be stress range, S_r, at which 50 percent of the specimens of a given sample would be expected to survive N cycles.

all beams and the theoretical strain at the top of bar was a constant percentage of that at the bottom of the bar. The test results were presented in the form of an S-N curve for each combination of the parameters under study. The test data was analysed to find an approximate fatigue limit and an equation for the mean S-N line for the test data in the finite life region.

The test data in the first phase showed considerable scatter in fatigue lives, which pointed out the need for replication and for a statistically designed experiment. At the same time, a need for a simple standardized fatigue test specimen was also realised, since testing a concrete beam was not only cumbersome and costly, but also might have added to the scatter in the results due to variations in the concrete beam parameters. Considering these factors and the specialised nature of testing required to investigate various bar surface characteristics, the simple reinforcing bar fatigue specimen described in Chapter III was developed. The tests in the second phase were planned and executed according to a statistically designed experiment. The main objectives of the tests were to determine whether deformations, decarburization of the rolled surface, and rust and mill scale had a significant influence on the mean fatigue limit and to quantify these effects by statistical analysis. The objectives of the project also included the determination of the stress concentrations produced by the deformations and the extent of bar surface decarburization.

The tests in the second phase included deformed bars, plain as-rolled bars, plain bars without rust and mill scale and machined polished specimens, all of the same reinforcing steel. Reinforcing steels of Grades 40 and 60 were used in the tests. In all, 88 reinforcing bar fatigue specimens and 32 machined polished specimens were tested in air under similar stress conditions. The tests results were statistically analysed to determine mean fatigue limits, and S-N-P curves for each series. An analysis of variance and multiple regression analyses were used to test the significance of specified variables and to quantify their influence on fatigue strength. These analyses are presented in Chapter VI.

Extensive metallographical investigations are reported in Chapter IV. These tests were conducted to study the general steel structure, to estimate the grain size and to determine the extent of the decarburization of the bar surface of all the reinforcing steels used in this project.

Stress concentrations produced by the deformations were investigated analytically and experimentally for the types of reinforcing bars used in this project. The influence of the geometrical parameters of the deformations on the theoretical stress concentration factor is outlined in section 5.4 of Chapter V.

The conclusions from the fatigue tests, the stress concentration analysis and the metallographical analysis are compared and discussed with the previous important test findings in Chapter VII. In this chapter, an engineering approach to estimate the fatigue limit of

high strength deformed bars is suggested. This approach is applied to previously published test data with considerable success.

The deformation requirements of reinforcing bars specified in ASTM, German, Swiss, Japanese and Canadian codes (3-7) are reviewed in Chapter VIII. Suggestions have been made on how the code specifications on deformation details could be modified to improve the fatigue strength of reinforcing bars without significantly impairing their bond properties. Finally, Chapter IX outlines the significant findings of this project and suggestions are offered for future research.

CHAPTER II

TEST PROGRAM AND PROPERTIES OF
REINFORCING STEELS STUDIED

2.1 Description of Test Program

This investigation was a study of the fatigue behavior of reinforcing bars of Grade 40, 60 and 75 steels, meeting ASTM (A615-68) requirements (3). The influence of six major variables; bar grade, bar size, minimum stress level, deformations, decarburization and rust and mill scale on the fatigue strength of bars was studied. The experiments were carried out in two phases.

The tests in the first phase included flexural fatigue tests of 72 reinforced concrete beams. The testing was divided into 12 series of reinforced concrete beams. Each series consisted of 6 beams of the same dimensions and reinforcement. A total of nine types of steels were investigated, including all combinations of the three grades of steel and three bar sizes. The outline of the test program is given in Table 2.1. These tests will be briefly described in this report, since a detailed description of these tests has been previously reported (29). However, the test data from these tests will be analyzed with those of the second phase.

A detailed description of the tests in the second phase is presented in this report. These tests were partly an extension of the

TABLE 2.1

OUTLINE OF TEST PROGRAM

(PHASE I)

Beam Series	Bar Size	Bar Grade	Minimum Stress Level
1	8	G40	0.1 fy
2	8	G60	0.1 fy
3	8	G75	0.1 fy
4	8	G40	0.4 fy
5	8	G60	0.4 fy
6	8	G75	0.4 fy
7	5	G40	0.1 fy
8	5	G60	0.1 fy
9	5	G75	0.1 fy
10	10	G40	0.1 fy
11	10	G60	0.1 fy
12	10	G75	0.1 fy

tests in the first phase. They were more comprehensive than the tests in the first phase and were based on a statistically valid experimental design. In designing these tests, emphasis was placed on accounting for scatter in the test results and on the determination of the mean fatigue limits. The influence of four major variables; deformation details, decarburization, rust and mill scale and bar grade on the fatigue limit of the bars was investigated. Axial tension tests were conducted under repeated loading in air on plain and deformed

No. 8 bars of Grade 40 and 60 steel. The details of specimens and experimental design of these tests is presented in Chapter III.

Although fatigue tests formed the major part of the test program, several miscellaneous tests were undertaken to explain the findings from the fatigue tests. These tests were the following:

(1) Metallographical investigations for steel structure, grain size and decarburization.

(2) Tests to determine stress concentration factors.

(3) Surface roughness measurements.

(4) Hardness tests.

(5) Analyses of failure surfaces.

2.2 Properties of Reinforcement

2.2.1 Description of Manufacturing Process

The majority of reinforcement used in this program was of three grades; Grade 40, 60 and 75, meeting ASTM (A615-68) specifications (3). Special plain No. 8 bars of Grade 40 and 60 were also tested. These bars were specially rolled for the tests and did not meet the deformation requirements of the ASTM code. All bars were supplied by The Steel Company of Canada (Stelco), a leading manufacturer of reinforcing bars in Canada.

All the reinforcing bars were manufactured by the hot rolling process from billets produced from steel scrap in a continuous casting mill. The steel scrap used was of wide variety coming from farm machinery, auto-wrecks, used machines etc. Steel billets for Grade 40

and 60 were cast from steel scrap remelted at 2100-2200°F in an
electrical furnace in the Edmonton Stelco plant. The Grade 75 steel
was produced in an open-hearth furnace at the Stelco plant in Hamilton.
In both plants no control of decarburization of the billet surface
was exercised in the furnace. The chemistry of the steel was controlled
to get the desired physical properties. Normally, additions of manganese,
chromium and vanadium were made to get higher strength. For each heat
a ladle analysis was made to comply with the specified chemistry clause
of the ASTM Standard.

The deformed reinforcing bars were made by successive rolling
of a steel billet through a series of 12 to 15 rolls depending upon
the final bar diameter. Bar sizes Nos. 5 and 8 were rolled from a
3-5/8 inch square billet and No. 10 bars from a 5-1/2 inch square
billet. In all cases, the length of the billets ranged from 10-12 ft.
The deformations were hot formed in the final pass by pressing the bar
between rolls having patterns cut into them.

The rolls wear out with continuous use, changing their geometry
at sharp corners. The rolls are normally not replaced until they reach
the minimum requirements of deformations in the ASTM Standard.

In the rolling plant, tests were made for yield strength,
tensile strength, bending properties, weight and deformation size in
compliance with the ASTM Standard.

The reinforcement in the first phase of the tests consisted
of three steels; Grades 40, 60 and 75, and three bar sizes; Nos. 5, 8
and 10. Two grades of steels were used in the second phase of tests.
The reinforcement in these tests consisted of plain and deformed No. 8

bars of Grades 40 and 60 produced in the Edmonton Stelco plant. The deformed and plain bars of each grade were rolled from two successive billets from the same heat. The deformed bars of both grades were rolled in two successive passes using newly machined final rolls, which produced essentially identical deformations on the two steels. Because the rolls were newly machined the deformations were extremely sharp. In a similar manner the plain bars of Grade 40 and 60 were rolled in two successive passes through round bar rolls.

To determine the change in the cross-sectional dimensions of deformed bars due to wearing out of the rolls, a few reinforcing bars were rolled using fully worn rolls. These No. 8 bars were not tested under fatigue loading, however.

2.2.2 Bar Dimensions and Mechanical Properties

Photographs of a typical deformed bar are shown in FIGURE 2.1. The deformed bar had two longitudinal lugs and uniformly spaced parallel transverse lugs inclined at 75° to the bar axis. In each case the transverse lugs merged into the longitudinal lugs. Except for the No. 8 Grade 75 bars, the transverse lugs were reversed in direction on each side of longitudinal lug as shown in FIGURE 2.1. The transverse lugs were parallel on both sides of the longitudinal lugs on the No. 8 Grade 75 bars. In all cases the bars met ASTM specifications on deformations.

FIGURE 2.2 shows typical mid-lug profiles obtained by sectioning bars along their longitudinal axes. The bars in the second test phase had the profile shown in FIGURE 2.2(a). Similar diagrams
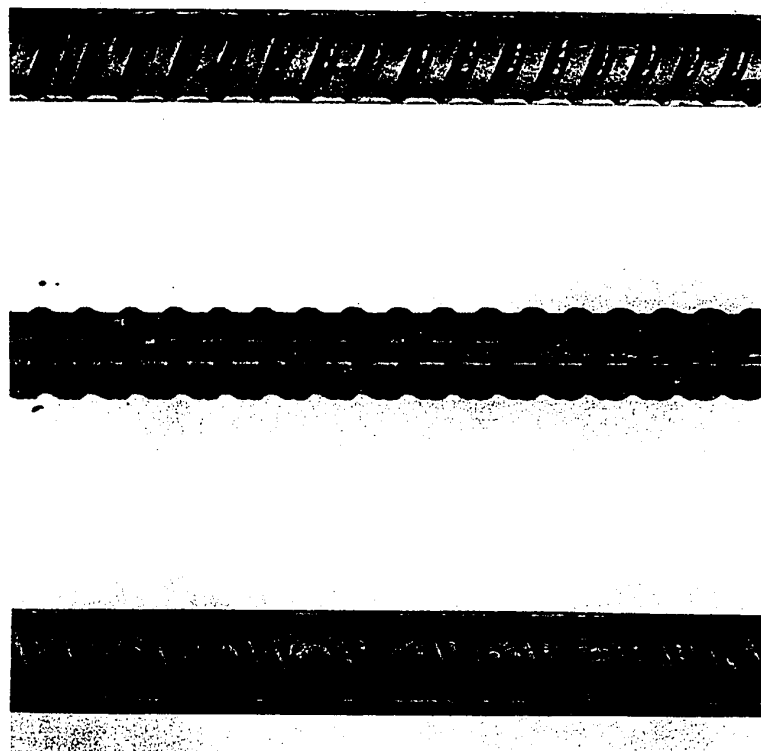
FIGURE 2-1   TYPICAL DEFORMED REINFORCING BAR
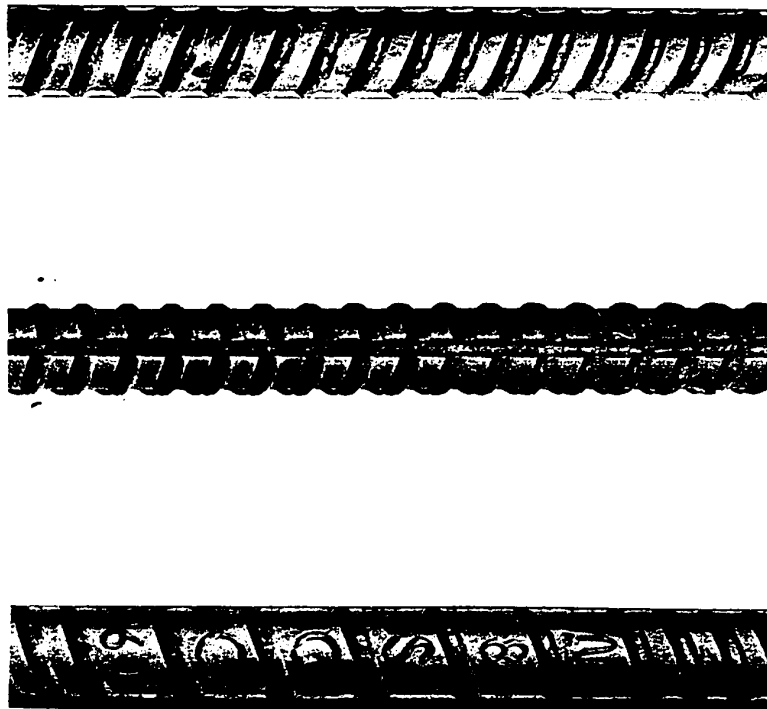
FIGURE 2-1   TYPICAL DEFORMED REINFORCING BAR

RADIUS = 0.015   RADIUS = 0.010

(a) FRESH ROLLS

RADIUS = 0.035   RADIUS = 0.030
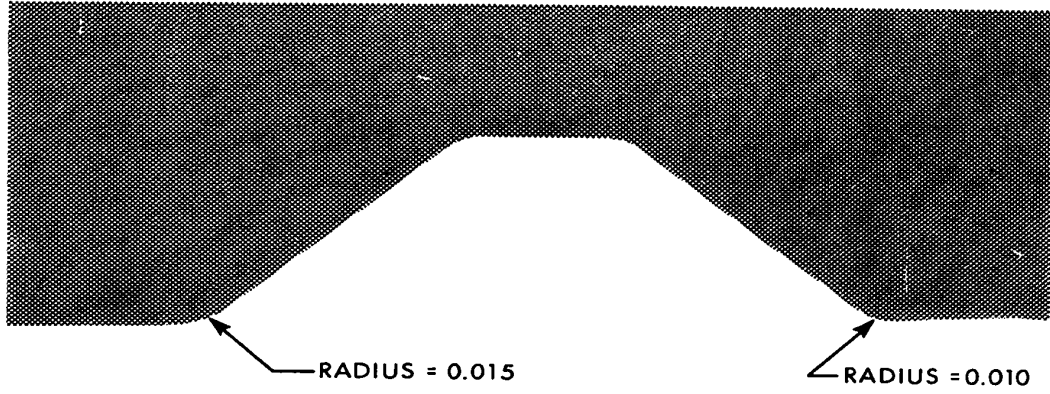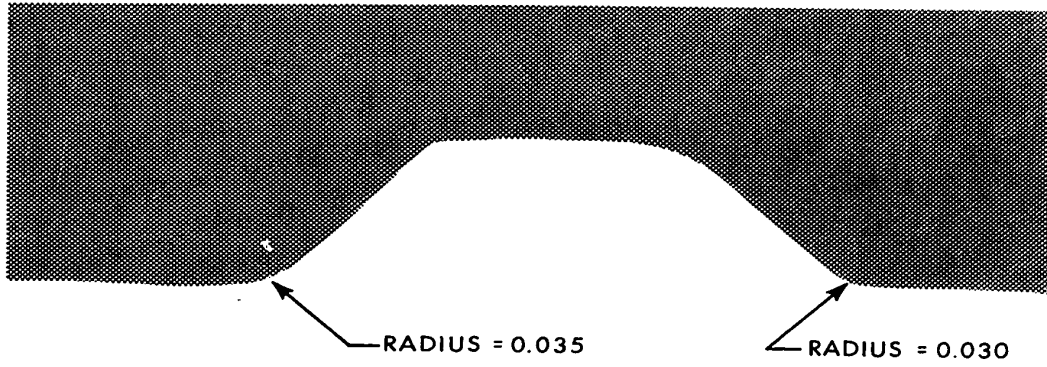
(b) FULLY WORN ROLLS

0   0.1
INCHES
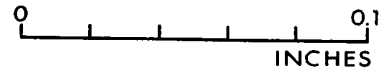
FIGURE 2-2   MID LUG PROFILES - NO. 8 BARS PHASE II

are presented in Reference 29 for the bars in the first test phase. The cross-sectional dimensions of the plain and deformed bars from both testing phases are given in Table 2.2. This table also contains data for the No. 8 deformed bars, which were rolled using fully worn rolls. The bar diameter, lug height, lug spacing etc., were measured with a micrometer. The radii at the bases of the lugs and the photographs of the mid-lug profiles shown in FIGURE 2.2 were obtained using an optical comparator.

Two reinforcing bars of each size in each grade of steel were tested in tension. The laboratory test data is summarized in Table 2.3. Three significant observations can be made from this data. First, for all steels used, the ratio between tensile and yield strengths ranged from about 1.35 for Grade 75 upto about 1.55 for Grade 40 steels, with an average of 1.5. This average ratio for the hot rolled steels is considerably higher than the average ratio of 1.2 found in cold rolled steels (11). Second, for all steels tested, the higher grade steels showed lower percentage of elongation. These results indicate that the ductility of the higher strength steels was lower. It has been observed in metal fatigue that steels with lower ductility generally have a lower fatigue strength. Finally, although the steel in the plain and deformed bars of each grade came from successive billets and had essentially the same chemistry, the strength and ductility of the plain bars was always greater than that of the deformed bars.

The stress strain curves are presented in FIGURES 2.3 and

TABLE 2.2

CROSS SECTIONAL DIMENSIONS OF BARS TESTED

BAR TYPE	EXPERIMENTS PHASE I									EXPERIMENTS PHASE II				
	DEFORMED BARS									PLAIN BARS		DEFORMED BARS		DEFORMED BARS FULLY WORN ROLLS
Bar Size	No. 5			No. 8			No. 10			No. 8		No. 8		No. 8
Grade of Steel	G40	G60	G75	G40	G60	G75	G40	G60	G75	G40	G60	G40	G60	G40
Unit weight lbs/ft	1.13	1.12	1.12	2.67	2.69	2.66	4.26	4.50	4.32	2.67	2.68	2.70	2.71	2.67
Diameter - inches	0.586	0.580	0.597	0.935	0.930	0.966	1.225	1.230	1.210	1.006	1.006	0.945	0.945	.930
Half width of lugs - inches	0.071	0.080	0.083	0.120	0.120	0.110	0.170	0.165	0.150	--	--	0.125	0.125	0.112
Height of lugs - inches	.042	.055	.040	.065	.065	.060	.076	.075	.074	--	--	.076	.076	.071
Spacing of lugs - inches	0.298	0.297	0.306	0.428	0.426	0.436	0.55	0.55	0.55	--	--	0.428	0.428	.428
Face angle of lugs Steeper side - degrees	56	56	42	41	45	43	44	43	45	--	--	45	45	47
Other side - degrees										--	--	41	41	45
Radius of Base of lugs, inches Steeper side - Average	.0125	.014	.0235	.020	.016	.020	.0317	.028	.019	--	--	.014	.014	.023
Standard deviation	.0025	.0025	.004	.003	.003	.005	.003	.002	.003	--	--	.004	.004	.004
Other side - Average	.0195	.0305	.042	>.075	.032	.061	>.075	.045	.038	--	--	.014	.014	.030
Standard deviation	.005	.006	.006	--	.019	.010	--	.002	.002	--	--	.00	.00	.006

TABLE 2.3

MECHANICAL PROPERTIES OF REINFORCING BARS

BAR TYPE	EXPERIMENTS PHASE I											EXPERIMENT PHASE II			
	DEFORMED BARS											PLAIN BARS		DEFORMED BARS	
Bar Size	No. 5			No. 8			No. 10					No. 8		No. 8	
Grade of Steel	G40	G60	G75	G40	G60	G75	G40	G60	G75			G40	G60	G40	G60
Yield Strength, ksi	50.0	67.7	89.4	52.7	65.6	84.4	49.7	64.2	83.0			54.2	67.0	50.6	61.4
Tensile Strength, ksi Bars	76.3	109.2	122.1	83.1	109.0	123.5	83.1	110.5	109.5			86.3	100.1	81.5	96.8
Machined Specimens	--	--	--	94.0	119.0	128.0	--	--	--			90.0	102.5	--	--
Elongation,* Percent	21.7	14.8	11.9	20.8	15.2	15.0	21.2	15.8	12.5			22.6	18.5	19.5	14.7
Reduction in Area, percent	--	--	--	--	--	--	--	--	--			45.6	44.6	--	--

*Measured on 8 inches gage length

2.4 for the nine steels used in Phase I and four steels used in Phase II. It is interesting to note that of the thirteen types of bars used, the Grade 75 size No. 10 bars were the only ones for which the stress strain curve deviated significantly from an elastic-plastic strain hardening stress strain curve. In addition, the measured tensile strength of the No. 10 Grade 75 bars was essentially the same as that determined for the No. 10 Grade 60 bars.

The differences in yield strength between the Grade 40 and Grade 60 plain and deformed bars of identical metallurgy can be seen in FIGURE 2.4. In both cases the plain bars had 4 percent higher yield and tensile strength than the deformed bars.

2.2.3 Chemical Composition of Steel

The chemical composition of steel has a major influence on its mechanical properties and micro-structure. Plain carbon steels used for reinforcing bars contain carbon and some of the more common additive agents such as manganese, silicon, chromium, molybdenum and vanadium. An increase of carbon content leads to an increase in the hardness, tensile strength and yield strength of a steel (30). Similar results may be obtained by the various additive agents, however.

The ASTM Specifications on the chemical composition of reinforcing bars (3) specify only maximum phosphorous content, leaving the rest of the chemical composition of the steel to the discretion of the manufacturer. The manufacturer generally selects the steel
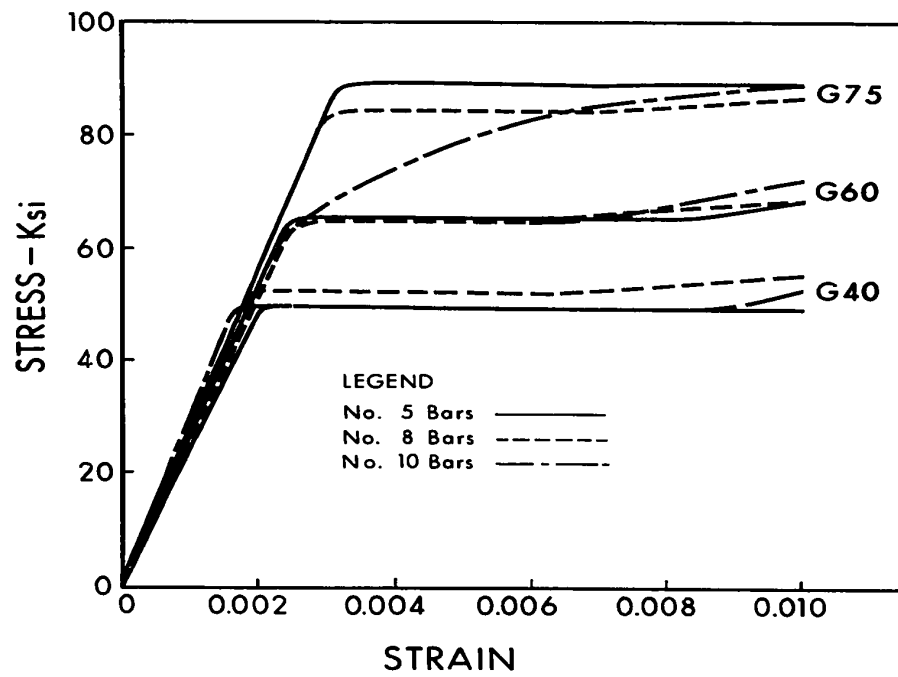
FIGURE 2-3   STRESS - STRAIN CURVES FOR BARS IN PHASE I
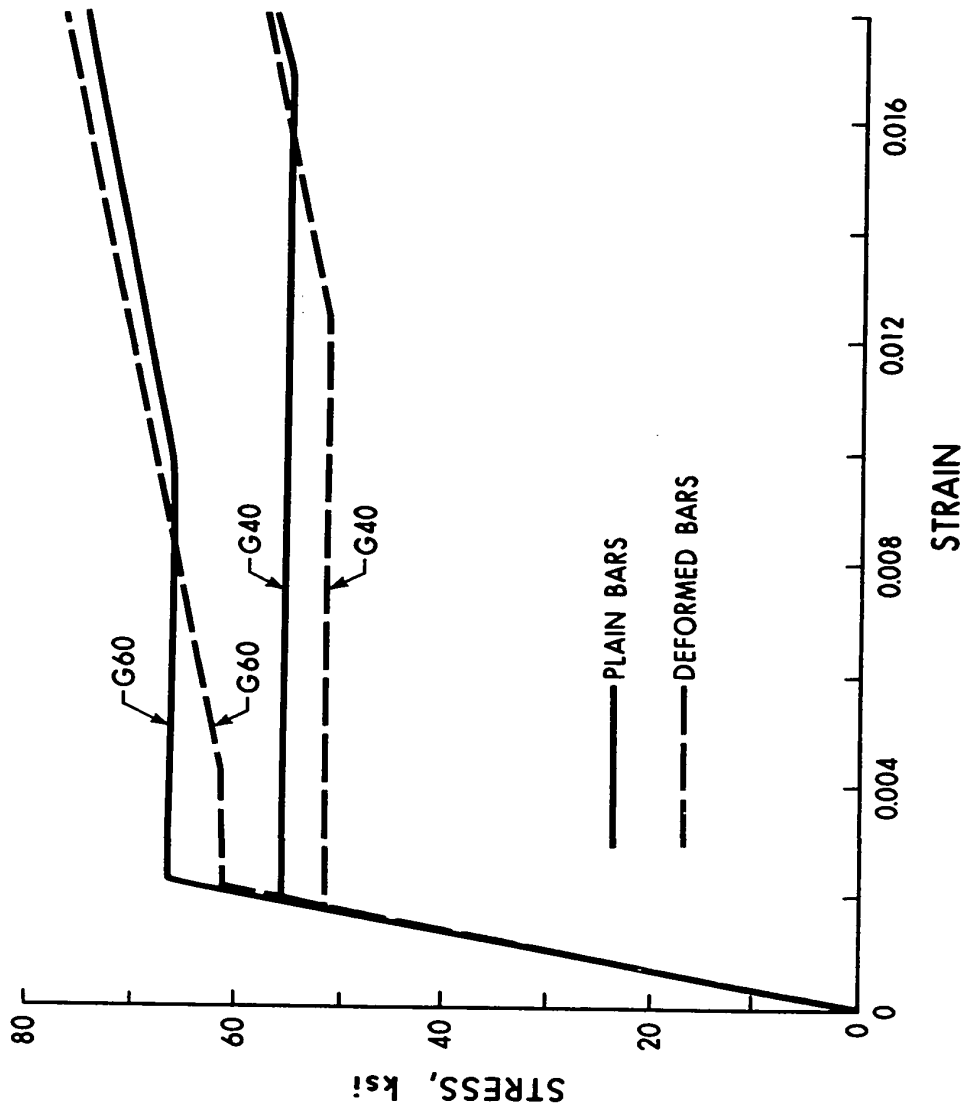
FIGURE 2-4   STRESS - STRAIN CURVES FOR BARS IN PHASE II

chemistry to achieve the specified mechanical properties without pay-
ing much attention to its micro-structure or grain size. The speci-
fications contain no requirements for the micro-structure and grain
size, which both affect the fatigue properties.

2.2.3.1 Chemical Analysis

To determine the chemical composition of the reinforcing
bars used in this project, tests were performed on a small sample of
each steel at the Stelco Edmonton plant. The chemical analysis for
all elements except carbon and sulphur was performed using an emission
spectrograph. The carbon and sulphur analyses were done separately.
The chemical analysis of the thirteen steels tested is given in
Appendix A.

The phosphorous content present in each case was less than
.05 percent as specified in the code (3). In the Grade 75 steels,
no phosphorous was detected. All the steels contained carbon contents
ranging from 0.36 - 0.52. The Grade 60 steels used for the first
phase of tests had carbon contents ranging from .42 - 0.52 percent,
much higher than the rest of steels. However, the Grade 60 steel
used for the second phase of tests had a carbon content of 0.34 percent
which is comparable to the carbon content of the rest of the steels.
From chemical analysis, it was apparent that the higher grade steels
were obtained partly by the increase in the carbon content and partly
by the additive agents such as manganese, chromium and vanadium,
some of which were probably present in the steel scrap used for bars.

CHAPTER III

FATIGUE TESTS

3.1 Choice of Type of Fatigue Specimen

Suitable fatigue test specimens had to be developed in order
to study the fatigue behavior of high strength deformed bars in con-
crete beams. Since a reinforced concrete beam under repeated loading
may fail in a mode of failure other than a fatigue fracture of the
tensile reinforcement (29), these modes of failure had to be eliminated
from the laboratory specimens by proper selection of the proportions
of the beam and the manner in which the load was to be applied. The
pioneer fatigue tests on deformed reinforcing bars at the University
of Münich, Germany (9) were performed on concrete beams having a bent
reinforcing bar as tension reinforcement. In these beams an adverse
stress condition was created in the bar by placing the bent section of
the bar in the highest tensile stress zone of the beam. Since in
actual structures, the probability of a bend being located in the maxi-
mum tensile stress region is low and since the radius of the bend it-
self affects the fatigue strength, most other investigators have used
one or more straight reinforcing bars as tensile reinforcement in
concrete beam specimens of rectangular or tee cross-section. Some in-
vestigators (16,18) used beam specimens with varying depths of reinforce-
ment. In all these cases, the beam cross-section or shape had no ef-

2 No. 3 Bars
No. 3 Stirrups
No. 5 Bar

7 1/2"

No. 8 Bar

12"

No. 10 Bar

15"

10 1/4"
6"

2 1/2"

45"

2 1/2"
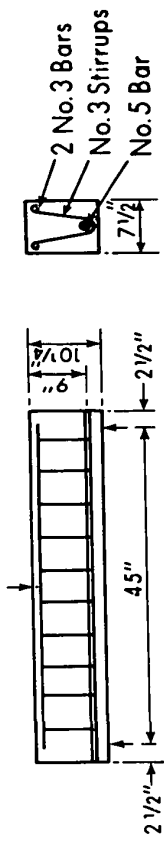
Series 7, 8 and 9 Beams - No. 5 Bars

12 1/2"
14"

4"

72"

4"
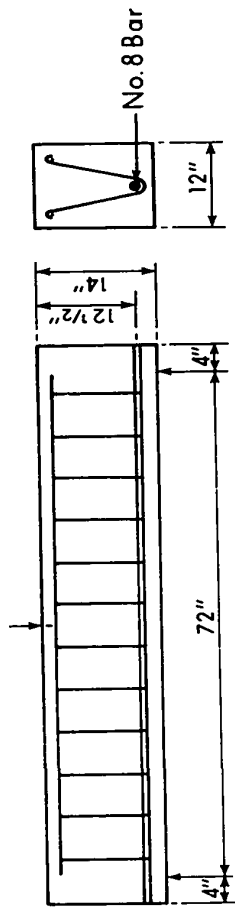
Series 1 to 6 Beams - No. 8 Bars

17 1/2"
15 5/8"

5"

90"

5"
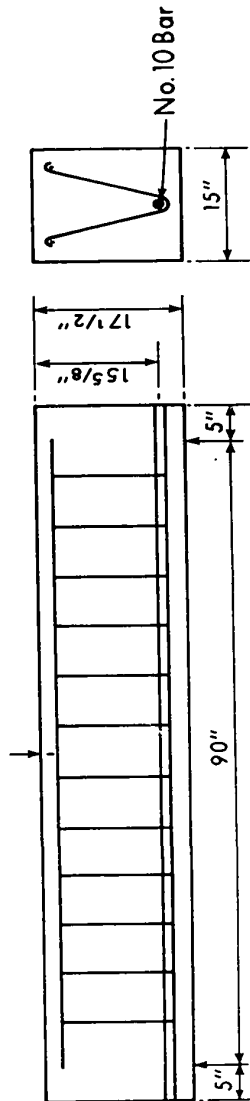
Series 10, 11 and 12 Beams - No. 10 Bars

FIGURE. 3-1   DETAILS OF BEAM SPECIMENS

25

SUPPORT ASSEMBLY

HYDRAULIC JACK

FATIGUE SPECIMENS

TEST FRAME

PULSATOR

LOADING BEAM

PULSATOR CONTROL PANEL

FIGURE 3-2   TEST SET - UP

SUPPORT ASSEMBLY

HYDRAULIC JACK

FATIGUE SPECIMENS

TEST FRAME

PULSATOR

LOADING BEAM

PULSATOR CONTROL PANEL

FIGURE 3-2   TEST SET - UP

25
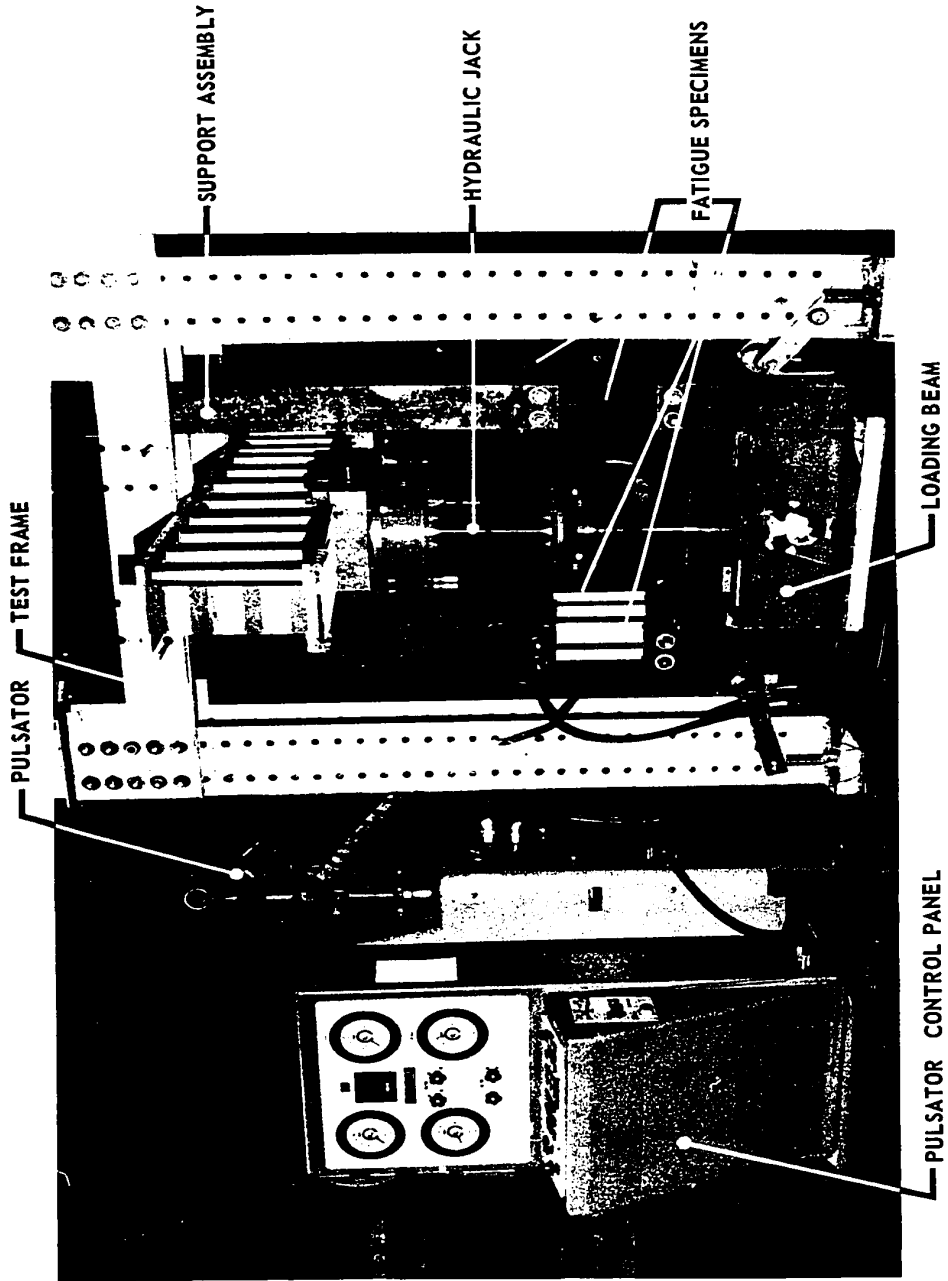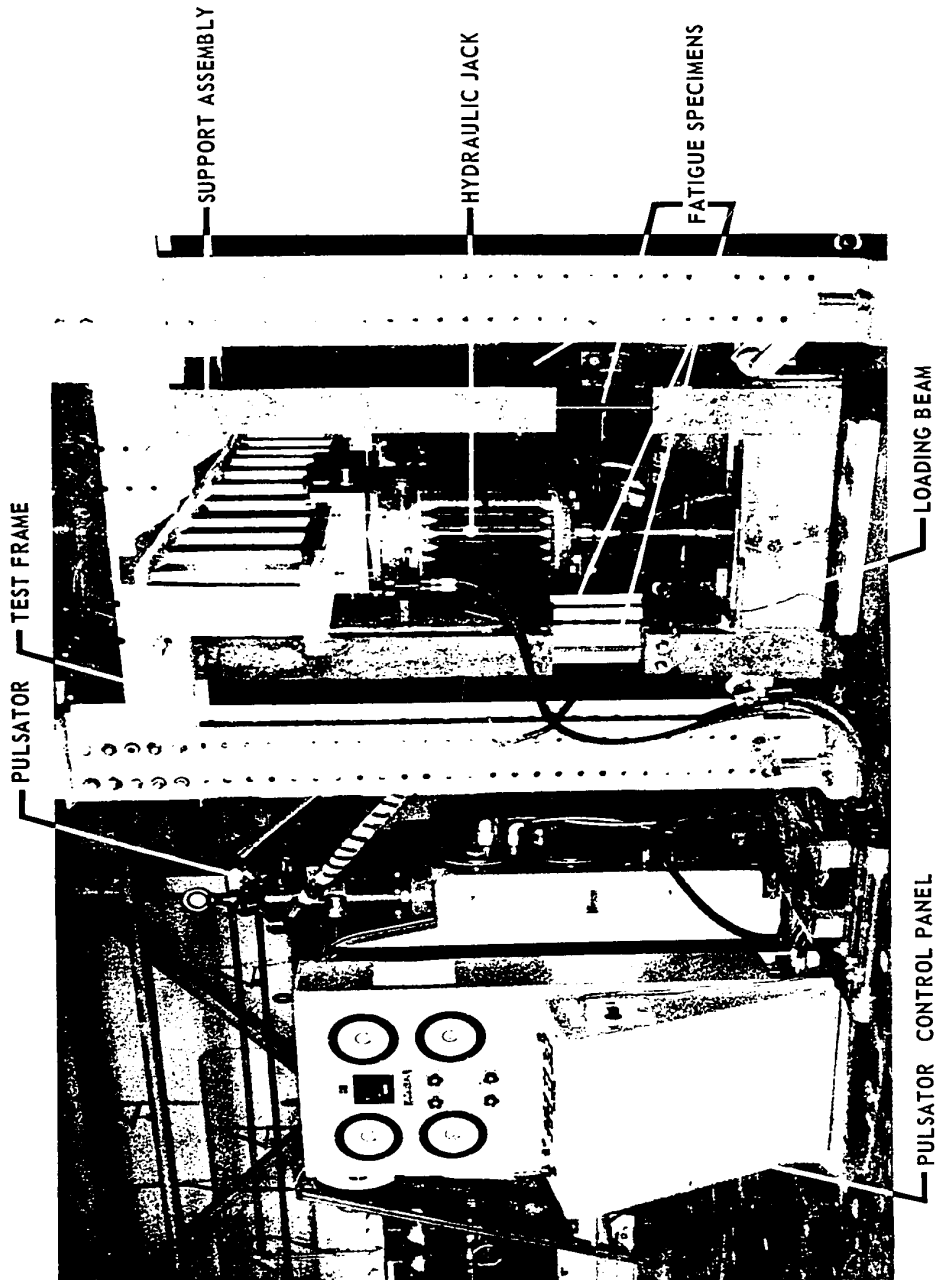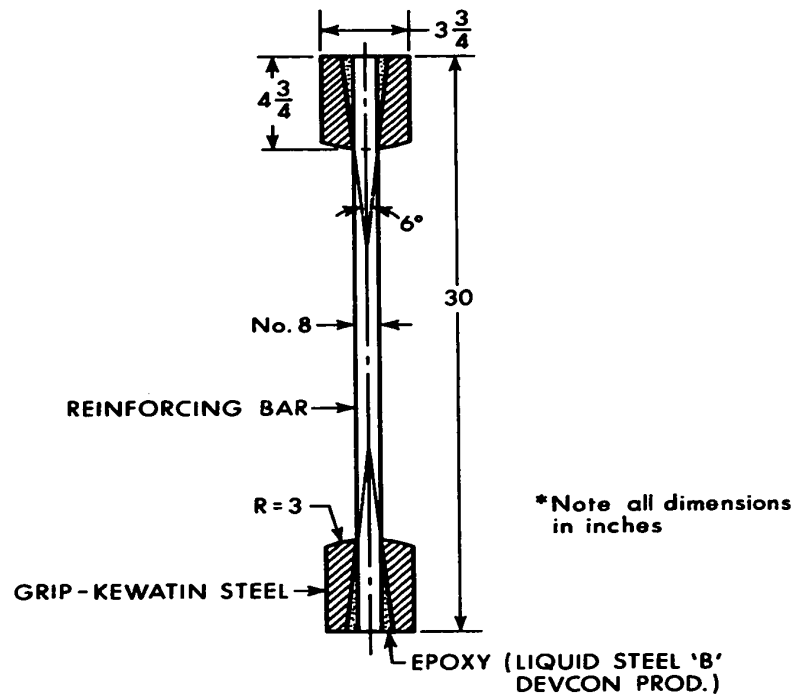
FIGURE 3-3   DETAILS OF FATIGUE SPECIMEN TESTED IN AIR
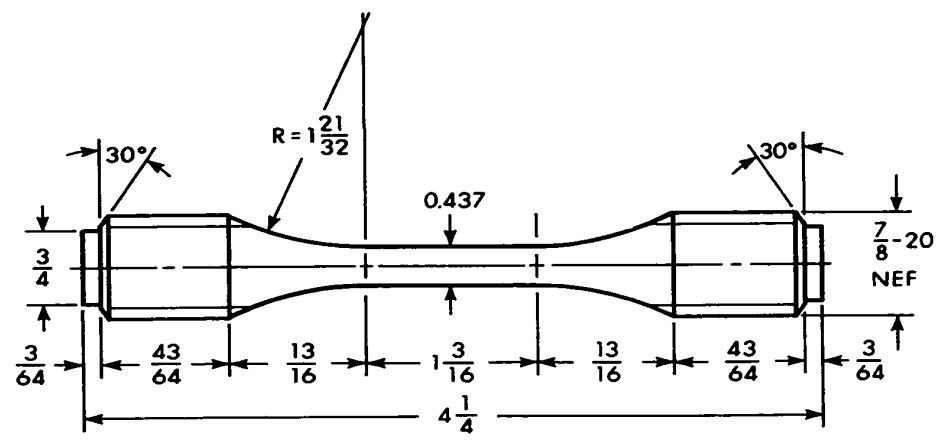
FIGURE 3-4   MACHINED POLISHED SPECIMEN

fect on the fatigue strength of reinforcing bars.

Rehm (9), Soretz (10) and Wascheidt (11) attempted to simplify the fatigue test specimen by testing reinforcing bars in air, since it is easier and more economical to test an individual bar in air than in a concrete beam. However, there is a disagreement on the effect of concrete encasement on the fatigue strength of bars. This aspect of the problem will be discussed in Chapter VII along with the results from this investigation.

In the first phase of tests, concrete beams with a single straight bar acting as tensile reinforcement were tested under repeated bending. The beam specimens used in this phase are shown in FIGURE 3.1. The fabrication, testing equipment and test procedures for these specimens will not be described in this report, but are given in detail in reference 29. In these tests, the beams were tested one at a time. The loads were applied at 500 stress cycles per minute and the total time required for testing 72 beams was eighteen months.

The second phase of tests involved testing deformed bars, as rolled bars, plain bars without rust and mill scale and machined polished specimens under identical stress conditions. These tests required more test specimens per series than in the first phase. For these reasons, a test set-up in which four bars were simultaneously tested in air was developed. A total of 88 bar specimens were tested at 500 cycles per minute in a period of six months. The test set-up and the fatigue specimens are shown in FIGURES 3.2 and 3.3 and are described more fully in

In addition, the second phase included tests of machined polished fatigue specimens as shown in FIGURE 3.4. These were tested under axially applied loading cycles in a vibraphore fatigue testing machine. The choice of specimen was dictated by the vibraphore fatigue testing machine.

3.2 Experimental Design

In the second phase of tests, a total of 88 No. 8 bar specimens and 32 plain machined specimens were tested in air under repeated loading. Six of the 88 No. 8 bar specimens were Grade 40 bars from the first phase of tests. These tests were intended to compare the fatigue strengths of bars in air to those in concrete beams under identical stress conditions. These six tests were considered a supplement to the tests in the first phase and hence were not included in the experimental design for the second phase of tests.

The main objective of the fatigue tests performed in the second phase was to carry cut a statistically valid experiment to determine the influence of the deformations, rust and mill scale, decarburization and grade of steel on the fatigue strength at long life, arbitrarily defined as 3 million cycles.

The first step in obtaining this objective involved determination of the mean fatigue limit defined for this test program as the fatigue strength at 3 million cycles for a specified confidence limit. This is frequently done using the test procedure known as the "sensitivity test" (28). Since from previous tests, it was known that reinforcing bars exhibited a practical fatigue limit (16) which was

known approximately, it was assumed that tests at four properly selected stress levels would yield the fatigue limit. Due to limitations in the testing facilities, it was not possible to strictly follow the sensitivity method. However, similar results were obtained by testing four specimens at each stress level. In these tests a stress increment of 2 ksi was used, which was considered adequate for practical purposes (31).

The outline of the experimental design is given in Table 3.1. The test program consisted of a two-way complete factorial design with 8 cells. Each cell was divided into four sub-cells which consisted of four test specimens. The grade of steel, bar surface characteristics, minimum stress and maximum stress were kept constant for a given sub-cell. Multiple tests in a sub-cell provided information on the distribution of fatigue life of bars. The four stress levels in one cell were not necessarily the same as that in another cell. The four sub-cells in a cell provided the information on the fatigue strength. The tests in all the cells formed a two-way complete factorial design (32).

A randomization procedure was adopted in the test program to minimize the effects of possible bias due to sampling, test sequence, machine and operator. The specimens in a sub-cell were randomly selected (33) and the testing sequence of the sub-cells was also randomized. In Table 3.1 the two numbers given in each sub-cell correspond to the group number of bars and testing sequence of the sub-cells, respectively.

Separate randomization procedures had to be adopted for machined polished specimens in cells 7 and 8 since these specimens were tested one at a time in a different machine. In general, it should be

TABLE 3.1
EXPERIMENTAL DESIGN

STEEL GRADE	STRESS LEVELS(*)	BAR SURFACE CHARACTERISTICS							
		DEFORMED AS ROLLED		PLAIN AS ROLLED		PLAIN WITHOUT RUST & MILL SCALE		MACHINED AND POLISHED	
		GROUP No.	TEST SEQUENCE	GROUP No.	TEST SEQUENCE	GROUP No.	TEST SEQUENCE	GROUP No.	TEST SEQUENCE
G40	I	1	4	9	8	17	12	25	25
	II	2	6	10	11	18	18	26	26
	III	3	9	11	15	19	21	27	27
	IV	4	13	12	20	20	24	28	30
G60	I	5	1	13	2	21	5	29	28
	II	6	3	14	7	22	14	30	29
	III	7	10	15	17	23	19	31	31
	IV	8	16	16	23	24	22	32	32

(*) STRESS LEVELS FOR ONE CELL MAY NOT NECESSARILY BE SAME FOR ANOTHER

** □ SERIES OR CELL NUMBER

noted that due to the special nature of fatigue tests, it is very diffi-
cult to completely randomize the whole experiment.

3.3 Fatigue Tests on Reinforcing Bars in Air

3.3.1 Fatigue Specimen

The specimen used to test reinforcing bars in air was essentially
a 30 inch long piece of No. 8 reinforcing bar. Special end grips were
designed to facilitate axial loading of the test piece without any
damage to the bar and to avoid fatigue fracture of the bars inside the
grips. The details of the fatigue specimen and the end grips are shown
in FIGURE 3.3. The end grips were made of a cylindrical block of
Kewatin Steel having a spherical shape on one end and a conical hole.
The spherical face of the grip and the grip housing seat (section 3.3.2)
were designed to facilitate true axial load application to the specimen.

The bars were cemented into end grips using a two component
epoxy, "Liquid Steel B" made by Devcon Products. To ensure alignment
of the grips and the bar, and to keep the grips a fixed distance apart,
a specially designed wooden mold was used. The epoxy was poured into
the end grips when the bar and end grips were positioned inside the
wooden mold. The epoxy hardened after 24 hours and developed a strong
bond with the bar. When tensile load was applied to the bar through
the grips, it was transmitted by the epoxy by wedging action to the end
grips.

For proper functioning of the above described grips, two
factors were important. First, adequate bond was required between the
epoxy and reinforcing bar and second, the slip between the bar and end
grips should be a minimum. Through experience, an included angle of

6° for the wedging cone was found to be most satisfactory.

Although the deformed fatigue specimen had excellent bond
with the epoxy, the plain bars did not develop comparable bond. This
problem was overcome by knurling a 3 inch length on both ends of the
bar specimen which provided good bond with the epoxy. The knurled
portion of the bar always started one inch inside the end grips.

In order to make the grips re-usable, a releasing agent (wax)
was coated on the conical hole wall of the grip, prior to cementing
the bars. This prevented bond formation between the epoxy and the grip.
After fatigue fracture of the bar, the broken bar pieces could be
forced out of the grips. As a result, of the waxing, the epoxy and
bar slipped 1/16 to 1/8 inch relative to the end grips when the load
was first applied.

Three types of bar specimens were used depending upon the
bar surface characteristics. The deformed and plain rolled bars were
cemented inside the grips as received from the mill. The plain bars
without rust and mill scale were plain rolled bars cleaned by the pro-
cedure described in the following paragraphs.

A chemical solution containing 10 percent EDTA (Diamino-
Ethate-Tetra-Acidic acid) and one percent sodium hydroxide dissolved
in water was used to remove rust and mill scale from the plain rolled
bars. A small percentage of sodium hydroxide helped in dissolving the
EDTA in water. This solution reacted only with the iron oxide and formed
an Fe EDTA complex compound (34).

For the cleaning operation, the bars were submerged in the

chemical solution in a galvanized tank. The tank was heated by two
small heaters to raise the solution temperature to about 70°C. The
solution was stirred intermittently and good ventilation was provided
for the escape of fumes. After about six hours a coffee brown pre-
cipilate of Fe EDTA complex was observed. The bars were kept in the
bath for 24 hours. Since the bars were only partially cleaned in this
operation the cleaning operation was repeated with fresh solution.
Immediately after the bars were taken out of the bath, they were washed
in a soap solution and a fine protective film of corrosion protective
oil was applied. The cleaned bars showed no blackish mill scale or
rust and had a shiny greyish color. Rolling defects such as longitudinal
seams, laps and flaws were visible on the bars. The bars showed no
signs of pitting due to the cleaning operation. One or two days after
the cleaning operation the bars were tested under fatigue loading.

3.3.2 Test Set-up and Testing Equipment

An overall view of the test set-up is shown in FIGURE 3.2
and the details of its various components are given in Appendix B.
The test set-up consisted of two reaction frames which were anchored
to the laboratory test floor. These two frames were connected by a
distributing beam on which two Amsler hydraulic jacks of 110 kips
dynamic capacity were mounted. These two jacks applied identical
sinusoidal loading on two identical loading beams, each supported by
two fatigue specimens, supported in turn by two identical assemblies
hanging from the distributing beam.

The grips at the ends of the specimens were housed in identical housings at their top and bottom ends. The bottom and top housings were bolted to the loading beam and overhanging support assembly, respectively. These housings had spherical seats compatible with the grips. The radius of curvature of the grips and the seats were the same, so that true axial load could be applied to the specimen. Both grips and housings were made of Kewatin Steel to reduce wear and the possibility of fatigue fracture. During testing, molybdenum grease was used to reduce friction between the grips and housings.

Each overhanging support assembly was supported by a pin which permitted free movement in the plane of loading beam. When one specimen failed, damage to the other specimen supporting the same loading beam was avoided through movement of the supporting assembly.

The loading ram of the jack was housed in a pocket provided at the center of the loading beam. Measurements showed that the load applied through the jacks was resisted equally by the four fatigue specimens.

Amsler equipment consisting of a hydraulic pulsator, two jacks and a control panel was used in the fatigue tests. Both jacks were connected to the same pulsator which was operated at 500 cycles per minute throughout the test program.

The testing equipment was capable of applying a sinusoidal load cycle varying between two limits. The minimum and maximum loads were set on two separate dials on the pulsator control panel which were calibrated in divisions representing one percent of the load capacity.

It was thus possible to estimate the reading upto 0.2 percent of the full jack capacity. The possible error in estimating the pulsator dial reading corresponded to 0.14 ksi.

A reset-counter indicated the number of stress cycles applied to the specimens. The machine stopped automatically when it reached a preset number of cycles; when a preset decrease in minimum load or increase in the maximum load occurred; when the machine on the test specimens started to vibrate significantly; or when one of the four specimens fractured. These controls assisted in obtaining undisturbed fractured specimens.

3.3.3 Laboratory Work and Testing Procedure

The reinforcing bars were received in 20 ft. lengths from the rolling mill. Eight bars of each grade and each bar type (plain or deformed) were obtained. Upon arrival at the laboratory, identification marks of paint and steel tags were put on each bar. Three deformed bars and five plain bars of each grade were randomly selected for the tests. These bars were cut into 30 inch long pieces. An identification mark was punched on one end of each bar piece according to a preplanned scheme. The bar specimens for each grade and bar type were then randomly grouped into four series, each series containing four groups and each group four specimens.

The groups of four bar specimens were chosen for testing according to the test sequence scheme outlined in Table 3.1. The bar specimens were then cemented into end grips in groups of four and these specimens were mounted in the fatigue testing assembly. Repeated loads

were simultaneously applied on these four specimens at predetermined
minimum and maximum stress levels. Minimum stresses of 5 ksi and
6.7 ksi were used for Grade 40 and 60 bars respectively. In all cases,
the bar stresses were calculated using a nominal area of 0.79 sq. inch
for the bars. The effect of the self weight of the loading assembly
was taken into account in calculating the bar stresses. The effect of
forced vibration on the bar stresses was approximated by assuming that
the load would overrun the top and bottom of the cycle set on the
machine by 2 percent of the stress range in the cycle. This was calcu-
lated using formulas provided in the Amsler Instruction Manual (35).

The Amsler pulsator was operated at 500 cycles per minute for
the entire test program. The initial load setting on the pulsator varied
slightly during the first hour or so and minor load adjustments upto
one-half of a pulsator dial division (about 0.35 ksi bar stress) were
made during this period. The Amsler dials were calibrated under static
load at the beginning, middle and end of the complete test program using
a 50 ton load cell. The pulsator calibration remained unchanged during
the three stages of tests.

The accuracy of bar stress calculations was checked by measure-
ments of strain in the bar. Electric resistance strain gages were glued
on two polished bars at mid-height and at both ends. The gages were
placed in pairs and were located on diametrically opposite faces of
the bar. A total of six 1/4 inch gages were glued on each bar. These
bars were mounted in the fatigue testing assembly with two other fatigue
specimens. Under static loading the stresses at the center and at the

ends varied between 99.8 and 100.3% and 97.5 and 102.5% of the nominal
stress respectively. When the location of the bars with gages was
interchanged with other bars in the test set-up, no appreciable dif-
ference in the stresses was observed. Part of the observed error was
due to bending stresses at the bar ends due to small misalignment in
the end grips. Since these bending stresses were small they were
neglected in the bar stress calculations.

When one out of the four specimens failed under the fatigue
loading, the machine stopped automatically. The number of cycles
applied to all the specimens prior to failure of the first specimen
was recorded. The failed specimen in the test assembly was removed and
was replaced by a dummy specimen. The dummy specimen was a plain
polished No. 8 bar of alloy steel having identical dimensions and end
grips as the rest of the fatigue specimens. Since the dummy bar had a
higher fatigue strength than the test specimens, it was not intended
to fail. When the second and third specimens failed, they were also
replaced by dummy bars. After fatigue fracture of the fourth specimen,
the next group of four specimens was tested. When fatigue failure did
not occur within 3 million cycles, the tests were terminated. These
specimens were called "run outs" and were not used for future tests.

After completion of tests on two groups of bars without
rust and mill scale of each grade, a statistical analysis of the data
showed that there was no significant difference between the lives of
these specimens and that of as-rolled bars at the same stress level
(see Chapter VI). Thus the tests on the remaining two groups of these

bars were abandoned.

The pieces of fractured bars were preserved for investigation of the initiation and progression of fatigue cracks. Two extra fatigue specimens of Grade 40 deformed bars were tested under identical loading with a 30 ksi stress range. After the fatigue failure of one specimen the load applications on the other specimen was terminated. This unbroken specimen was used in the investigation of probable zones of fatigue crack initiation. The observations from these tests will be discussed in section 6.2.

3.4 Fatigue Tests on Machined Polished Specimens

The design and details of the machined polished specimen shown in FIGURE 3.4 were taken from the "Instruction Manual" for the Amsler Vibraphore Fatigue Testing Machine. The selection of the minimum test diameter of the specimen was based on the maximum size of specimen which could be machined out of a No. 8 plain reinforcing bar. In the tests, a specimen minimum diameter of 0.437 inch was used.

One plain bar of each grade was taken for machining plain polished specimens. Eighteen pieces of the required size were cut from each grade and identification marks were stamped on the bar pieces. The specimens were turned with light cuts on a precision automatic lathe following a template. Each specimen was identically polished in three stages: (1) with No. 120 emery cloth, (2) with No. 240 emery polishing paper and (3) with No. 320 silicon carbide paper, successively. Polishing was done in the longitudinal direction on a lathe rotating at

100 rpm. After the final polishing no surface defects such as circumferential tool marks, scratches or nicks were visible to the unaided eye. After polishing a light coat of oil was applied to the specimen and great care was taken not to touch the polished surface. Within a week after polishing, all the specimens were tested.

Out of eighteen specimens of each grade, sixteen were used for fatigue tests and the remaining two for tension tests. The results of these tension tests were reported in Table 2.3.

The axial fatigue tests were performed on a high frequency Amsler Vibraphore Fatigue Testing Machine. This machine operates on the resonance principle, the test frequency coinciding with the natural frequency of the oscillating elements. A test frequency of 213 cycles per second was used for these tests.

A 10 ton load cell was used for the tests. The load on the specimen was indicated on a scale calibrated in divisions of one fifth of a pound. It was possible to adjust loads upto one quarter of a dial division. The corresponding error in the estimation of the specimen stress was 0.33 ksi.

The force exerted on the specimen could be chosen to fluctuate between any desired minimum or maximum loads. The load amplitude could be regulated exactly and maintained constant by means of a special photo-electric regulating device. Initially the tests were intended to apply a stress cycle similar to that used in the reinforcing bar tests, but, due to inability of the testing equipment to maintain maximum stresses above yield stress, a different stress cycle was selected.

This stress cycle consisted of 12 ksi and 6 ksi minimum compressive stresses for Grade 40 and 60 bars respectively. The tests were performed under a constant minimum compressive and maximum tensile stress cycle.

The specimens were tested one at a time according to the test scheme given in Table 3.1. The tests were divided into eight groups, each group consisting of four specimens. Four specimens belonging to one group were tested under identical stress cycles.

The testing equipment stopped when the specimen failed or when a preset number of cycles was reached. The specimens which did not fail after 5,000,000 cycles of load application were designated "run outs" and they were not re-tested. The fractured specimens were properly identified and preserved for examination of the fracture surfaces.

CHAPTER IV

METALLOGRAPHICAL AND OTHER INVESTIGATIONS

The surface characteristics of a structural member have a pronounced influence on its fatigue strength because the stress is usually greatest on the surface, particularly when stress concentrations are present. Moreover, the surface may be inherently weaker and as a result, fatigue failures almost always originate at the free surface. Metallographical investigations were undertaken to study characteristics of the surface and interior of the bars.

Tests were also performed to measure the surface roughness of the various fatigue specimens and to investigate the residual stresses in deformed bars.

4.1 Metallographical Investigations

The metallographical investigations included studies of macro-* and micro-structure, mill scale, decarburization and the grain size of reinforcing bars. Micro-hardness tests and carbon analyses of the decarburized bar surfaces were carried out to determine the depth and the approximate strength of the decarburized layer.

4.1.1 Structure of Reinforcing Steels

In order to observe the macro-structure of the reinforcing

---

*Magnification upto 10 x (36).

bar surface, six inch long pieces of all types of reinforcing bars in-
vestigated were macro-etched in 50 percent commercial hydrochloric acid
at 70°C for a half hour. The etched bar pieces revealed well defined
flow lines along the bar lengths. These flow lines indicated the di-
rection in which steel was worked during the rolling process. Rolling
defects such as seams, laps and inclusions were distinctly visible to
the unaided eye. Although the seams did not seem to be deep, they were
continuous along the entire length of the bar in some cases.

The bars were sliced along longitudinal and transverse planes
to observe the macro-structure in these planes. Bar specimens were cut
about 1/2 inch long by an abrasive cut off saw. While cutting, bars
were kept submerged in a cooling agent to avoid any change in the metal
structure due to heat. To facilitate polishing, the sliced bar specimens
were mounted in Araldite blocks in a mounting press.

The polishing of the specimens was done in four gradual stages,
using silicon carbide belts, silicon carbide discs, diamond abrasive and
alumina coated discs. The final finish of the surface was approximately
1/4 micron.

Polished specimens were macro-etched in a 50 percent hydro-
chloric acid solution. The macro-structure of the specimens revealed
non-uniformity of the metal structure in the cross-section of the bar.
Evidence of segregation in the ingot in all steels was indicated by wide
banding near the center of the bar. In some specimens dark black spots
were seen in the center of the bar which under high magnification, were
identified as carbon and phosphorous rich zones. The non-uniform

structure observed in the bars is common in rolled steels (36) which generally have directional and positional metal properties. However, defects such as surface cracks, pipes, cavities or blow holes were not observed in any of the specimens observed.

Microscopic observations for non-metallic inclusions were made on un-etched specimens. The inclusions were generally discontinuous and mostly oriented along the bar axis. Three typical photomicrographs at 100X magnification showing inclusions are shown in FIGURE 4.1. The intensity of inclusions was almost the same in all steels. These inclusions, when compared to standard ASTM Charts were classified as C^+ (background classification). The inclusions present were not excessive and their influence on fatigue strength is probably not significant since they were oriented in the direction of stress.

Metallographical observations for micro-structure were made on specimens etched in Nital (Nitric acid 2%, Ethanol 98%). The micro-structure in the longitudinal section at the center of the bars showed wrought or banded structure which essentially disappeared as the outside of the bar was approached. Close to the bar surface a zone of decarburization and oxidation was observed in all the specimens. Three photomicrographs showing decarburization and mill scale close to the base of a transverse lug in No. 8 reinforcing bars of the three grades used in first phase of tests are shown in FIGURE 4.2. In these photomicrographs an oxide layer is identified by a black boundary and a decarburization zone by a white fine grain structure close to the surface. Decarburization of steel occurs due to the loss of carbon
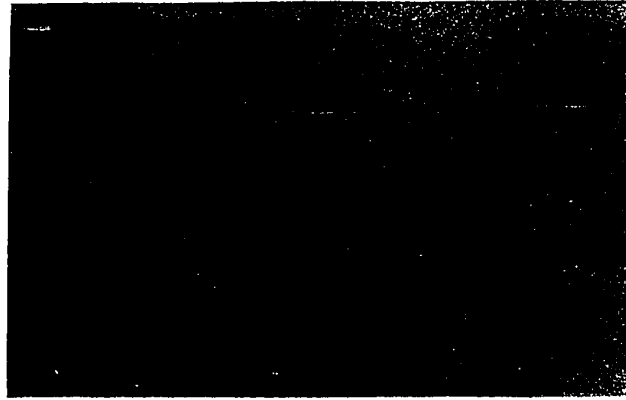
(a) ASTM A15 BAR

(b) ASTM A432 BAR

(c) ASTM A431 BAR
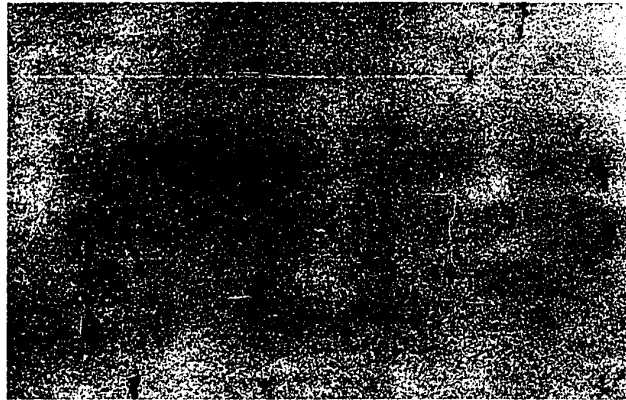
DIRECTION OF ROLLING

0   0.01   0.02

SCALE   INCHES

FIGURE 4-1   NON-METALLIC INCLUSIONS IN LONGITUDINAL SECTIONS OF NO. 8 BARS USED IN PHASE I TESTS.

(a) ASTM A15 BAR

(b) ASTM A432 BAR

DIRECTION OF ROLLING

(c) ASTM A431 BAR

0   0.01   0.02

SCALE   INCHES

FIGURE 4-1   NON-METALLIC INCLUSIONS IN LONGITUDINAL SECTIONS OF NO. 8 BARS
USED IN PHASE I TESTS.

(a) ASTM A15 BAR (b) ASTM A432 BAR (c) ASTM A431 BAR

DIRECTION OF ROLLING

SCALE — INCHES
0   0.01   0.02

FIGURE 4-2   MICRO-STRUCTURE AT BASE OF DEFORMATION LUG OF NO. 8 BARS USED IN PHASE I TESTS.

(a) ASTM A15 BAR (b) ASTM A432 BAR (c) ASTM A431 BAR

DIRECTION OF ROLLING

SCALE — INCHES

0   0.01   0.02

FIGURE 4-2   MICRO-STRUCTURE AT BASE OF DEFORMATION LUG OF NO. 8 BARS
USED IN PHASE I TESTS.

and due to grain boundary oxidation which usually occurs on the billet surface while in the furnace. The presence of oxide and decarburized zones may significantly lower the fatigue strength of reinforcing bars (37,38). The decarburization of the steel was determined by hardness tests and the carbon analyses. Both these tests were undertaken to estimate the depth of decarburized bar surface and its approximate tensile strength. These tests are described in the following sections.

4.1.2 Micro-Hardness Tests

The rolled surface of reinforcing bars makes hardness tests on the bar surface very difficult since most hardness testers require a smooth plane specimen surface. The hardness determination becomes even more complicated when the hardness of the surface layer of a rolled bar is desired. Micro-hardness tests are generally used when the hardness of very small layer is required, but these require a metallographic surface finish on the test surface. For this reason micro-hardness tests were made on a polished bar cross-section from close to the surface rather than on the surface of the bar itself.

A Tukon Micro-Hardness Tester with a Knoop diamond indenter was used for the tests. A Knoop indenter is a diamond ground to pyramidal form, that produces a diamond shaped indentation having an approximate ratio of 7:1 between long and short diagonals. The depth of indentation is 1/30 of its length. Due to the unique shape of the indenter, it is possible to use small loads up to 1 Kg to determine the hardness of very small layers.

Three-eighth inch long pieces of reinforcing bar were polished
to 1/4 micron in a thermoplastic mold by the procedure previously de-
scribed in section 4.1.1. Knoop indentations were made on the bar
cross-section using a 1 Kg load. On each specimen indentations were
made starting 0.1 mm from the surface and a total of 15 indentations
were made at 0.1 mm spacing towards the center of the bar. Photo-
micrographs showing Knoop indentations in reinforcing steels are given
in FIGURES 4.3, 4.4 and Appendix C. In these figures the Knoop Hard-
ness Numbers corresponding to each indent are also plotted for illu-
stration. The horizontal scale is the same in the graph and the indent
micrograph in part (b) of these Figures. Though several sets of hard-
ness tests were made on each bar specimen, only one representative set
of data for each steel is presented in these figures. It may be noted
in these figures that the hardness of the decarburized surfaces was
much lower than in the center of reinforcing steels. The decarburiza-
tion zone seen in the indent photomicrographs and that estimated from
micro-hardness results agreed closely.

The thickness of mill scale and decarburization layers was
measured by a Microtone attached to the Tukon hardness tester. The
approximate tensile strengths of decarburized surfaces and bar steels
were obtained from Knoop hardness numbers using conversion charts.

The average thickness of the mill scale was 0.10 to 0.20 mm
and 0.15 mm in Phase I and Phase II, respectively. The decarburiza-
tion thicknesses, and the average tensile strengths of the steel in
the decarburized surface layers and the interior of the bar are given

(a) GRAIN STRUCTURE

(b) KNOOP HARDNESS AND CARBON CONTENT
GRADIENTS THROUGH DECARBURIZED
SURFACE

FIGURE 4-3 GRAIN STRUCTURE, MICRO-HARDNESS AND
CARBON CONTENT DATA FOR GRADE 40
NO. 8 PLAIN BARS

(a) GRAIN STRUCTURE   0 __INCHES__ 0.01

(b) KNOOP HARDNESS AND CARBON CONTENT
GRADIENTS THROUGH DECARBURIZED
SURFACE
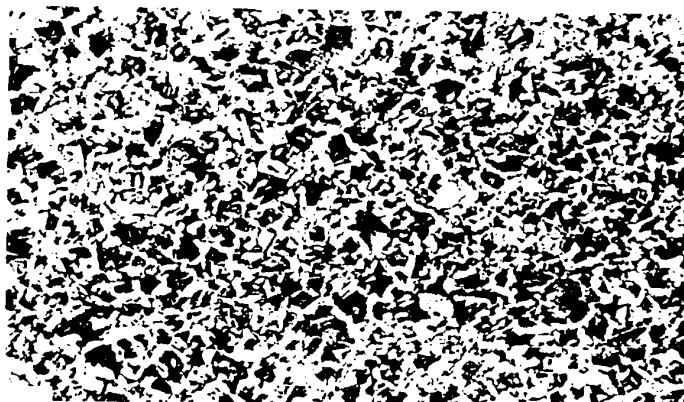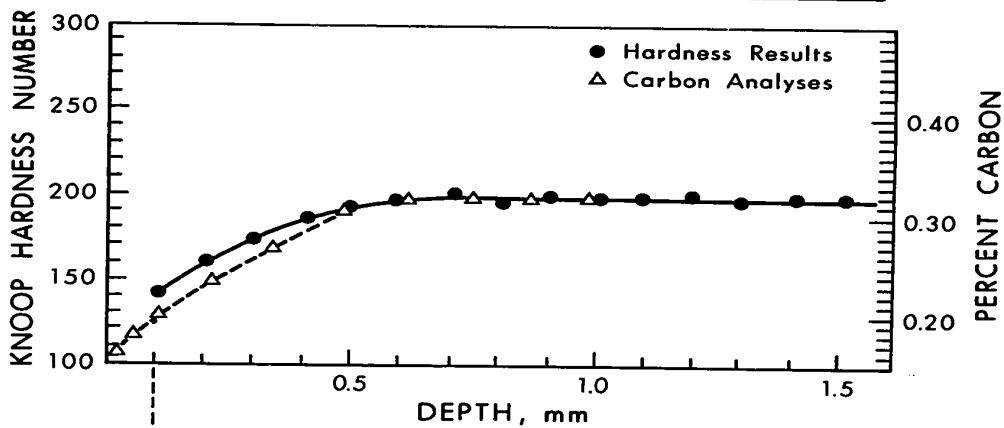
FIGURE 4-3   GRAIN STRUCTURE, MICRO-HARDNESS AND
CARBON CONTENT DATA FOR GRADE 40
NO. 8 PLAIN BARS

(a) GRAIN STRUCTURE

(b) KNOOP HARDNESS AND CARBON CONTENT
GRADIENTS THROUGH DECARBURIZED
SURFACE
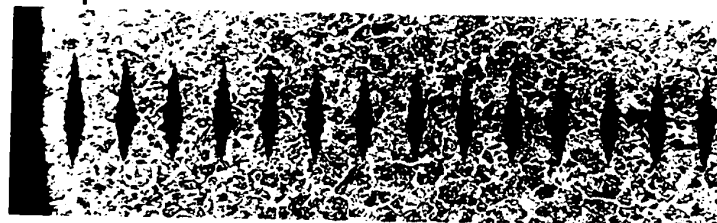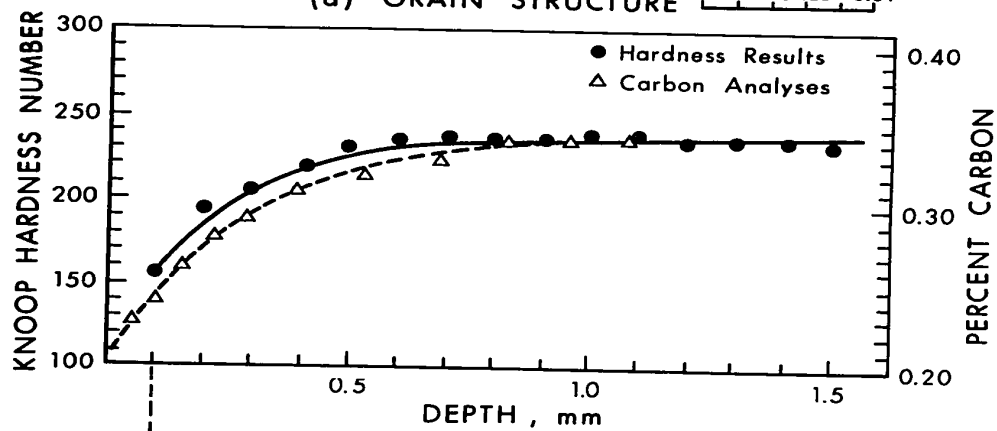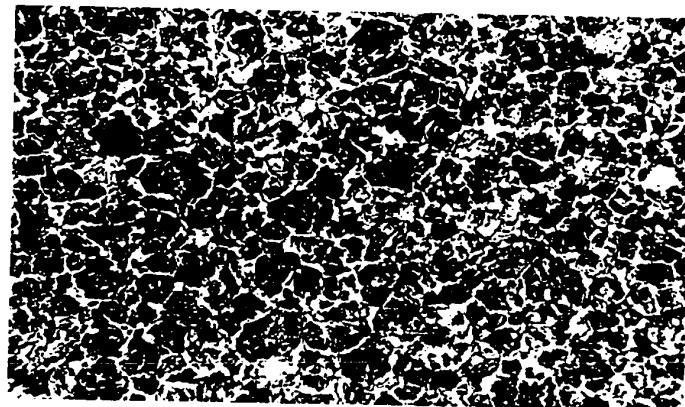
FIGURE 4-4   GRAIN STRUCTURE, MICRO-HARDNESS AND
CARBON CONTENT DATA FOR G60
NO. 8 PLAIN BARS
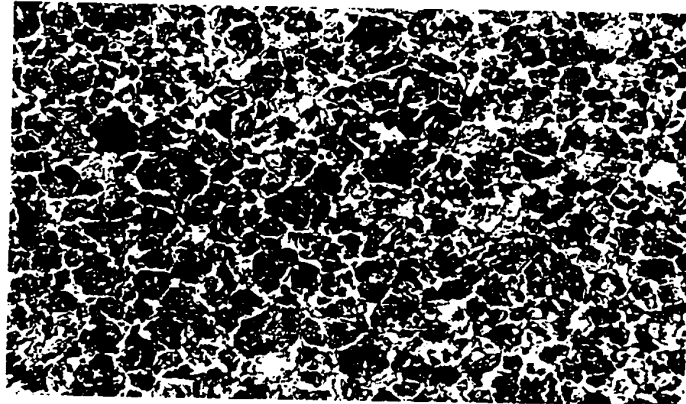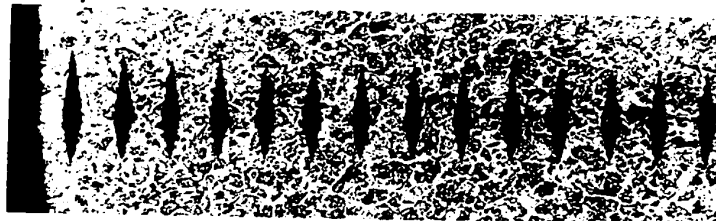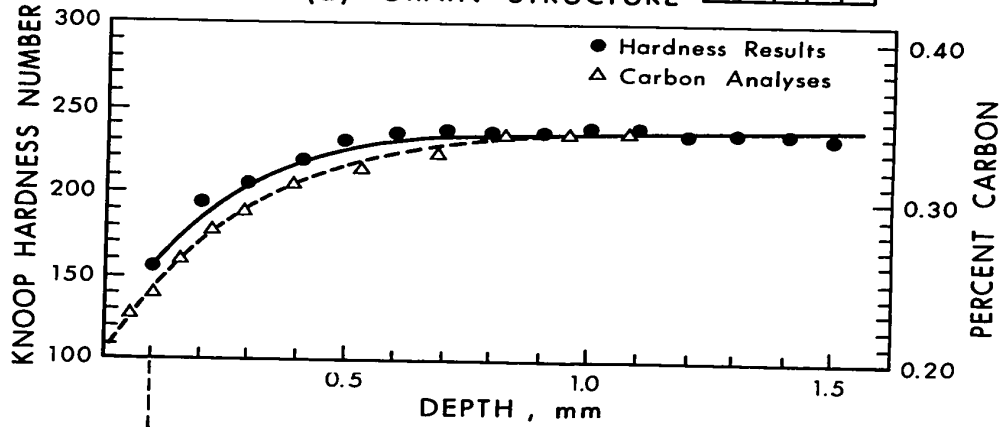
(a) GRAIN STRUCTURE

(b) KNOOP HARDNESS AND CARBON CONTENT
     GRADIENTS THROUGH DECARBURIZED
     SURFACE

FIGURE 4-4   GRAIN STRUCTURE, MICRO-HARDNESS AND
               CARBON CONTENT DATA FOR G60
               NO. 8 PLAIN BARS

in Table 4.1.

4.1.3 Carbon Analyses of Bar Surface

To further confirm the findings from the metallographic ob-
servations and micro-hardness tests regarding the presence of decarburi-
zation, carbon analyses of the bar surface were made in the laboratory
at the Stelco plant in Edmonton. These analyses were restricted to the
plain reinforcing bars of Grade 40 and 60 steels. The bar surface was
machined off in layers. Five cuts of 0.002 inch and eight cuts of
.005 inch were made. The shavings from each cut were sealed in separate
containers and sent for carbon analyses. In order to avoid contamination
of the shavings, the cutting tool used was cleaned with alcohol and
subsequently sharpened; and in the machining operation no oil or cooling
solution was used.

The results of carbon analyses are given in FIGURES 4.3 and 4.4.
In these figures, it may be noted that carbon contents as low as 0.15%
and 0.18% were obtained in the bar surface of Grade 40 and 60 steels,
respectively. The carbon content was lowest at the bar surface, in-
creased towards the bar center and became equal to the carbon content
of the bar steel at the end of decarburized zone. Since the strength
of steel increases with an increase in the carbon percentage (37), it
is reasonable to assume the steel strength varies in the same manner
as the carbon percentage inside the decarburized zone. This assumption
was supported by the micro-hardness results.

TABLE 4.1

DECARBURIZATION AND GRAIN SIZE DATA(*)

Experiment Phase	Bar Type	Bar Size	Bar Grade	Tensile Strength(**) ksi	Decarburization Thickness mm	Approximate Tensile Str(ksi)		Grain Size at Center of Bar	
						Bar Steel	Decarb. Layer (+)	ASTM Index	Grains/sq.in. (***)
I	Deformed	#5	G40	--	0.30~0.40	88.0	72.0	8.5	165
			G60	--	0.30~0.40	105.0	82.0	8	120
			G75	--	0.25~0.55	124.0	85.0	10	330
		#8	G40	94.0	0.20~0.40	92.0	74.0	8	102
			G60	119.0	0.20~0.45	120.0	80.0	7.5	80
			G75	128.0	0.35~0.60	130.0	84.0	6.5	45
		#10	G40	--	0.30~0.50	88.0	75.0	7.5	80
			G60	--	0.30~0.50	120.0	86.0	6.5	45
			G75	--	0.40~0.60	142.0	82.0	5.5	26
II	Deformed	#8	G40	90.0	0.40~0.60	88.0	76.0	8	98
			G60	102.5	0.40~0.60	110.0	80.0	7.5	75
	Plain	#8	G40	90.0	0.40~0.60	90.0	75.0	8	102
			G60	102.5	0.40~0.60	108.0	80.0	7.5	80

(*) Average data is reported.
(**) Tensile strength of Plain Polished Specimens machined from center of bar.
(***) At 100X magnification .
(+) Average in layer.

4.1.4 Grain Size

While examining the micro-structure of the reinforcing steels, it was observed that the austenitic grain sizes of the various steels varied considerably. Since it has been observed that a fine grain size* results in a higher fatigue strength than a coarse grain size (2), grain size measurements were undertaken for the various reinforcing steels.

The Comparison Technique and Grains per unit Area Method of estimating grain size were used due to their simplicity and wide acceptance (37). The bar specimens were etched in Nital to reveal the micro-structure. The etching solution darkened the pearlite, gave contrast between pearlite colonies and revealed ferrite boundaries which facilitated the grain size measurements.

Generally the grain size of one type of steel was found to be uniform except in the very thin layer close to the bar surface which was non-uniform and had finer grain size. Grain size measurements were made anywhere in the bar cross-section except near the bar edges. Photomicrographs taken at exactly 100X magnification for all steels are given in FIGURES 4.5 to 4.8. These photomicrographs were compared to the standard ASTM charts to determine the Grain Size Index (37). The measured grain sizes are given in Table 4.1. A higher ASTM Grain Size Index corresponds to a finer grain size.

Though Comparison Technique is simpler and less laborious than

---

*Grain size everywhere refers to austenitic grain size.
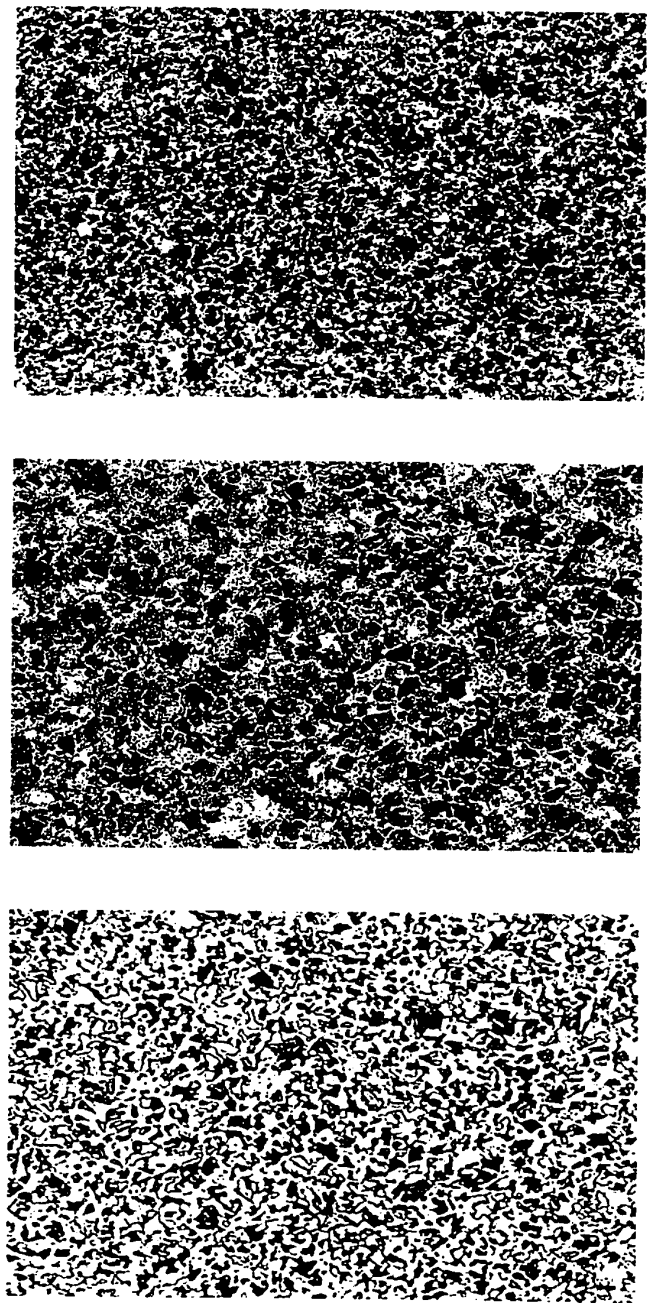
(a) GRADE 40   (b) GRADE 60   (c) GRADE 75
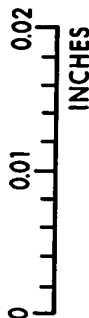
0   0.01   0.02

INCHES

FIGURE 4-5   MICRO-STRUCTURE OF NO. 5 BARS

(a) GRADE 40

(b) GRADE 60

(c) GRADE 75

0   0.01   0.02

INCHES

FIGURE 4-5   MICRO-STRUCTURE OF NO. 5 BARS

(a) GRADE 40 (b) GRADE 60 (c) GRADE 75

INCHES

0   0.01   0.02

FIGURE 4-6   MICRO-STRUCTURE OF NO. 8 BARS USED IN PHASE I TESTS

54
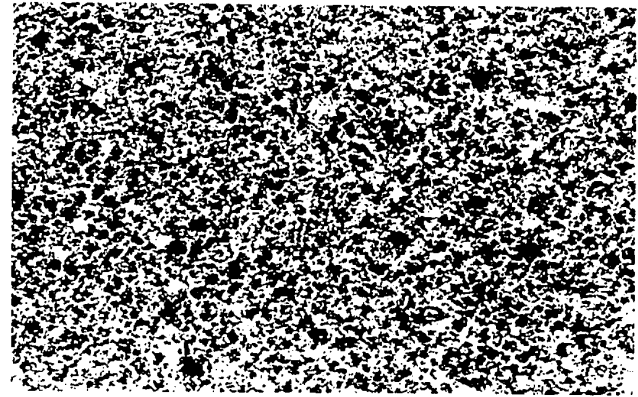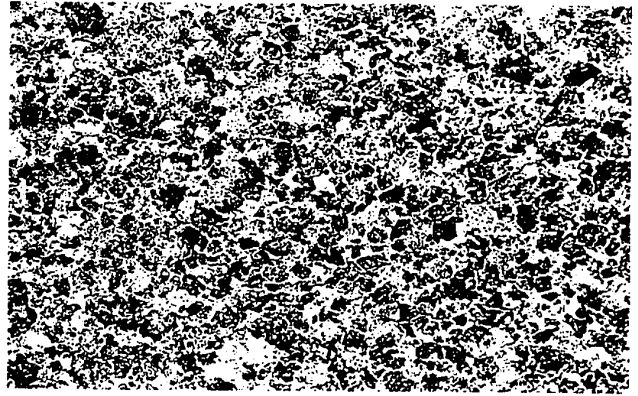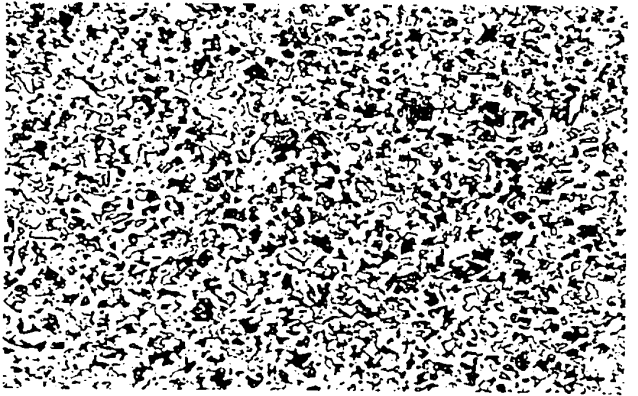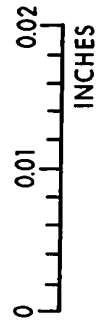
(a) GRADE 40 (b) GRADE 60 (c) GRADE 75

0   0.01   0.02
INCHES
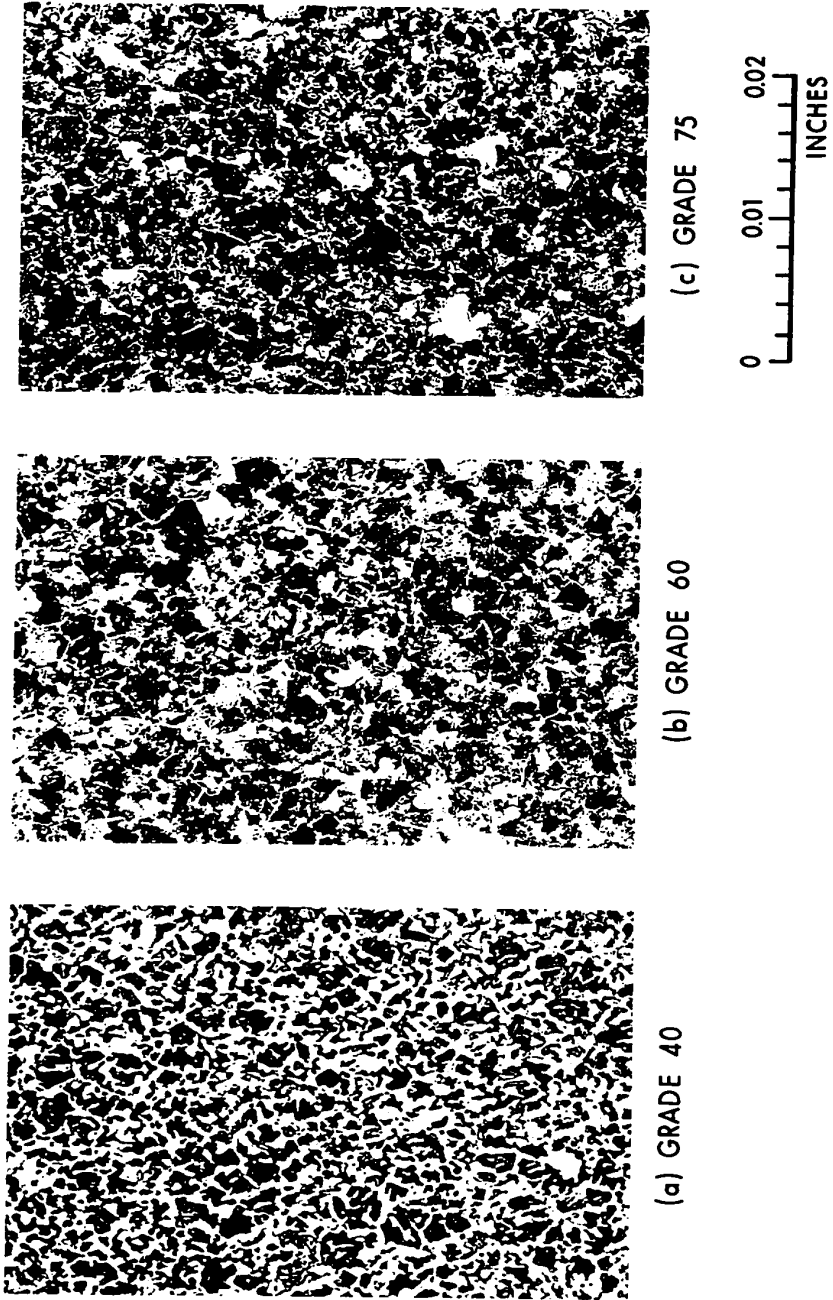
FIGURE 4-6   MICRO-STRUCTURE OF NO. 8 BARS USED IN PHASE I TESTS

(a) GRADE 40

(b) GRADE 60

(c) GRADE 75

INCHES

0   0.01   0.02

FIGURE 4-7   MICRO-STRUCTURE OF NO. 10 BARS

(a) GRADE 40   (b) GRADE 60   (c) GRADE 75

0   0.01   0.02
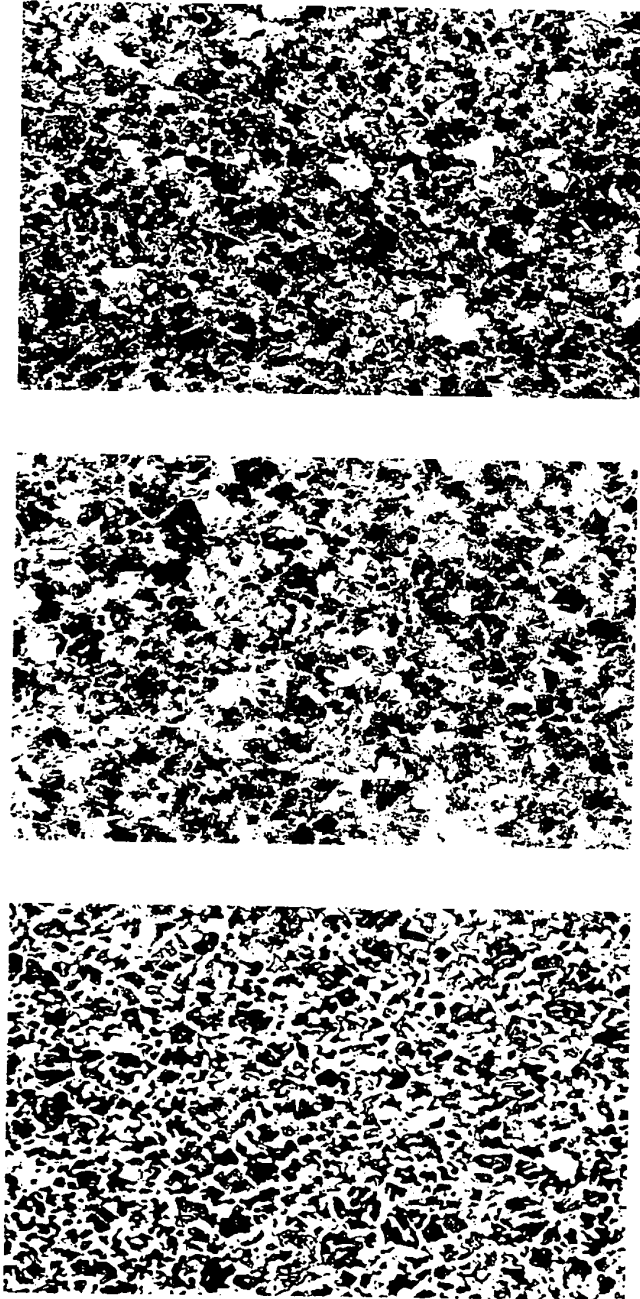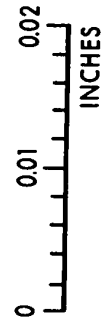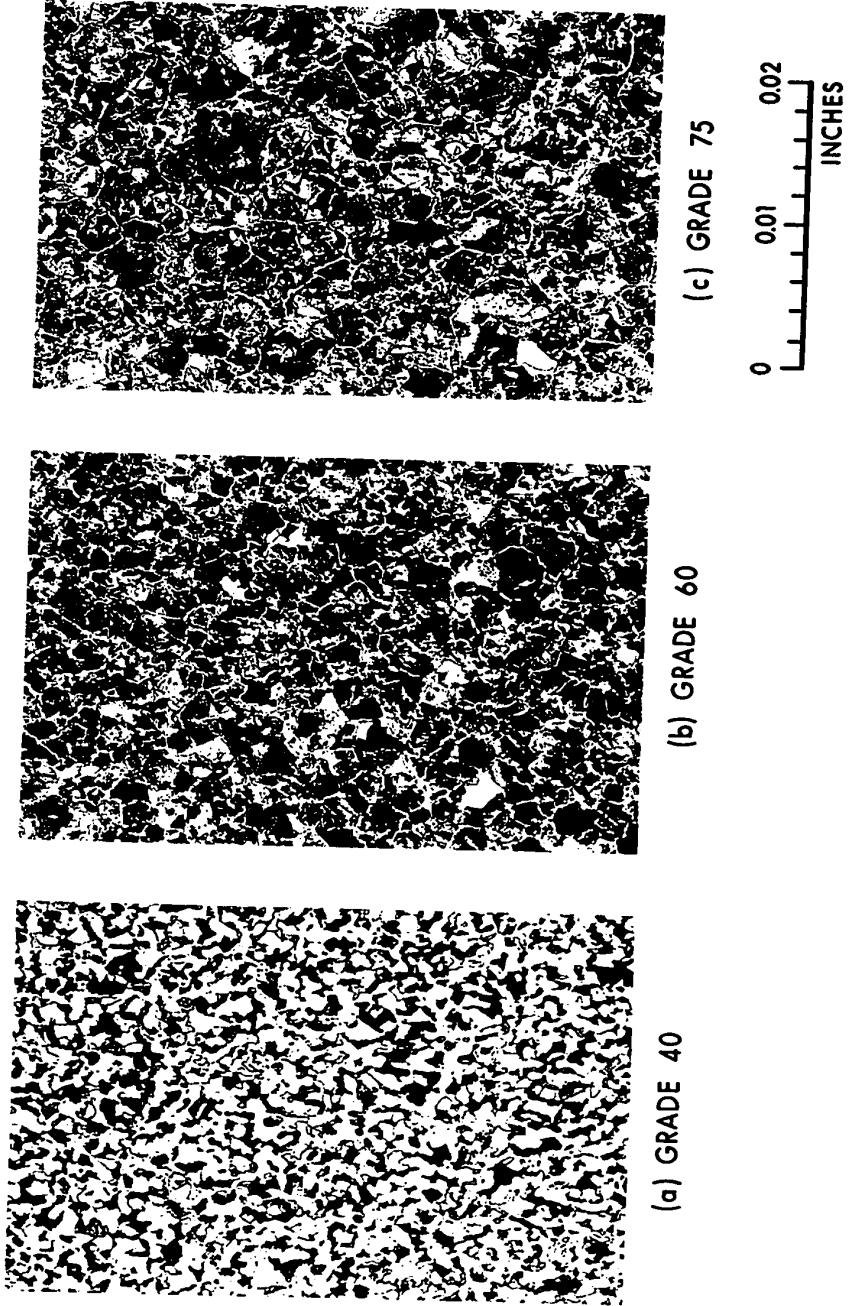
INCHES

FIGURE 4-7   MICRO-STRUCTURE OF NO. 10 BARS

(b) GRADE 60

(a) GRADE 40

0 0.01 0.02

INCHES
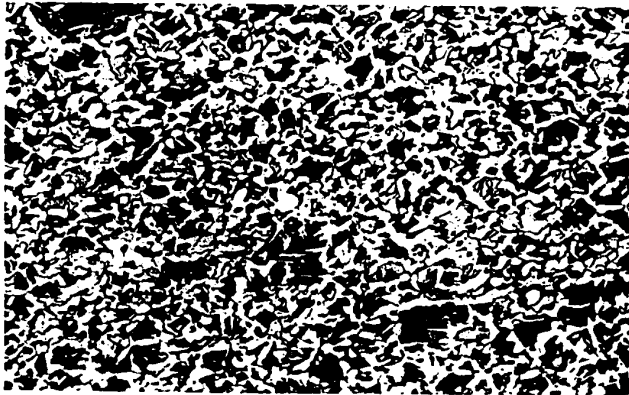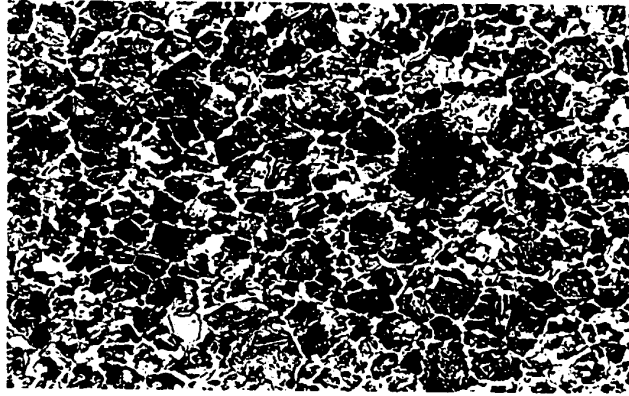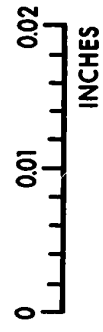
FIGURE 4-8   MICRO-STRUCTURE OF No. 8 BARS USED IN PHASE II TESTS

(a) GRADE 40   (b) GRADE 60

INCHES
0   0.01   0.02
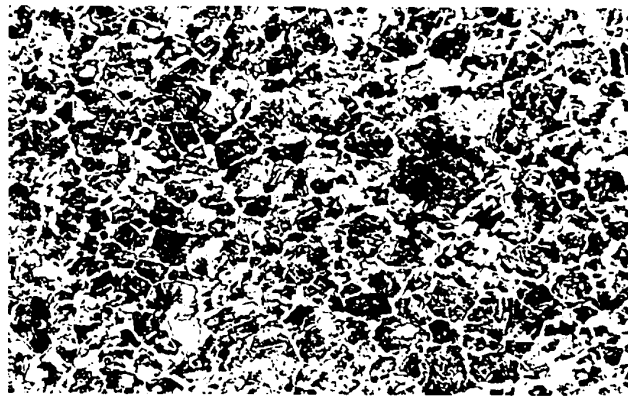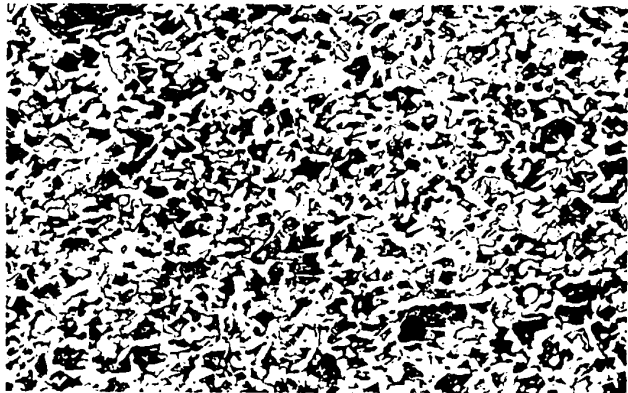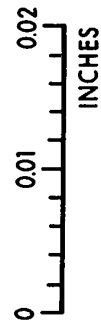
FIGURE 4-8   MICRO-STRUCTURE OF No. 8 BARS USED IN PHASE II TESTS

other grain size measuring methods, it is wholly dependent on visual judgement. To obtain a more accurate estimation of grain size, the grains per square inch of micrograph were counted from the photomicrograph of each steel at several locations. The results are given in Table 4.1.

Results obtained from both grain size measurement methods showed that the grain size increased with the increase in the bar grade and/or increase in the bar diameter except for the Grade 75 No. 5 bar. This bar had the finest grain size among all the steels investigated. Referring to the steel chemistry of this bar given in Table A-1 in Appendix A, it may be seen that this steel had .09 percent vanadium. Additions of .05 percent or higher of vanadium have been found to be a powerful deoxidizing agent resulting in a strong carbide formation which inhibits grain growth. This alloying agent might have been responsible for the fine grain structure observed in the No. 5 Grade 75 bars. This conclusion is not supported by the chemistry and grain sizes of Nos. 8 and 10 bars of Grade 75 steels, however.

4.2 Surface Roughness

The importance of the surface roughness of the fatigue specimen has long been realized by investigators. Generally the smoother the surface of a specimen, the higher is its fatigue strength (2). When this conclusion is applied to plain reinforcing bars, their lower fatigue strength as compared to plain polished specimens observed in

fatigue tests must have been partly due their rougher surface.

The fatigue specimens investigated, had three basic surfaces; as-rolled, rolled with rust and mill scale removed, and machined and polished. The roughness of these three surfaces was measured using a "Talysurf 4" surface measuring instrument. The instrument consists of a sharply pointed stylus, an electrical pickup and control unit with a graph recorder. The stylus was placed on each specimen surface and traces of surface profiles along the length of the specimens were recorded. The typical surface trace records for three surfaces along with their equivalent CLA values (a measure of roughness) (41) are given FIGURE 4.9. The surface roughnesses of as-rolled surfaces with and without rust and mill scale were found to be about the same, having CLA values ranging between 250 to 400. Although the surface trace record of the machined polished fatigue specimen is plotted with a vertical magnification ten times greater than that used for the other two traces in the figures it still has smaller peaks. The CLA values for the machined polished specimen was about 13 and had much smaller variation than for the other two surfaces.
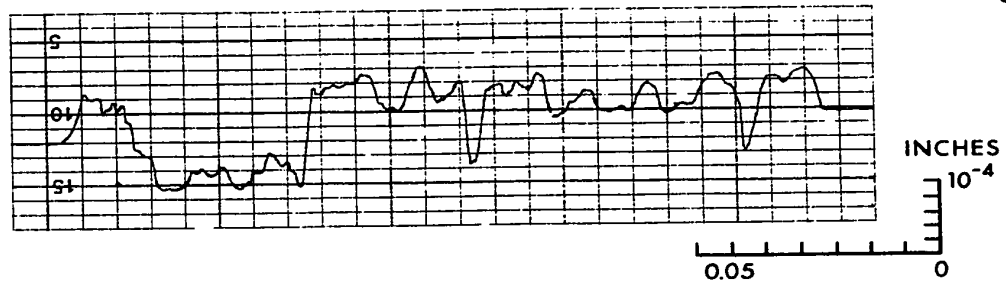
(a) As - ROLLED BARS   CLA = 250 - 400

INCHES
10^{-4}

0.05   0
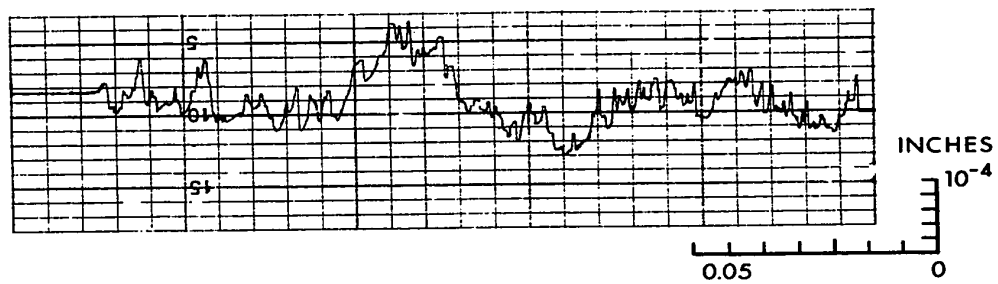
(b) ROLLED BARS WITHOUT RUST AND MILL SCALE
CLA = 260 - 380

INCHES
10^{-4}

0.05   0
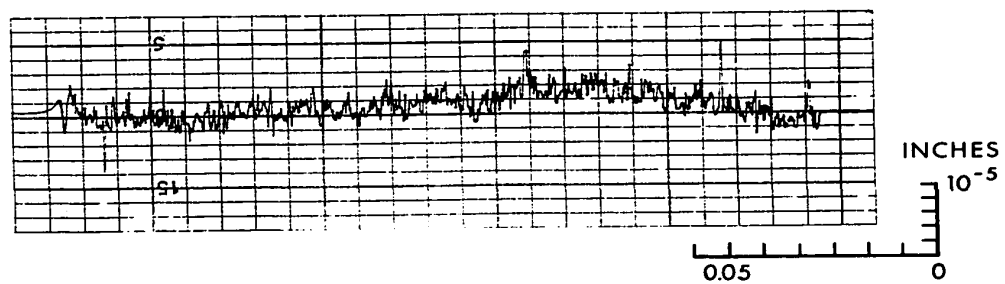
(c) MACHINED POLISHED SPECIMEN   CLA = 12 - 14

INCHES
10^{-5}

0.05   0

FIGURE 4-9   SURFACE ROUGHNESS PROFILES

CHAPTER V

STRESS CONCENTRATION DUE TO DEFORMATIONS

5.1 Significance of the Stress-Concentration Factor, K_T

Research on metal fatigue has shown that fatigue failures tend to occur in regions of high stress concentrations. In structural members, stress concentrations are caused by sudden changes in the member cross-section, sharp corners, fillets, holes, etc, all of which are more popularly known as notches. The severity of a notch is measured by the stress concentration factor (K_T), which is defined as the ratio of the maximum elastic stress in the region of the notch to the nominal stress in the member. Determination of K_T should be based on an elastic stress analysis.

One logical conclusion from the preceding paragraph is that regions of high stress concentrations (notches) should be avoided in structural members designed for fatigue loading. Unfortunately, in reinforcing bars this is not practical without significantly reducing their bond properties. An alternate approach to the design of structural components against fatigue failure is to minimize the stress concentration factor for a notch by correctly proportioning its geometry.

A typical hot rolled deformed reinforcing bar contains two longitudinal ribs and a regular pattern of equally spaced transverse lugs. The ribs and lugs cause stress concentrations in the reinforcing

60

bar. To study the fatigue behavior of reinforcing bars, it was felt
necessary to determine the stress concentration factors for the de-
formations.

Although technical literature (41,42) contains K_T values for
numerous types of notches, none of the published cases truly represent
deformations on reinforcing bars. Therefore, an investigation was
undertaken to determine K_T for the deformations. This investigation
was carried out in two phases. In the first phase, the technique
of direct strain measurement using electric resistance strain gages
was employed to determine the locations of high stress concentration
and the maximum stresses for the deformed reinforcing bars used in this
project. The experimental work is described in section 5.2. In the
second phase, a theoretical stress analysis was performed for circular
bars having axi-symmetrical projecting lugs. The K_T values for a
wide variety of projecting lug shapes similar to deformations in
reinforcing bars were determined. This phase of the investigation
is presented in section 5.3.

5.2 Experimental Investigation for K_T using Strain Gages

5.2.1 Description of Tests

Electrical resistance strain gages with 0.3 mm gage lengths
were used for the strain measurements. These gages were Kyowa (KFC-
03-C1) foil type gages bonded to an epoxy insulation.

Stress concentration measurements were made on the deformed
reinforcing bars used for fatigue tests in air. Since the deformation

details on bars of grade 40 and grade 60 were identical, it was imma-
terial which grade of steel was selected for stress measurements and
a grade 60 steel bar was chosen due to its higher yield strength.
A 30 inch long specimen, machined 4 inches at both ends to ensure con-
centric mounting in the testing machine, was used for stress measure-
ments.

Prior to mounting the gages, the surface of the bar was
prepared by a light glass bead blast cleaning to remove rust and mill
scale. Following this the gage locations were polished with size 120
emery paper and cleaned with trichloro-ethlyne solution. In these
processes, special care was taken to ensure uniform cleaning of the
bar specimen without altering the geometry of the deformations.

The strain gages are shown in FIGURES 5.1 and 5.2. Gages 1
and 2 were of 1/4 inch gage lengths. These two gages were mounted
on to the body of the bar midway between two transverse lugs at a
point adjacent to the manufacturer's markings, where the lugs were
further apart than normally. These gages were mounted on the dia-
metrically opposite sides of the bar. The rest of the gages shown in
FIGURES 5.1 and 5.2 were of 0.3 mm gage length. These gages were
located at possible zones of high stress concentrations.

The deformed bar with strain gages was tested under static
tension in a 100 ton Baldwin Universal testing machine. The strains
were measured using Budd Strain indicators and a multiple channel
switch box. Separate strain indicators and dummy gages were used for
1/4 inch and 0.3 mm gage length strain gages.

As previously mentioned, the determination of K_T should be

GAGES #1-12

GAGES #13-21

FIGURE 5-1 PHOTOGRAPHS SHOWING STRAIN GAGES ON DEFORMED BAR
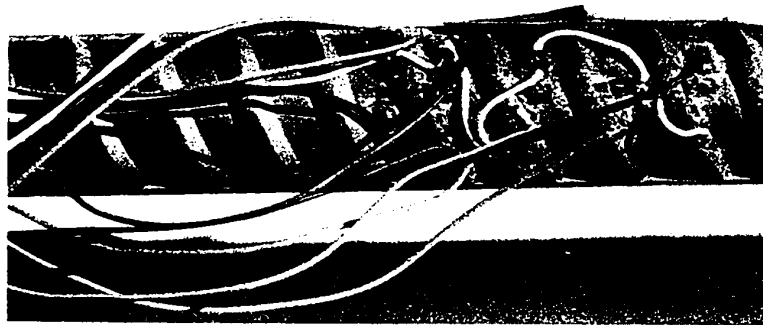
GAGES #1 - 12

GAGES #13 - 21

FIGURE 5-1   PHOTOGRAPHS SHOWING STRAIN GAGES
ON DEFORMED BAR
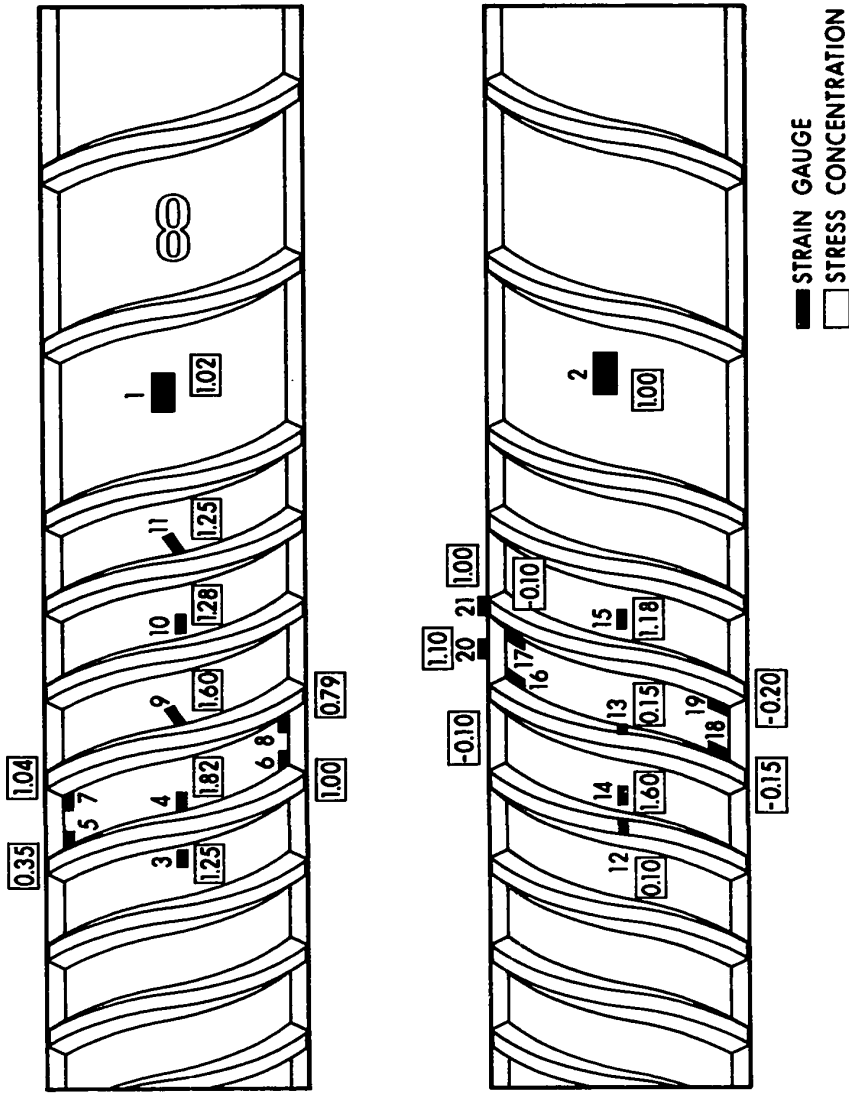
FIGURE 5-2   STRESS CONCENTRATION MEASUREMENTS ON DEFORMED BAR

based on an elastic stress analysis. Therefore, precautions were taken
so that the stress in the bar did not exceed the elastic limit of the
test specimen at any point. This was done by placing an upper limit
on the loads and the measured strains in the tests.

Strains were recorded at load levels of 0, 5, 10, 15 and 20
kips. This operation was repeated three times. In all cases con-
sistent observations were obtained. The average of the three ob-
servations was used for the stress calculations. The modulus of
elasticity of steel was assumed to be 29 x 10^6 psi in these calcula-
tions.

5.2.2 Presentation and Discussion of Test Results

The ratio of measured stress to the nominal stress corres-
ponding to each strain gage is shown in FIGURE 5.2. Referring to
this figure, the stress concentration at each gage location will be
discussed in the following paragraphs.

Gages 1 and 2, due to their location and longer gage lengths
than the rest of the gages, were intended to show the nominal stress in
the bar. The measured stresses in these two gages were within 2 per-
cent of the nominal stress. The center of these gages was 10 mm from
the nearest lug.

Gages 4 and 9 were mounted parallel to the bar axis and
perpendicular to the transverse lug, respectively. The centerline of
these gages was located at 0.15 mm from the transverse lug. Gage 4
always showed 14% higher stresses than gage 9. Gages 10 and 11 were

mounted in an identical fashion to gages 4 and 9, except that gages 10 and 11 were 0.7 mm away from the lug base. Gage 10 measured 5% higher stresses than gage 11. From these observations, it may be noted that though the radius at the base of the rib is smaller in the plane perpendicular to the transverse rib than in the plane of the bar axis, lower stresses were observed in the former case. Higher stresses were obtained for gages parallel to the bar axis because the plane of load application and that of stress measurement was the same.

In order to find whether the stresses were higher on the steeper side of the transverse lug than on the other side, gages 10 and 3 were located 0.7 mm away from a lug base on the steeper and the other sides respectively. The stresses in the steeper side of the lug were found 5% higher than the other side.

To determine stresses at the intersection of the transverse lugs and longitudinal ribs gages 5, 6, 7, 8, 16, 17, 18 and 19 were located in these regions. Gages 5, 6, 7 and 8 were located parallel to the bar axis, whereas gages 16, 17, 18 and 19 were located parallel to transverse lugs as shown in FIGURE 5.2. All these gages except 6 and 7 showed stresses less than the nominal stress. Gages 6 and 7 measured stresses equal to the nominal stress and 4 percent higher than the nominal stress, respectively.

Gages 20 and 21 were mounted on the longitudinal rib to measure stress along the bar axis. As shown in FIGURE 5.2, Gage 20, located midway between intersecting transverse lugs showed 10 percent higher stresses than the gage 21, located at the intersection.

The stress concentration measurements at gages 12, 13, 4, 14, 10 and 1 are plotted in FIGURE 5.3. These gages were located at 2.5, 1, 0.15, 0.3, 0.7 and 10 mm respectively, from the base of a transverse lug in the direction parallel to the bar axis. In FIGURE 5.3, the theoretical results obtained from the analysis of an axisymmetrical projecting lug having identical dimensions to the deformation lugs of the bar specimen used for stress concentration measurements are also plotted for comparison. The horizontal scale has been non-dimensionalized. (The theoretical analysis will be described in section 5.3.3). It may be seen in this figure that the experimental results lie very close to the theoretical curve, however, the maximum stress concentration factor 1.82 obtained by experiments is lower than the value 2.16 obtained from theoretical analysis. It was not possible to place a gage at the point of maximum stress concentration, however.

From the experimental investigation of stress concentrations in this deformed bar, three main conclusions may be derived:

(1) The stresses at the base of the lugs were 14% higher in the direction of the bar than at the same location but perpendicular to the transverse lug.

(2) Stresses at the intersection of the longitudinal and transverse ribs were not as critical as those at the bases of transverse lugs.

(3) The stresses were observed to be 5% higher on the steeper side of the transverse lug than on the other side.
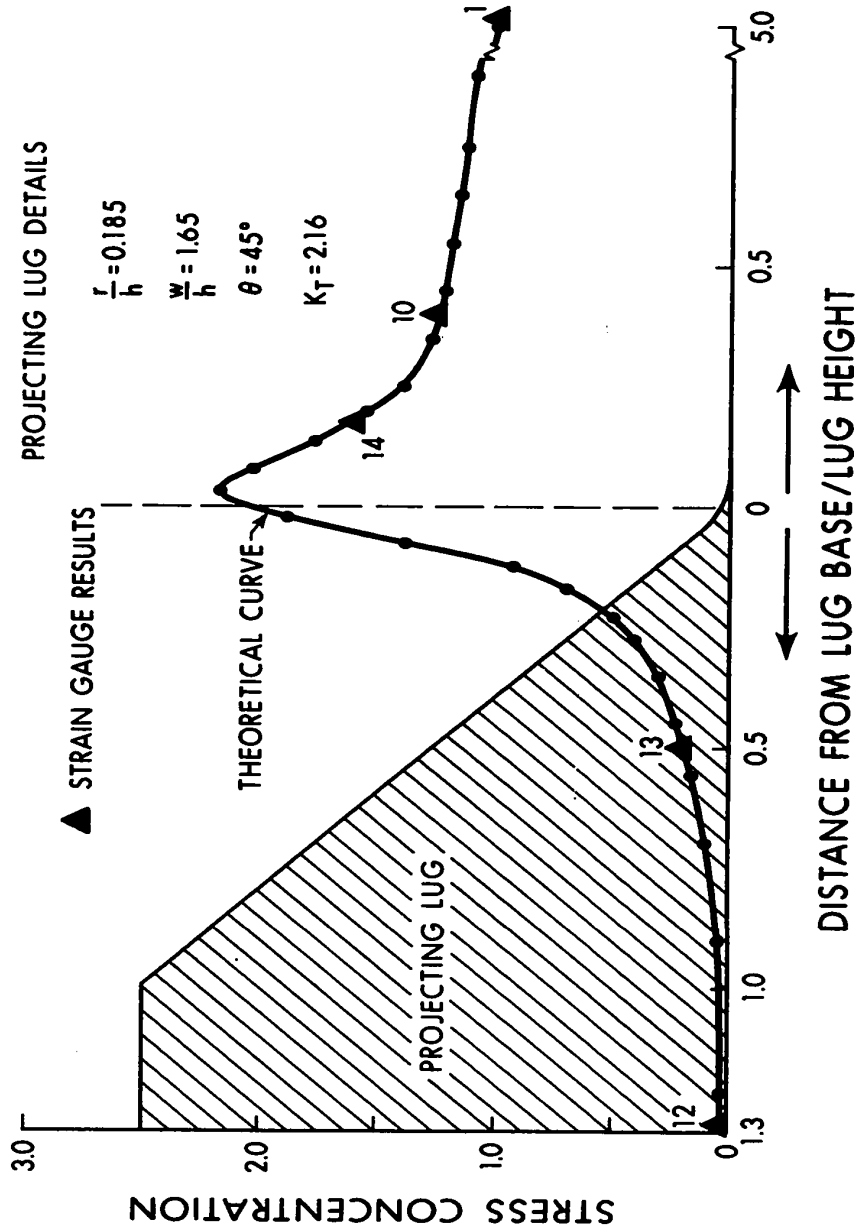
FIGURE 5-3   STRESS GRADIENT AT BASE OF PROJECTING LUG

68

5.3 Determination of K_T using Finite Element Stress Analysis

Although there is extensive data in the literature covering the stress concentrations for notches in flat plates, etc. no systematic study exists for the case of circular bars with protruding notches resembling reinforcing bar deformations. A series of finite element Analyses were used to study this problem. Since the computer program used was restricted to axisymmetric solids, the results are strictly applicable only to the "bamboo pattern" of reinforcement deformations. However, the strain measurement in section 5.2 showed that the 75° lugs could be represented by axi-symmetrical lugs having the same lug base radius in the plane of the bar axis.

5.3.1 Finite Element Computer Program

A finite element computer program entitled "Finite Element Analysis of Solids with Non-linear Material Properties" (43) was used in this investigation. The finite element method of stress analysis is based on the approximation that a continuous structure can be replaced by a system of elements which are inter-connected at the joints or nodal points. The equilibrium equations are developed at each nodal point in terms of unknown nodal point displacements. A solution of this set of equations constitutes a solution to the system.

The computer program used considers triangular and quadrilateral elements. With the use of these elements, it is possible to create practically any desired geometry. The program is quite general with respect to loading and boundary conditions. However, the applica-

tion of this program is limited to plane structures or axi-symmetrical structures.

To facilitate the checking of the input mesh a program was written to plot the finite element mesh on the Calcomp Plotter. Adjustments were made in the finite-element program for the use of files and input/output format statements compatible with the IBM OS system. The program was run on the IBM/360 computer at the University of Alberta Computing Centre.

5.3.2 Check for Accuracy of Results

The accuracy of the finite element computer program results was checked in the following three stages:

    (1) Check on the computer input-data.

    (2) Convergence of results.

    (3) Comparison with Previous Analyses .

1. Check on the Computer input-data

The input-data for any finite element program consists of data cards describing material properties, "node cards" describing the coordinates and boundary conditions at each node, and "element cards" describing the location of each element in the structure. Due to the large number of data cards, there is a high probability of error in the input data cards. Some errors are detected by the self diagnosis error messages in the program, however, errors in nodal point coordinates as well as in the location of elements in the structure could only be found using the element plotter program described in section

5.3.1. The plotter program made use of several built-in plotter sub-routines in the University of Alberta Calcomp Library. A typical plot of a finite element mesh plotted in this way is shown in FIGURE 5.4.

2. Convergence of the Results

In finite element analysis, the selection of the number of mesh elements to approximate a structure is governed by two factors: first, the geometry of the structure and second, the desired accuracy of the results. Structures with notches require a larger number of elements to describe their complex geometry than do structures with plain configurations. In addition, the local peak stresses near the notch are of more significance than the nominal stress. In order to determine these peak stresses these zones have to be defined by a finer mesh than the rest of structure. The computer program computes the average stress in each element. If a significant stress gradient exists across an element, it is not revealed. If this element with high stress gradient is further divided into two or more elements, a more accurate estimate of the peak stress can be obtained.

On the other hand, repeated sub division of elements will not always lead to more accurate results. After reaching a certain number of elements in a region, a further sub-division in the elements may not appreciably change the stress results. This will be true if strong convergence exists in the computer solution. Thus in order to minimize the data preparation and computation time, a proper selection of the element mesh is very important.

Convergence of the test results in the analysis of axi-

$\theta = 60°$

$w = 50$ $D = 500$

$h = 50$ $r = 12.5$
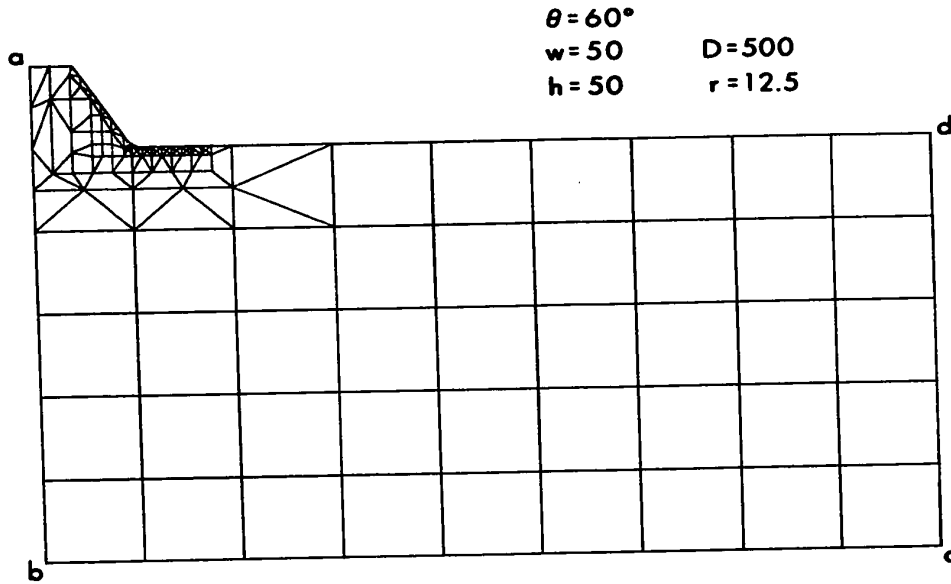
FIGURE 5-4   TYPICAL FINITE – ELEMENT MESH
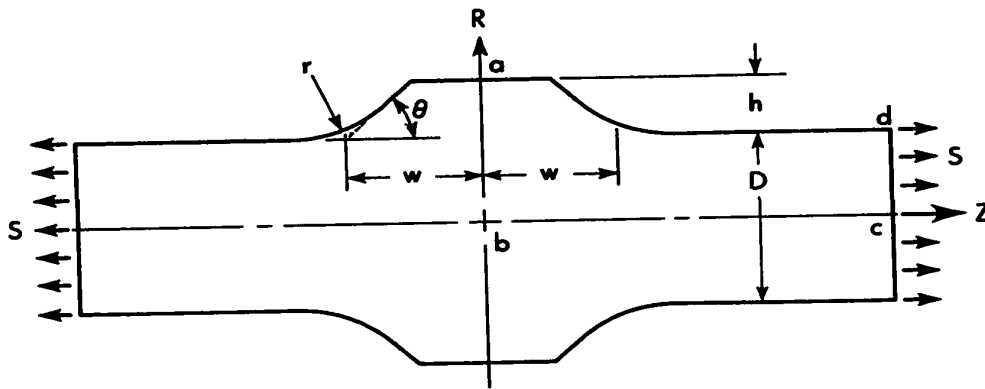
FIGURE 5-5   AXI – SYMMETRICAL PROJECTING LUG MODEL

symmetrical notches was tested by varying the number of elements at the base of the projecting lug. The details of the structure analysed and the results obtained are given in Table 5.1.

TABLE 5.1

EFFECT OF NUMBER OF ELEMENTS ON CONVERGENCE OF RESULTS

Dimension of Structure: r/h = 0.1, h/D = 0.1,

w/h = 2, θ = 45°

(Symbol definition see section 5.3.3.2)

No. of Elements	K_T
100	2.232
150	2.523
200	2.547

From the results in Table 5.1, it may be seen that the value of K_T increased from 2.232 to 2.523, with an increase in the number of elements from 100 to 150, but that no appreciable difference was found between 150 to 200 elements. Hence a structural model with 150 elements was used for the investigation reported in section 5.3.3. In examining these results, it should be noted that the number of elements was increased in the critical region only.

3. Comparison with Previous Analyses

As an additional check, the results obtained from the use of the finite element computer program were compared to published results. For this purpose, two previously analysed notches (41,42) were analysed under axial tension using the computer program. The data pertaining to these investigations are as follows:

Notch #1 - Fillet

Ratio fillet radius over smaller dia = 0.4

Ratio bigger dia over smaller dia = 2.0

Type of Structure	K_T	
	Obtained	Literature(41)
Plane Structure	3.10	3.12
Axi-symmetric	2.75	2.75

Notch #2 - Projecting Lug

Ratio lug radius over lug height = 0.25

Ratio lug width over lug height = 1

Lug face angle = 60°

Type of Structure	K_T	
	Obtained	Literature(42)
Plane Structure	1.809	1.80
Axi-symmetric	1.904	--

5.3.3 Determination of K_T for Projecting Lugs

5.3.3.1 Assumptions in the Analysis

Because the finite element computer program was limited to axi-symmetric solids or planar structures, it was not possible to include the longitudinal deformations or to consider a lug inclination other than perpendicular to the bar axis. A section through a diameter of the simplified model used to compute K_T for the bar deformations is shown in FIGURE 5.5.

In the analysis of projecting lugs the material was assumed to be elastic, homogeneous and isotropic. A uniform axi-symmetrical tensile loading was applied on the face c-d of the idealised model shown in FIGURE 5.5. The boundary conditions on the face a-b were assumed symmetrical. Radial deformations were not permitted along the center line c-b.

To determine whether the K_T value obtained for a single lug would be applicable to a deformed bar, consisting of many equally spaced lugs, single and multiple notch finite element models were analysed. Element meshes for a single lug and a multiple lugs model containing three lugs are shown in FIGURE 5.6. In both cases the geometrical parameters of the lugs were identical. The spacing between the adjoining lugs was kept comparable to that in deformed bars. The K_T values obtained in these two analyses are also given in FIGURE 5.6. It may be noted that the K_T value obtained for middle lug was about 2 percent less than that obtained for a single lug. This reduction

$K_T=1.913$

(a) STANDARD MODEL

$K_T=1.917$
1.918
1.907

(b) MULTIPLE NOTCH MODEL
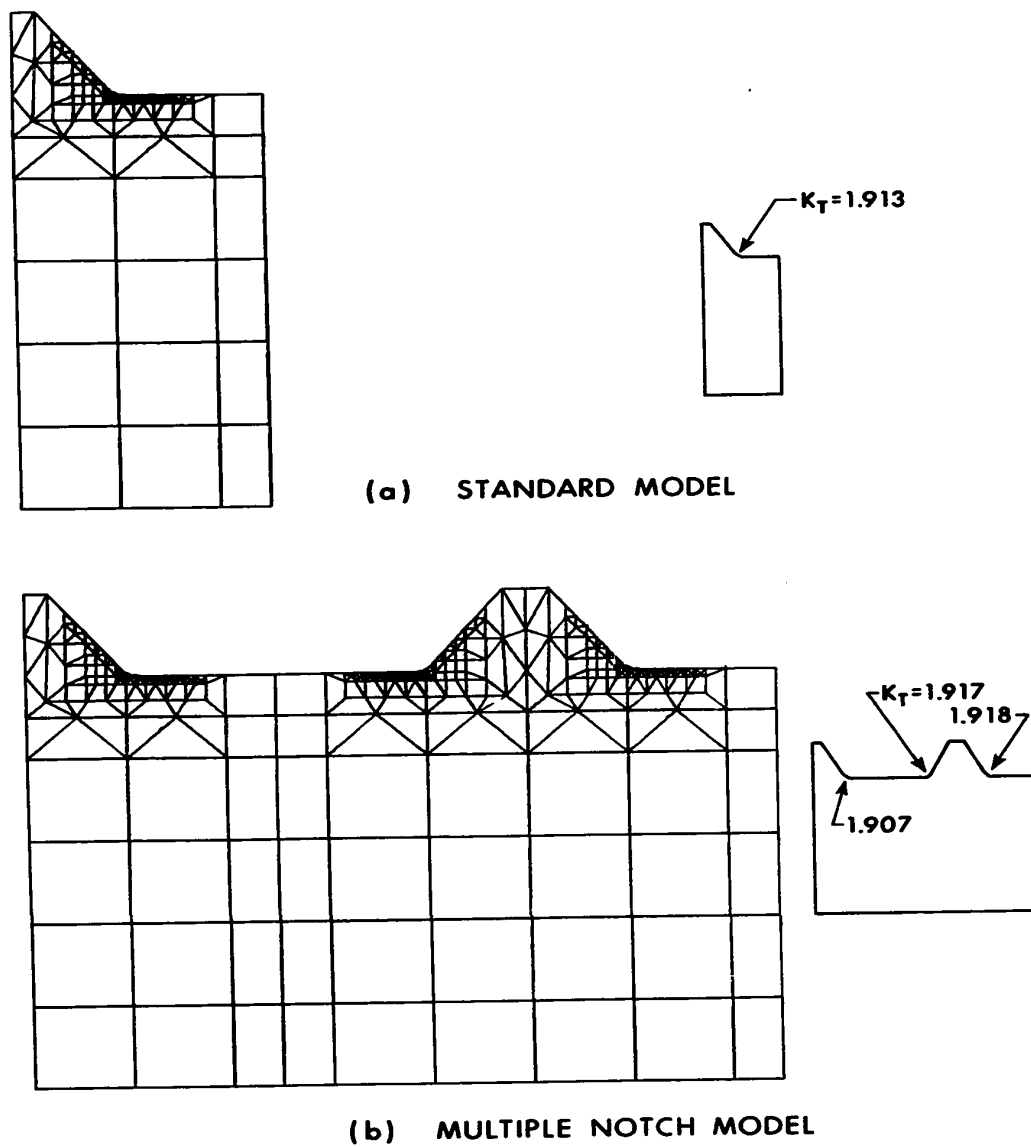
FIGURE 5-6 FINITE ELEMENT MODELS FOR SINGLE
AND MULTIPLE LUGS

in K_T due to multiple lugs was considered insignificant and a standard single lug model was used for the analysis of cases reported in section 5.3.3.2.

5.3.3.2 Presentation of Results of Analyses

Referring to FIGURE 5.5, it may be seen that the following parameters of projecting lugs geometry, adequately define the discontinuity:

r   = lug base radius (radius of the circular transition curve)

h   = height of lug, measured from the base of lug away from transition curve

w   = one-half width of the lug, measured from centerline of lug to the intersection of the transition curve tangents

θ   = lug face angle

D   = bar diameter

The selection of the ranges for the above parameters for the analyses reported herein, were based primarily on the comparable ranges of these parameters specified in ASTM A615-68 except that a wider range of radii at the base of lugs was analysed than expected in North American reinforcing bars.

For each set of these five parameters defining a lug it was possible to develop a finite element model. In this model attention was paid to accurately simulating the geometry close to the lug base. Since the smooth circular transition curve at the lug base was simu-

lated with straight lines, these straight lines were kept very small. On the average the triangles close to the surface defining the lug were .004 times the diameter of the bar. The stresses in these triangular elements were calculated at a distance equal to .0013 times the diameter below the surface.

From computer output of each finite element model analysed the stress state in each element was available. FIGURE 5.7 presents this data in the form of contours of equal ratio of calculated stress to nominal stress. In this figure it may be seen that the contours of high value are concentrated very close to the base of the lug. The type of stress state shown in FIGURE 5.7 is similar to that observed in photo-elastic notched models. The maximum value of this ratio is the stress concentration factor (K_T) for the notch.

Finite element models were analysed to study the variation in K_T for various combinations of the variables. Initially, the effects of two variables, radius at the lug base (r) and bar diameter (D) on K_T were investigated, for constant values of lug height (h), lug width (2w) and lug face angle (θ). A total of ten finite element models were analysed for this purpose. The value of K_T obtained in each case is reported in Table 5.2. It may be noted that the values of K_T are almost the same for the two bar diameters. From these results it was concluded that for practical ranges of the diameter and lug parameters, the K_T of the lug is independent of bar diameter. Although this conclusion may not hold for cases outside the ranges considered, such cases would be beyond the current ASTM Standard (A615-68)

PLANE STRESS STRUCTURE
PROJECTING LUG DETAILS

o POINTS WHERE
  STRESSES COMPUTED

$\frac{r}{h} = 0.25$

$\frac{w}{h} = 1.0$

$\theta = 60°$

$K_T = 1.83$
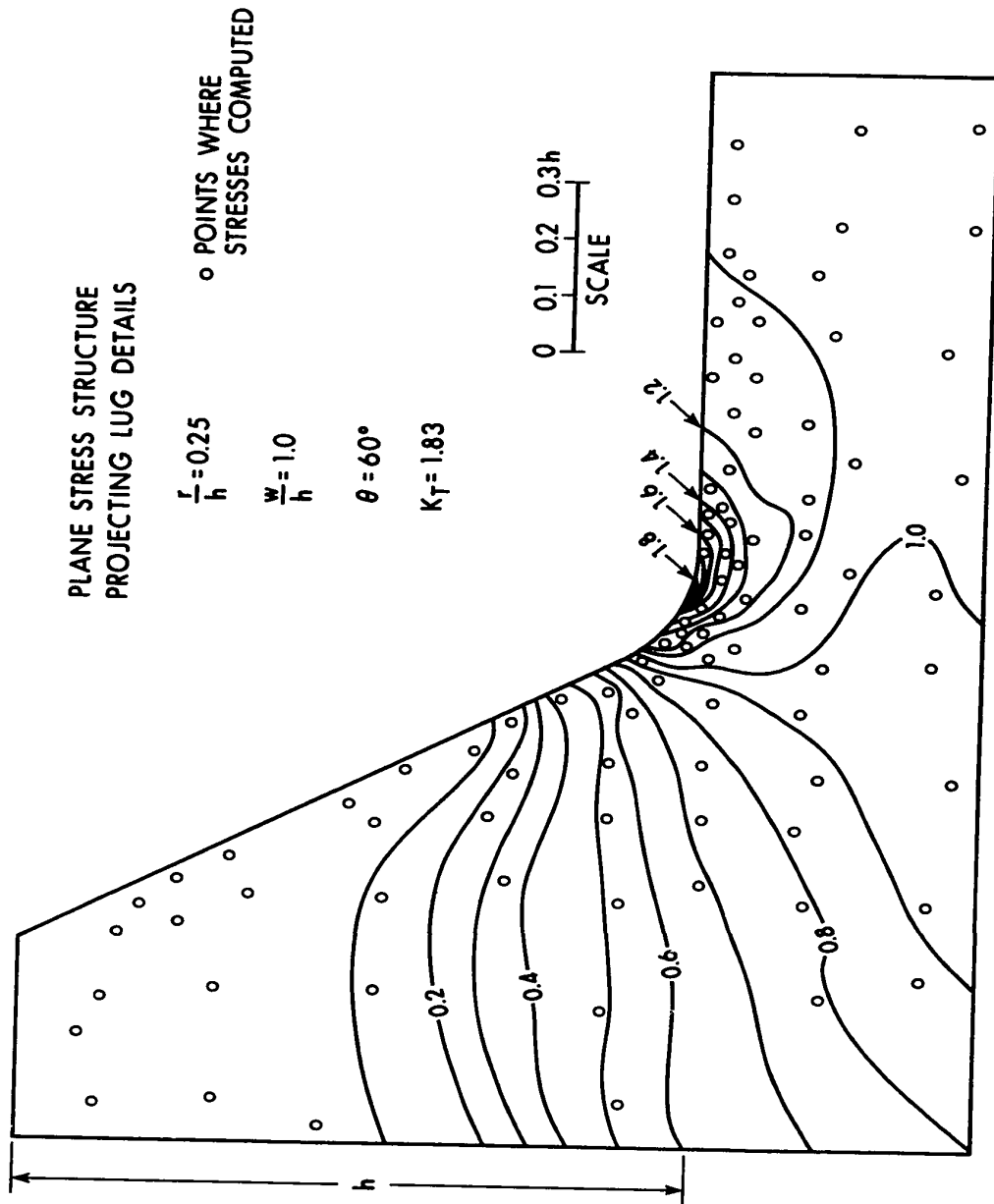
FIGURE 5-7   CONTOUR MAP OF STRESS CONCENTRATIONS AT THE BASE OF PROJECTING LUG

TABLE 5.2

K_T FOR PROJECTING LUGS

r/h	h/D = 0.05						h/D = 0.1
	w/h = 1			w/h = 2			w/h = 2
	θ=45	θ=52.5	θ=60	θ=45	θ=52.5	θ=60	θ=45
0.1	2.084	2.095	2.141	2.527	2.568	2.664	2.523
0.2	1.850	1.861	1.904	2.225	2.284	2.303	2.222
0.3	1.656	1.680	1.714	1.934	1.971	2.020	1.933
0.4	1.446	1.491	1.533	1.638	1.688	1.716	1.634
0.5	1.440	1.442	1.453	1.532	1.595	1.623	1.527

for deformations. In the subsequent analysis, all combinations of h/D equal to 0.1 with other lug parameters shown in FIGURE 5.5 were dropped on the assumption that the results of h/D equal to 0.05 would be applicable to all practical h/D ratios. Table 5.2 summarises the stress concentration factors for all the cases studied.

5.4 Effect of the Geometrical Parameters of Projecting Lugs on K_T

The stress concentration factors (K_T) for projecting lugs previously reported in Table 5.2 are shown in FIGURE 5.8. In this figure, four geometrical parameters: radius at lug base (r), one-half width of lug (w), lug height (h), and the bar diameter (D) are grouped into three non-dimensional variables. The stress concentration factors are plotted on a linear ordinate scale and the r/h ratios are plotted on a logarithmic abscissa. The plots of K_T versus r/h are shown for two values of w/h and three values of lug face angle (θ) in FIGURE 5.8. Since it was concluded in section 5.3.3.3 that the stress concentration factor (K_T) was independent of the h/D ratios in the practical region, this ratio has not been considered in FIGURE 5.8.

Referring to sections 5.3.3.1 and 2 and the K_T vs r/h plot in FIGURE 5.8, the following conclusions may be made regarding the effect of projecting lug parameter on stress concentration factors:

(1) The K_T of the projecting lugs increases with a decrease in the lug base radius. This conclusion is in agreement with the theory of notch stresses (41,42) and has been suggested in other studies of reinforcing bars (15,17).
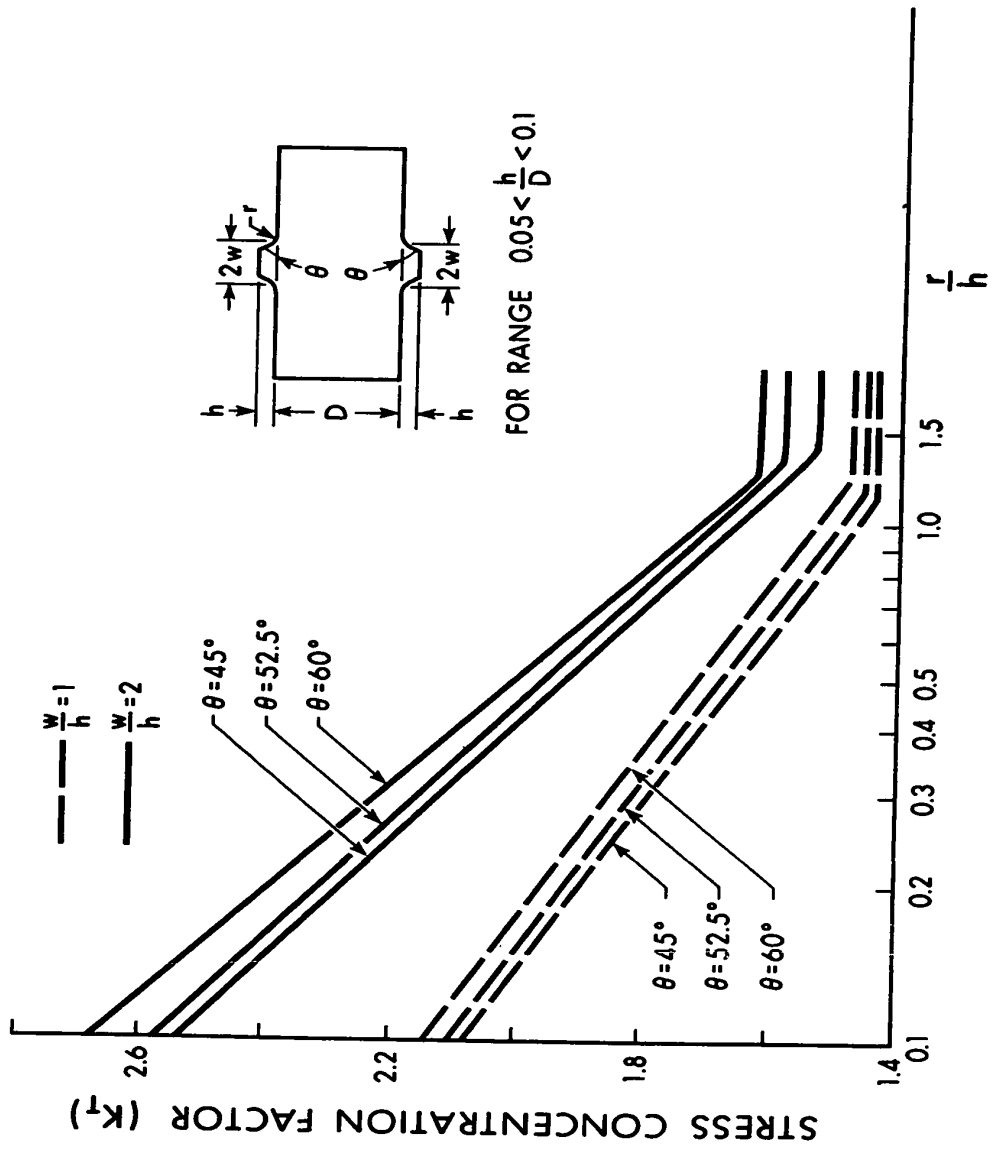
FIGURE 5-8   EFFECT OF PROJECTING LUG PARAMETERS ON K_T

(2) For all the cases of projecting lugs investigated, the K_T vs r/h plot may be approximated by straight lines on a semi-logarithmatic plot. The higher the r/h ratio, the lower the stress concentration factor. For r/h ratios greater than 1.25, there seems to be no appreciable further reduction in the stress concentration factors.

(3) The stress concentration factor increased with an increase in the w/h ratio. As shown in FIGURE 5.8, there are two distinct families of curves for w/h = 1 and w/h = 2, the latter being much above the former.

(4) The stress concentration factor increased with an increase in the lug face angle (θ). This increase in K_T is not as significant as those reported in items 2 and 3.

(5) The stress concentration factor was independent of the h/D ratio in the range studied.

(6) The reduction in the stress concentration factors due to multiple lugs was insignificant in the cases studied and could be ignored.

These six conclusions on stress concentration factors for projecting lugs can be used as a guideline for designing the deformations on reinforcing bars. The first major attempt in proportioning the deformation pattern parameters should be to keep the r/h ratio equal to or greater than 1.25. Second, it would be desirable to keep w/h closer to 1 than 2. The lug face inclination will not have much

significance if r/h and w/h are kept to the desired ratios. However, lug face angles (θ) less than 45° are not desirable from standpoint of bond.

CHAPTER VI

FATIGUE TEST RESULTS

6.1 Presentation of Fatigue Data and Description of Failures

6.1.1 Concrete Beams

The essential data from the fatigue tests of the concrete beams are presented in TABLE D-1 in Appendix D. This data consists of computed bar stresses and applied number of cycles for each specimen. The bar stresses were computed using the straight line theory of flexure assuming the modulus of elasticity of concrete given in ACI 318-63 (44) and that of steel as 29,000 ksi. Throughout the calculations, nominal areas of 0.31, 0.79 and 1.27 sq. in. were used for the No. 5, 8 and 10 bars respectively.

In Table D-1, in addition to the twelve series of concrete beams, a thirteenth series of reinforcing bar specimens has been included. The specimens in this series had same reinforcement as that used in Series 1 but were tested in direct tension in air.

In all the reinforced concrete beams that failed, the failures were due to fatigue failure of the tension reinforcement. In general, three major cracks appeared in each beam at the application of minimum load. A central vertical crack started at the crack initiator at midspan and extended approximately as far as the neutral axis cf the beam. The other cracks were shear cracks symmetrically

located on either side of the central crack. Longitudinal cracks were observed on the bottom of the beam below the bar. These cracks extended each way from each of the three flexural cracks about half a crack space in each direction. On removing the bars from the beams the bond between the bar and concrete was found to be excellent in this region, however.

In most cases the fatigue fracture of the reinforcement occurred at or close to the preformed crack at midspan. In four cases out of 72 beams, the reinforcement fractured just over the stirrup nearest to midspan. In these cases there were distinct marks of rubbing between the reinforcing bar and the stirrup. Six beams failed at the first major inclined crack in the shear span at distances ranging from 2 to 9 inches from midspan.

Following the fatigue fracture of a beam specimen, the details of the fracture surface and its location on the bar were recorded. In all cases, the failure surfaces had two or three failure zones, a familiar feature of fatigue failure (45). These zones can be seen in FIGURE 6.1. The zone of crack nucleation was smoother than other two zones, in some cases conchoidal or beach markings were seen in this zone. However, in most cases, it was difficult to distinguish between the zones of crack nucleation and progression. The final fracture zone could be easily recognised by its crystalline appearance. In general, the area of the fracture zone increased with an increase in the grade of steel and/or an increase in the stress range.

In all beams, the fatigue fracture in the reinforcing bars

(a) FRACTURE STARTING AT BOTTOM OF BAR, BEAM 10-G40-4
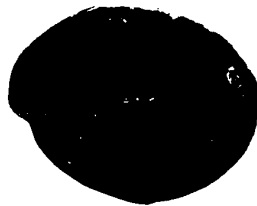
(b) FRACTURE STARTING BETWEEN BOTTOM AND
LONGITUDINAL LUG, BEAM 10-G60-6
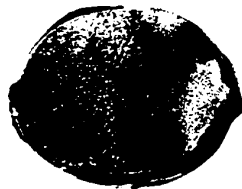
(c) FRACTURE STARTING CLOSE TO LONGITUDINAL LUG,
BEAM 10-G75-5

FIGURE 6-1   TYPICAL FRACTURE SURFACES FROM CONCRETE
BEAM SPECIMENS

(a) FRACTURE STARTING AT BOTTOM OF BAR, BEAM 10-G40-4

(b) FRACTURE STARTING BETWEEN BOTTOM AND
LONGITUDINAL LUG, BEAM 10-G60-6
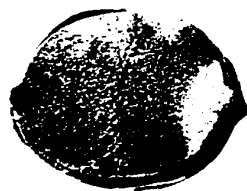
(c) FRACTURE STARTING CLOSE TO LONGITUDINAL LUG,
BEAM 10-G75-5

FIGURE 6-1   TYPICAL FRACTURE SURFACES FROM CONCRETE
BEAM SPECIMENS

started on the bottom side of the bars between the two longitudinal lugs. It should be noted that the longitudinal lugs were in a horizontal plane in all beams. In all but two cases, the fatigue failures originated at the bases of the transverse lugs.

Three typical orientations of the crack initiation zones observed in the beam tests are shown in FIGURE 6.1(a), (b) and (c). Bar failures appear to have started at the bottom in (a), between the bottom and a longitudinal lug in (b) and close to a longitudinal lug in (c). In 86 percent of the beams, the bar fracture originated closer to the bottom of the bar away from the lugs, while in the remaining 14 percent of the beams the fractures originated close to the intersection of the longitudinal and transverse lugs.

6.1.2 Reinforcing Bar Specimens

The fatigue test results on reinforcing bar specimens tested in air are presented in Table D-2 in Appendix D. For each specimen the data consists of an identification mark, test sequence, tensile stress, yield stress, minimum stress, stress range and number of cycles to failure. The test sequence of each group of four specimens was the same as was planned in the experimental design, except for groups No. 18 and 22. These two groups could not be tested as planned due to a delay in getting the chemical compound used for removing rust and mill scale from the plain bars. These two groups were tested at the end of test program.

Deformed bar specimen D-G40-16 was damaged during test because of its improper positioning inside the test assembly. This

specimen failed at 1,423,300 cycles, while its companion specimens of the same group survived 3 million cycles under identical stress conditions. The failed specimen upon examination was found to have evidence of rubbing on the bar surface close to the grip, where it failed. Because of this, the test result was considered unreliable for this specimen and was not included in the statistical analysis of the data.

Plain bar specimens P-G60-16 and P-G60-21 failed partly inside the grips, when tested under a 46 ksi stress range. In these two specimens the failures initiated outside the grips but extended inside the grips up to the knurled portion of bar. The results of these two specimens were treated with suspicion. The observed fatigue lives of these two specimens were higher than the other two specimens of the same group, however.

All the reinforcing bar specimens failed by fatigue failure. The failed specimens and the specimens which survived the 3 million cycles of loading were used for the failure analysis, which will be discussed in section 6.2. However, a general description of the fracture surfaces is presented in the following paragraphs.

In all the deformed bar specimens, the fatigue failure originated at the base of a transverse lug as shown in FIGURE 6.2. In 71 percent of the specimens, the failure started at the steeper side of a lug, in the remaining 29 percent of the specimens the failure originated on the other side of the lugs. No specimen failed at the manufacturer's marks despite the fact that such marks were present on 21 percent of the specimens.

From observations on the failure surfaces similar to those shown in FIGURE 6.2, it appeared that several cracks nucleated close to the bar surface in most bars and that the crack locations varied considerably along the base of transverse lug.

In the plain as-rolled bar specimens and specimens without mill scale or rust, fatigue failure generally started from a surface defect such as a lap, a depression or an inclusion as shown in FIGURE 6.3. In some cases, it was difficult to find the cause of bar failure. Most of the specimens showed some necking close to the fracture plane as shown in the figure. Two types of rupture zones, brittle and ductile, were again observed in the plain bar specimens.

The fracture surfaces of plain bars without rust and mill scale were identical to those of the plain as-rolled bars. In the cleaned bars the surface defects were more distinct than in the as-rolled bars, thus the cause of failure initiation could be identified with ease.

6.1.3 Machined Polished Specimens

Series 7 and 8 given in Table D-2 in Appendix D contain fatigue data for machined, polished specimens. During the testing of specimen M-G40-12 the load in the vibraphore machine dropped due to a misadjustment of the load maintaining knob, this mistake was found after about 2 million cycles of stress application. This mistake was not corrected and the specimen was tested at 51 ksi stress rather than intended at 52 ksi.
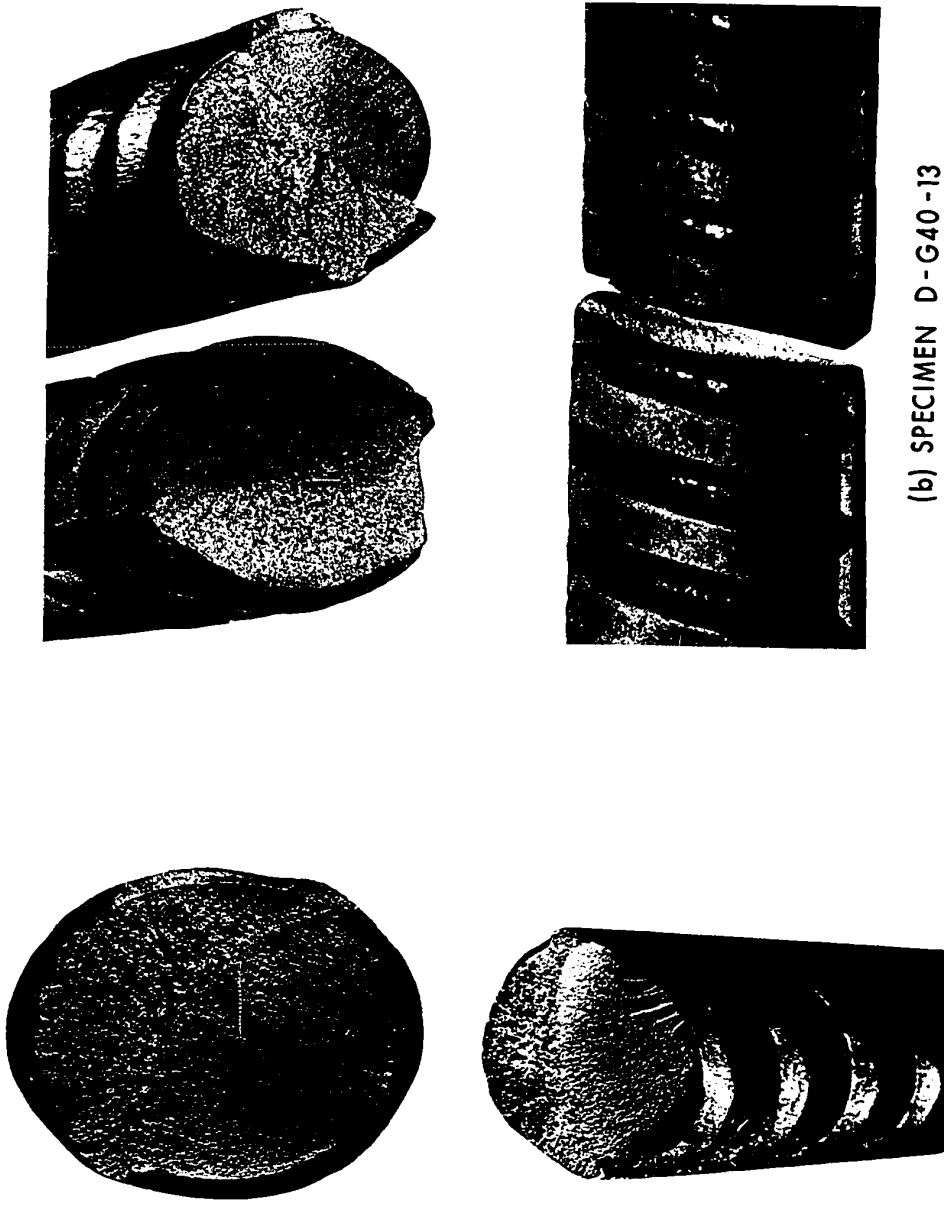
(b) SPECIMEN D-G40-13

(a) SPECIMEN D-G60-9

FIGURE 6.2 FRACTURE SURFACE FROM DEFORMED BAR SPECIMENS
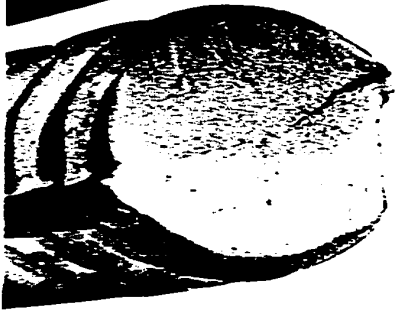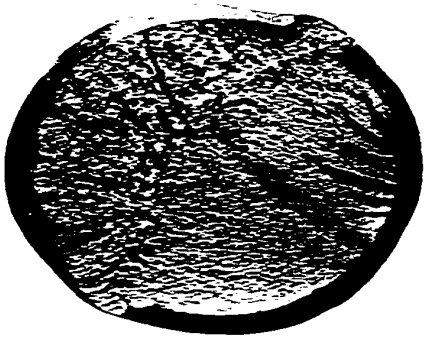
(b) SPECIMEN D - G40 - 13

(a) SPECIMEN D - G 60 - 9

FIGURE 6.2   FRACTURE SURFACE FROM DEFORMED BAR SPECIMENS

(a) SPECIMEN P-G40-4, AS ROLLED

(b) SPECIMEN W-G60-24, WITHOUT RUST AND
MILL SCALE

FIGURE 6.3   FRACTURE SURFACE FROM PLAIN REINFORCING BAR SPECIMENS

92
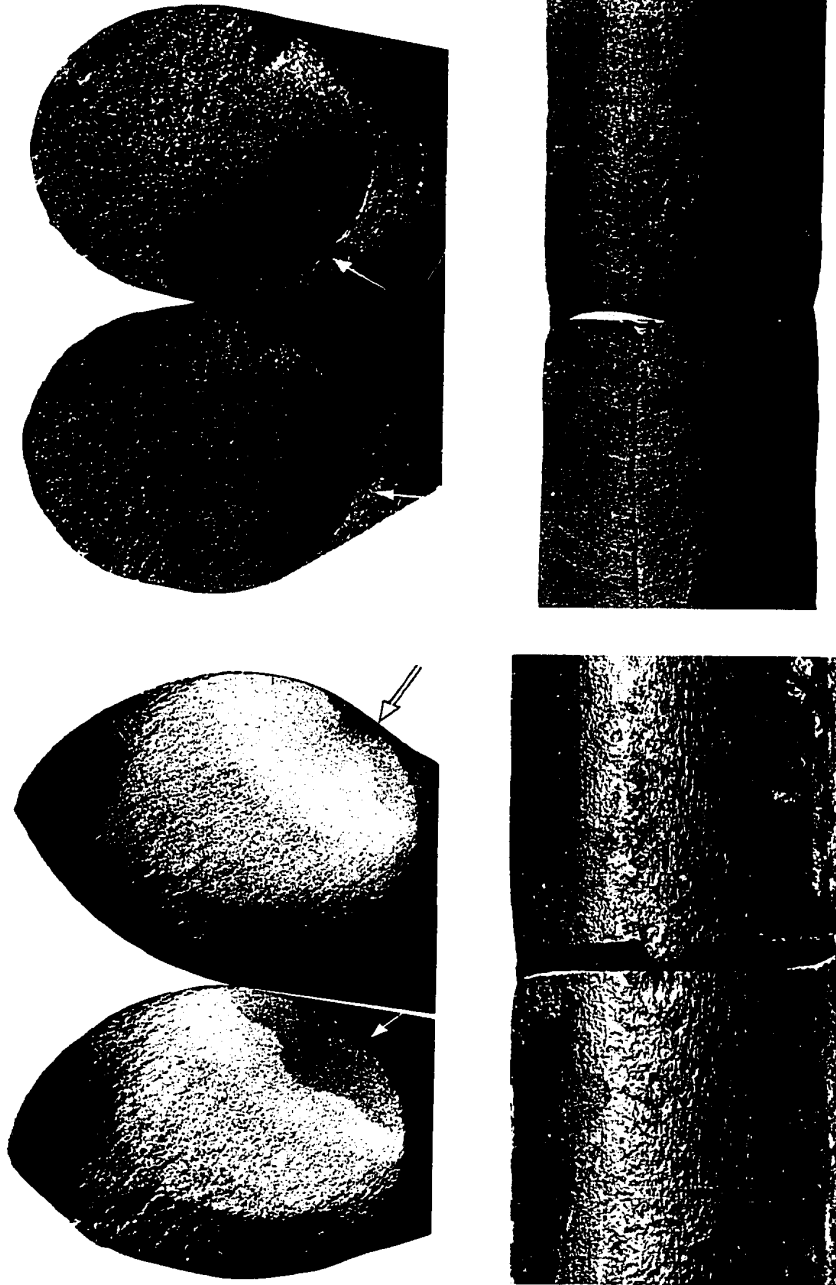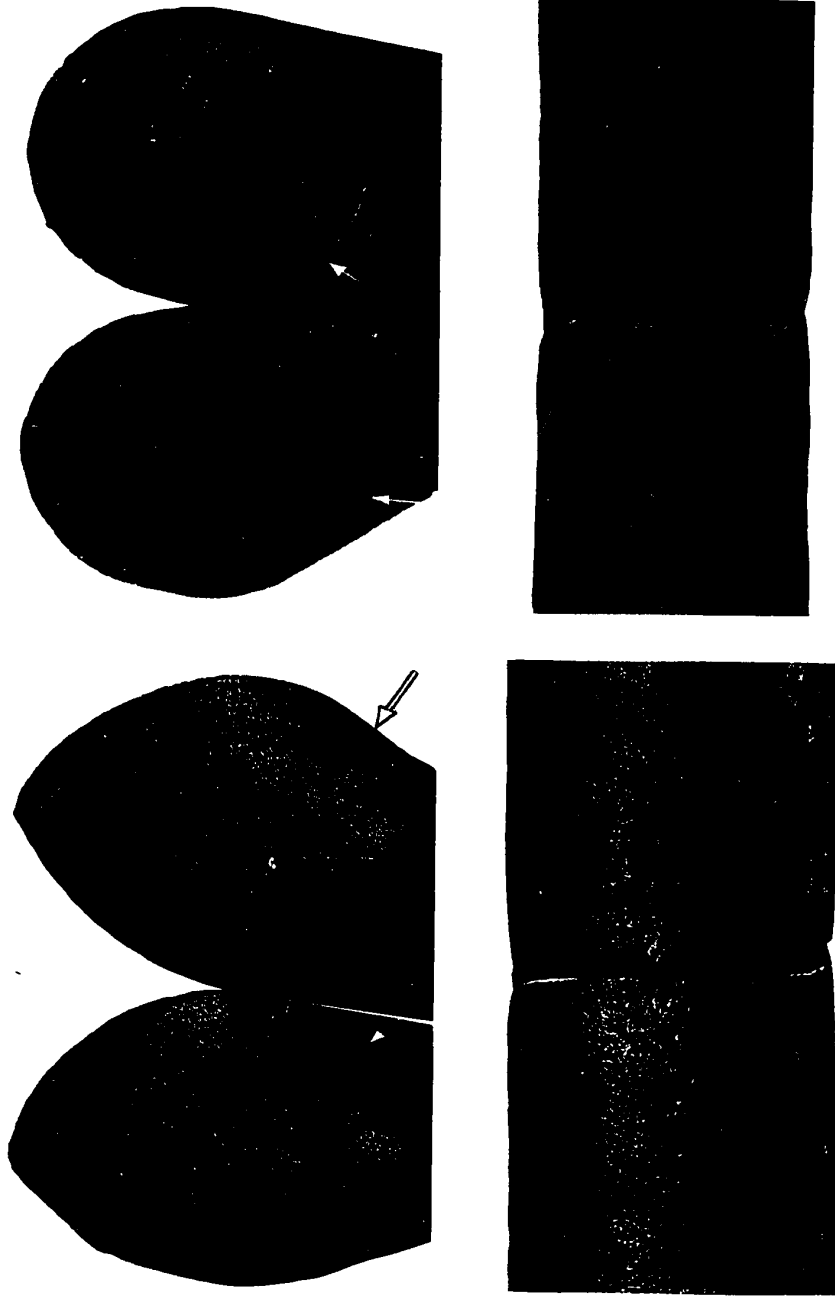
(a) SPECIMEN P-G40-4, AS ROLLED

(b) SPECIMEN W-G60-24, WITHOUT RUST AND
MILL SCALE

FIGURE 6.3   FRACTURE SURFACE FROM PLAIN REINFORCING BAR SPECIMENS

(a) SPECIMEN P-G40-4, AS ROLLED

(b) SPECIMEN W-G60-24, WITHOUT RUST AND MILL SCALE

FIGURE 6.3 FRACTURE SURFACE FROM PLAIN REINFORCING BAR SPECIMENS

92

All the specimens failed due to fatigue failure and again the fracture surfaces had two distinct failure zones; the zone of crack initiation and progression and the final rupture zone. The failure generally started from a minute polishing defect or an inclusion.

6.2 Discussion of Fatigue Failure Phenomenon in Reinforcing Bars

A knowledge of how reinforcing bars fail in fatigue can greatly contribute in the development of reinforcing bars with optimum fatigue strength. In the following paragraphs an attempt will be made to discuss this aspect of the problem within the scope of this project.

The reinforcing bar specimens tested in air were uniformly stressed along the length of the bar under the applied fatigue loading. Thus the probability of failure of the specimen was essentially the same at each deformation along the length of the specimen. Since fatigue failures originated at the bases of the transverse lugs in all deformed bars tested in air, the base of the transverse lugs must be the weakest region in the bar under a cyclic loading. This conclusion is supported by the stress concentration analysis presented in section 5.3.

Though the reinforcing bars embedded in concrete beams were most highly stressed in only a short length adjacent to the center crack, the failure always originated at the base of a transverse lug in a manner similar to the failures of the reinforcing bar specimens. The similar failure origin in the beam and the bar specimens

can be attributed to the close spacing of the deformations which ensured that a deformation occurred within the highly stressed region in a beam test.

From the observations on failure surfaces of the deformed bars, it was suspected that the failure might have been caused due to nucleation of several cracks at the free bar surface at the lug base rather than a single crack as suggested by others (15,16,23). To investigate this possibility the failure surfaces were examined under a Scanning Electron Microscope (SEM) and cracks on the surface of the bar specimens were detected by magnetic and penetrant methods (2).

(a) Observations under Scanning Electron Microscope

Following the fatigue failures of some bar specimens, a test piece 12 mm wide and 3 mm thick was cut from the fracture surface close to the crack origin zone. These test pieces were protected from oxidation and contamination in a container filled with inert gas. Because of its high resolution, a "Stereoscan S4" Scanning Electron Microscope was used to observe the fracture surfaces.

While observing the test specimen through the SEM, the surface was searched for the crack nucleus. Generally, the crack nucleus could be identified by its smooth surface and the beach markings. However, when several crack nuclei are present the beach markings are difficult to identify (45). This was the case in most of the test pieces observed. A typical photograph showing details of crack origin is given in FIGURE 6.4(a), (b) and (c). FIGURE (a) shows the overall view of the failure initiation region. From this photograph it is

(a) GENERAL VIEW OF CRACK INITIATION ZONE IN DEFORMED BAR

(b) DETAIL AT **X**

(c) DETAIL AT **Y**

FIGURE 6.4   DETAILS OF ZONE OF CRACK ORIGIN

95

(a) GENERAL VIEW OF CRACK INITIATION ZONE IN DEFORMED BAR

(b) DETAIL AT X

(c) DETAIL AT Y
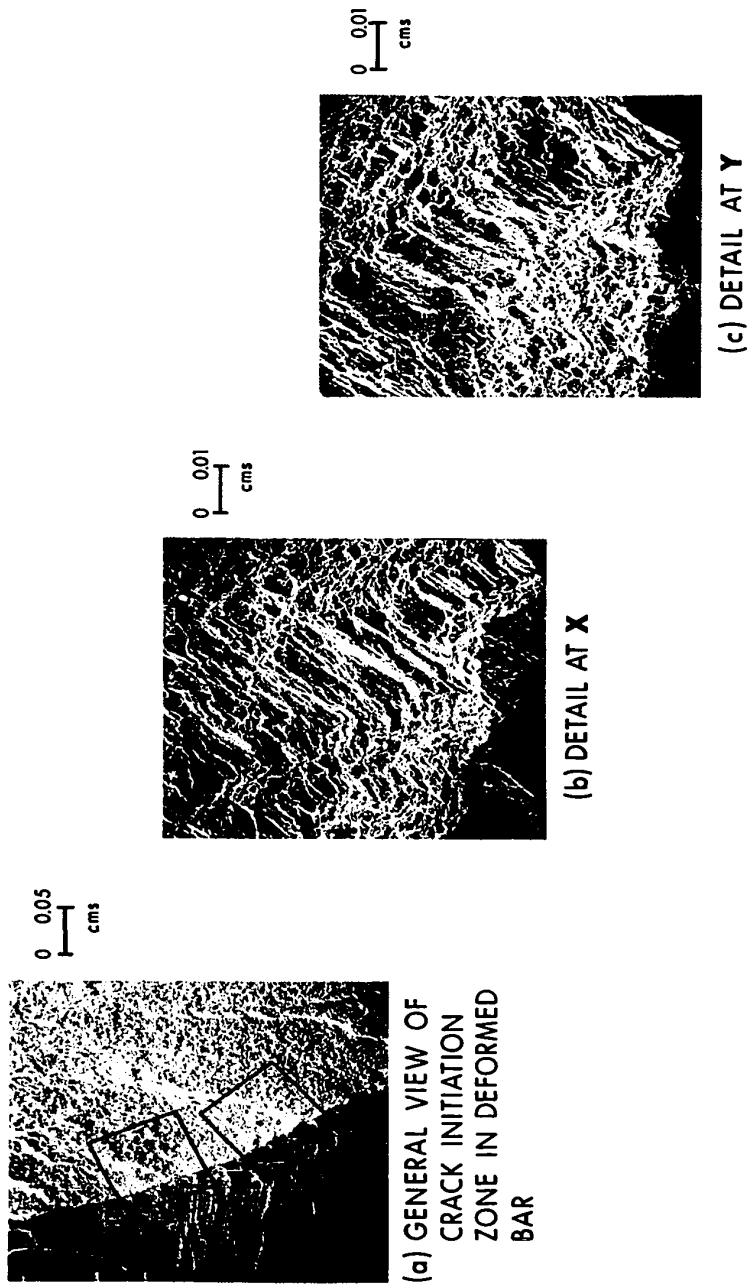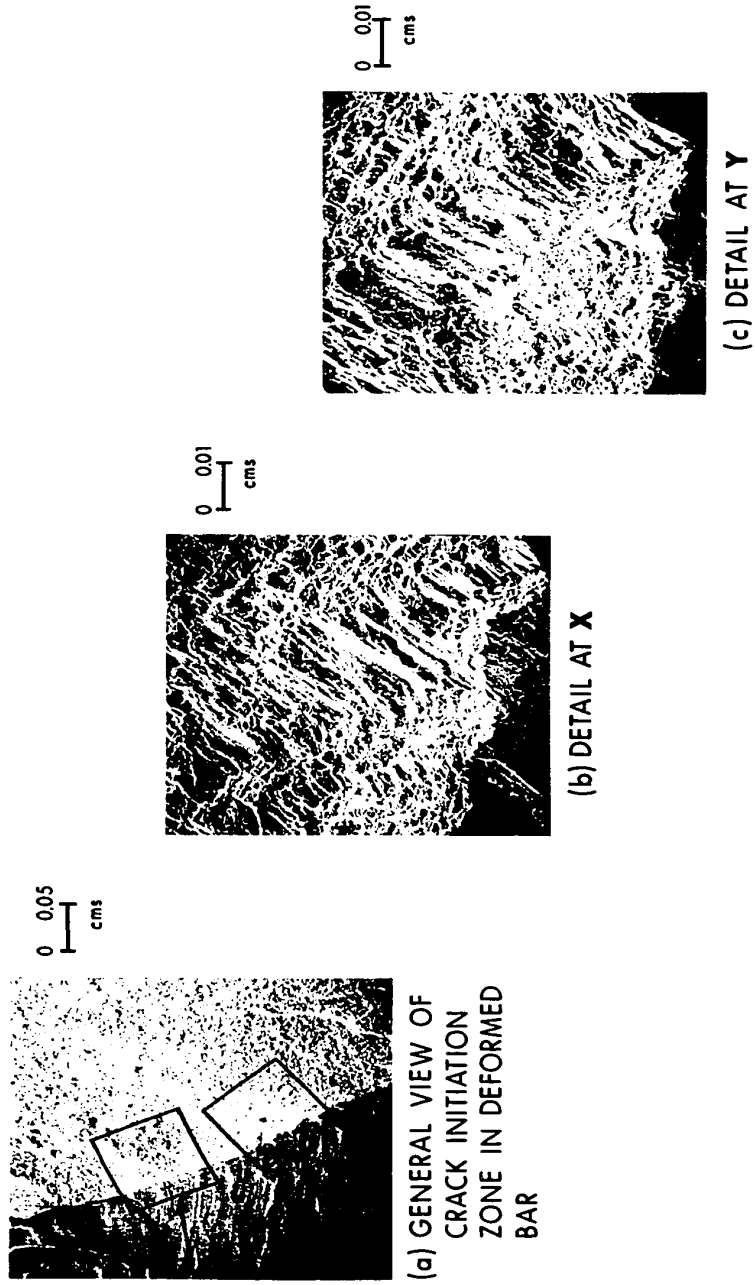
FIGURE 6.4   DETAILS OF ZONE OF CRACK ORIGIN

not apparent that the failure was caused by the origin of single crack.

Magnified views of two locations marked as X and Y in FIGURE 6.4(a) are shown in (b) and (c). It may be seen that the failure structural features and the roughness is almost the same in both the locations. In place of concoidal markings close to the surface, there are almost parallel crack fronts moving towards the interior of the bar. These observations indicate nucleation of several cracks rather than a single crack.

The general observations on the fracture surface suggest that the cracks progressed rapidly and abruptly in the early history of fatigue failure. This was evident from the changes in the surface structure. In the vicinity of a larger crack, several smaller cracks appeared to have joined the larger crack within about 1/30 inch (0.1 cm.) from the surface. Following this region a relatively smaller number of cracks progressed towards the bar interior.

FIGURE 6.5 shows the details of a growing crack. In photograph (a) the bar failure surface is shown to indicate the area of interest shown in (b) at much higher magnification. FIGURE (b) was constructed from several overlapping photographs taken along one crack which progressed into the bar.

Several micro-cracks are seen close to the bottom in FIGURE (b). These cracks are located very close to the fracture face in a region of high stress concentration at the base of a transverse deformation. Such cracks were also observed in several other specimens. Close to the origin of the crack some plastic deformation is evident
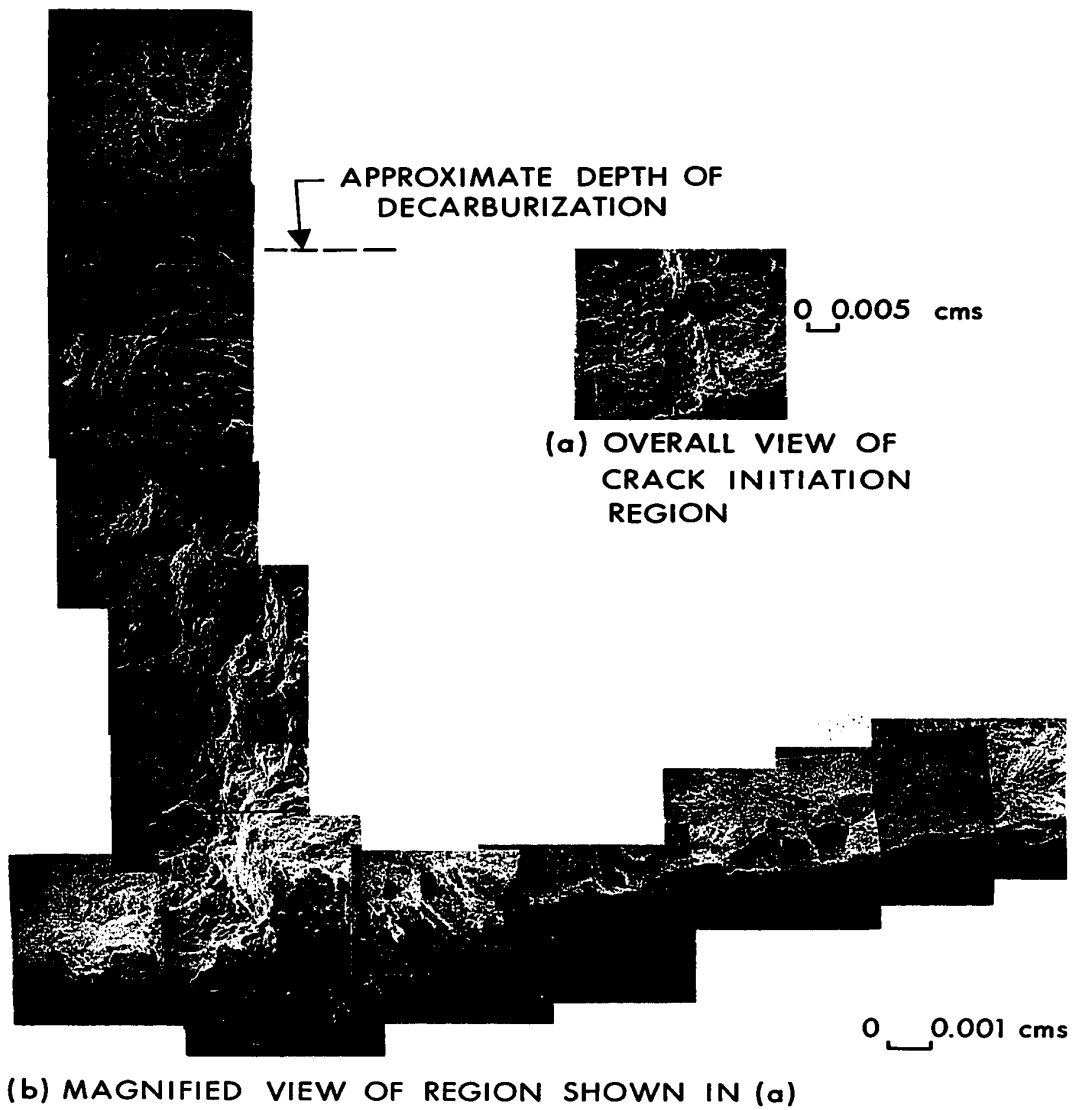
APPROXIMATE DEPTH OF
DECARBURIZATION

0 0.005 cms

(a) OVERALL VIEW OF
CRACK INITIATION
REGION

0 0.001 cms

(b) MAGNIFIED VIEW OF REGION SHOWN IN (a)

FIGURE 6.5 DETAILS OF ZONE OF CRACK NUCLEATION AND GROWTH

APPROXIMATE DEPTH OF
DECARBURIZATION

0 0.005 cms

(a) OVERALL VIEW OF
CRACK INITIATION
REGION

0 0.001 cms

(b) MAGNIFIED VIEW OF REGION SHOWN IN (a)
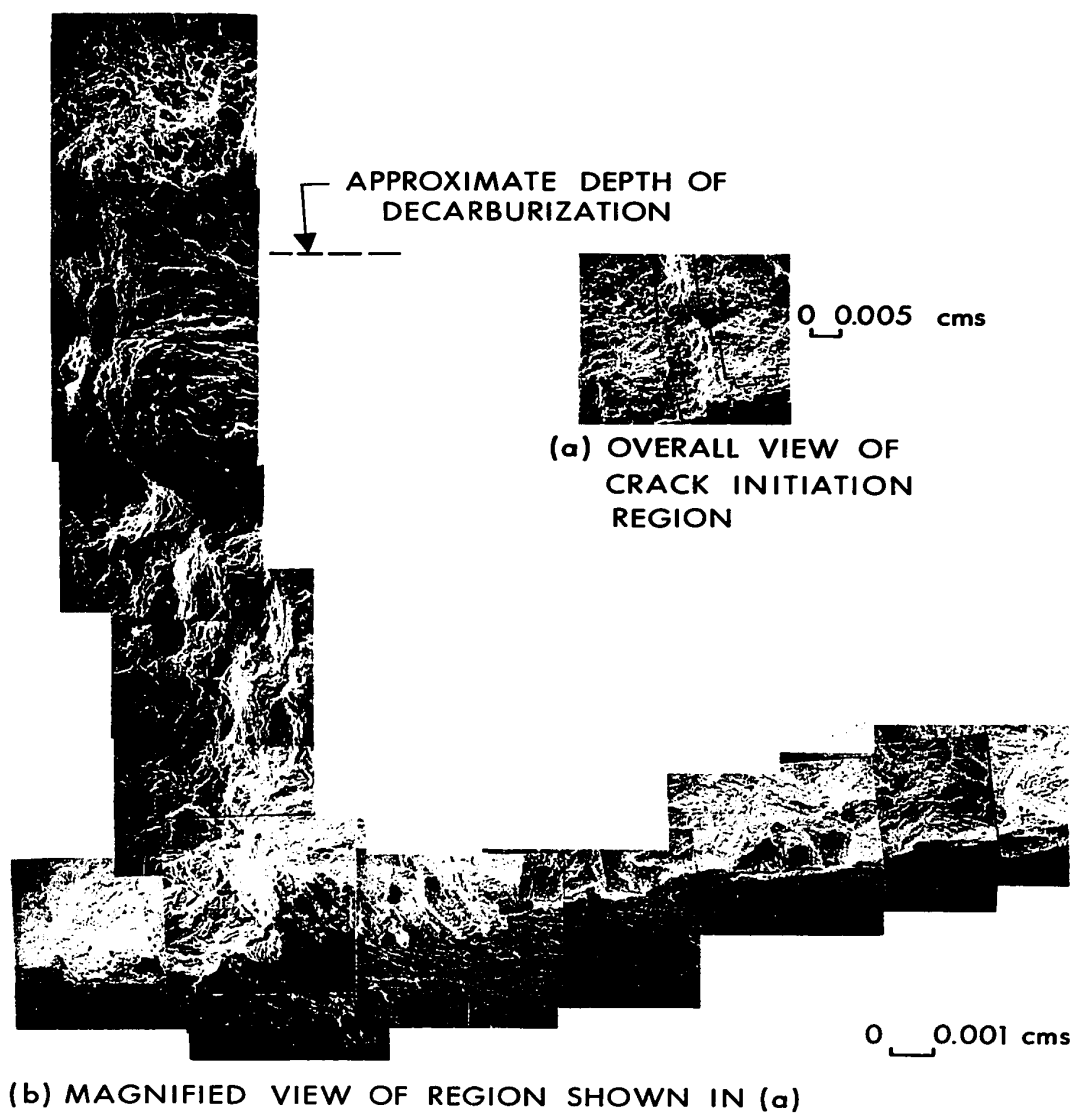
FIGURE 6.5   DETAILS OF ZONE OF CRACK NUCLEATION AND GROWTH

from the surface structure. Due to the absence of beach markings, it is difficult to trace the advancing crack. At the bottom left in FIGURE 6.5(b), however, finite increments of cracking with each cycle are evident on some grains. Several subsidiary cracks are visible in the valley, these generally occur as the crack grows. The direction of the progressing crack was diverted due to the presence of an in-homogeneity which can be identified in the pictures as a hugh block lying on the fracture surface.

(b) Detection of Cracks

Magnetic and penetrant methods were used to detect macro-cracks at, and close to, the bar surface of thirty-five reinforcing bar specimens which had failed in fatigue. In addition, two deformed reinforcing bar specimens of Grade 40 were simultaneously tested at a 28 ksi stress range. When one of the specimens failed at 876,500 cycles, the test was discontinued and the second specimen was examined for macro-cracks.

In most of the deformed bar specimens which had failed in fatigue, cracks were detected at the bases of lugs adjacent to the failure plane. Cracks were also detected in the deformed bar speci-men whose companion specimen failed under identical stress conditions. In the latter case, cracks were located at the bases of six adjacent lugs and two lugs located far away from the group of six. Cracks were not detected in any of the run out specimens.

To confirm the above findings, and to facilitate visual inspection of cracks, mill scale was removed by macro-etching in a

(a)   STAGE I

(b)   STAGE II

(c)   STAGE III

FIGURE 6.6   INITIATION AND GROWTH OF FATIGUE CRACKS

(a) STAGE I

(b) STAGE II

(c) STAGE III
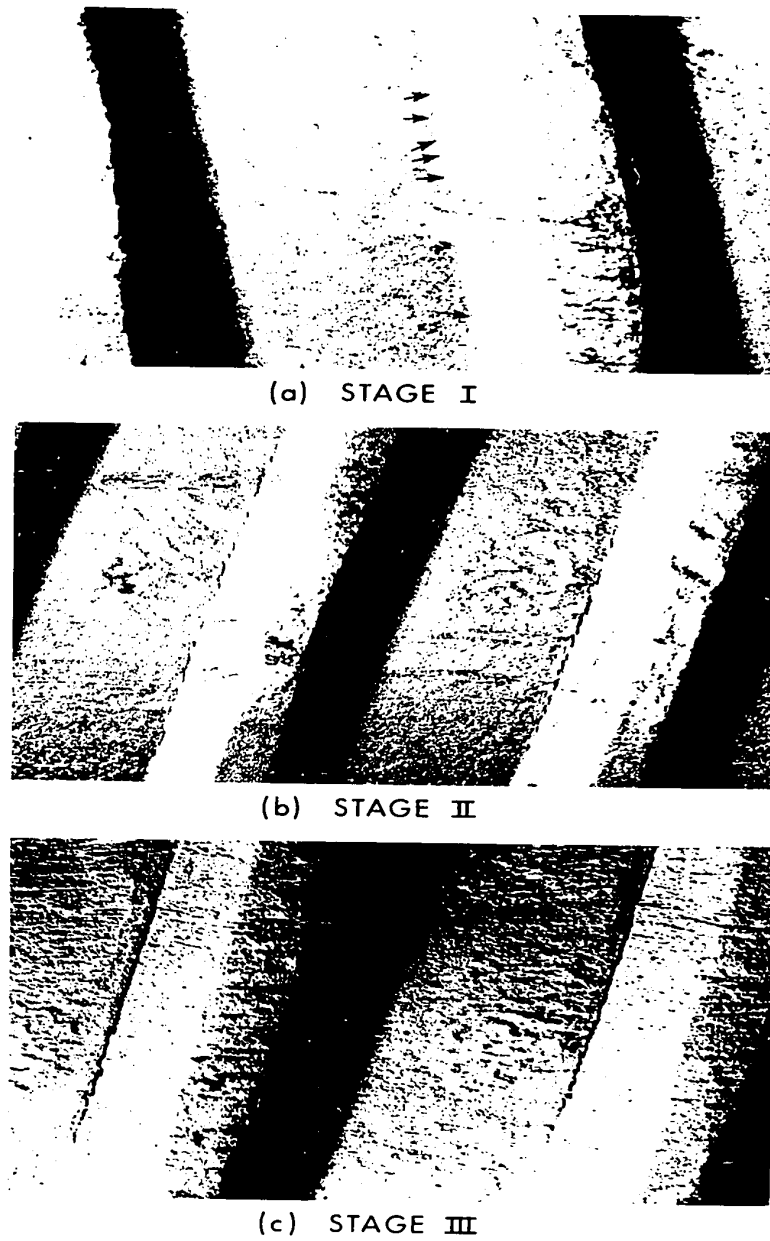
FIGURE 6.6   INITIATION AND GROWTH OF FATIGUE CRACKS

50 percent hydrochloric acid solution for 5 minutes and a penetrant "ZYGLO" produced by Magnaflux Corporation, Chicago was used for crack detection.

The results from the penetrant tests confirmed the findings from the magnetic tests. In these tests, it was also revealed that independent cracks started at several locations along the base of a single lug.

FIGURE 6.6(a) shows a selected lug base of the specimen whose companion specimen failed. A careful examination of the lug base would show several small cracks parallel to lug base. This stage was probably the first stage of crack nucleation. Two other specimens in which these cracks appear to be joining and forming a single crack are shown in FIGURES 6.6(b) and (c). It should be noted that the specimens shown in (b) and (c) were over etched for illustration.

(c) Probable Crack Growth Mechanism

In deformed reinforcing bars, several micro-cracks nucleated at the base of the deformations. The micro-cracks which were located in the region of the highest stress concentrations grew more rapidly than other cracks. These cracks progressed with a considerable plastic deformation. The rate of the advancing cracks was probably higher in the zone of decarburization. In this region the cracks progressed non-uniformly. Eventually several cracks joined to form a crack front which advanced a finite increment with each stress cycle until the re-

maining bar cross-sectional area could not support the load. This was followed by the final rupture.

6.3 Statistical Analysis of Data from Fatigue Tests in Air

The main objectives of the statistical analyses were to determine S-N-P curves for each test series, to find which of the bar surface characteristics had a significant effect on the fatigue strength and to quantify these effects. In the following paragraphs these analyses will be discussed briefly and their results presented. Some of the statistical calculations are discussed and tabulated in Appendix E.

The fatigue test data for the bars tested in air are given in Table D-2 in Appendix D and are plotted in S-N diagrams in FIGURES 6.7 to 6.9. The various lines in these figures will be discussed more fully later in this section.

6.3.1 Check of Uniformity of Loading in Tests

The test set-up used to test bars in air was designed to apply identical loads to the four specimens belonging to a test group. Though the accuracy of the load application was checked by static calibration tests, the possibility of bias in the bar stresses under repeated loads due to small errors in the fabrication of the test assembly could not be rejected. This possibility was examined by analysing the order in which the specimens failed and their corresponding failure location in the test assembly. This data is summarized
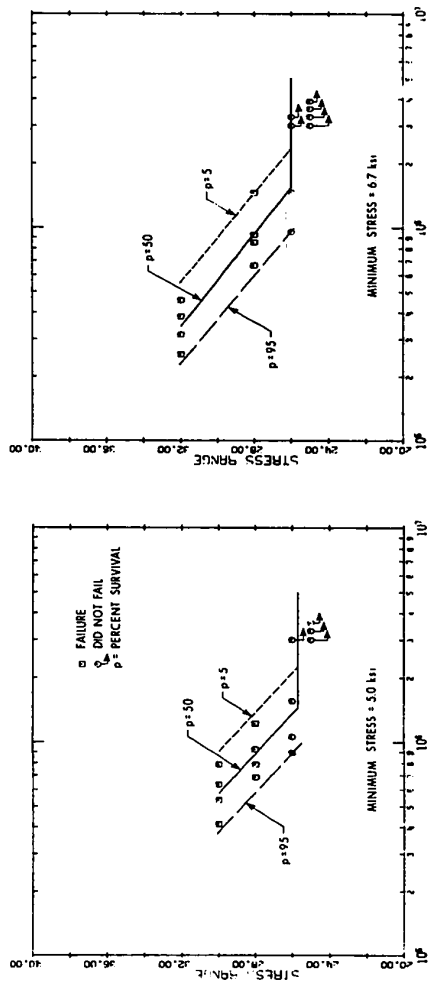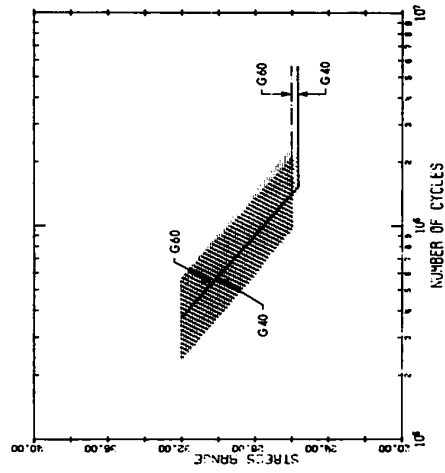
FIGURE 6-7   S-N-P CURVES FOR DEFORMED BAR SPECIMENS TESTED IN AIR, MINIMUM STRESS = 0.1 f_y
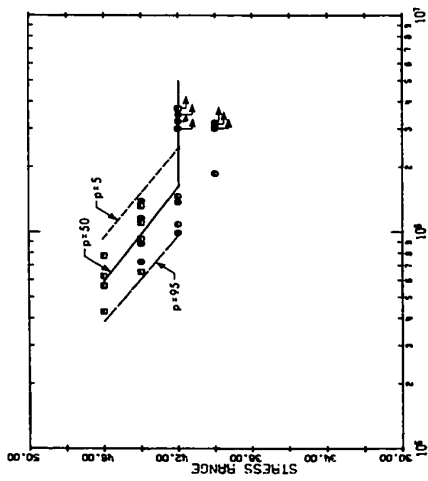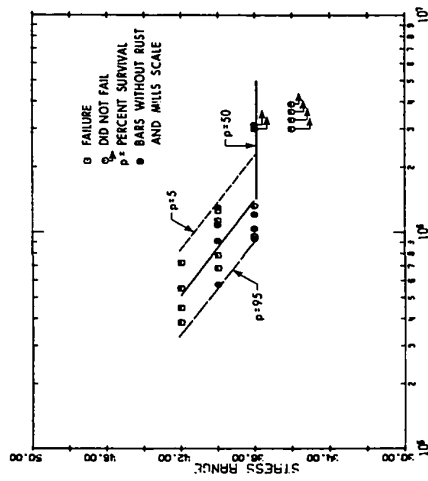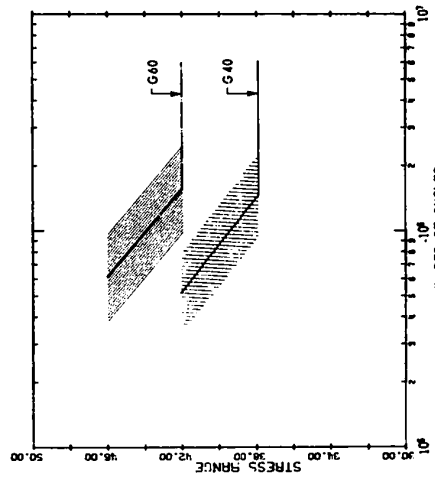
FIGURE 6-8 S-N-P CURVES FOR PLAIN BARS SPECIMENS TESTED IN AIR,
MINIMUM STRESS = 0.1 f_y
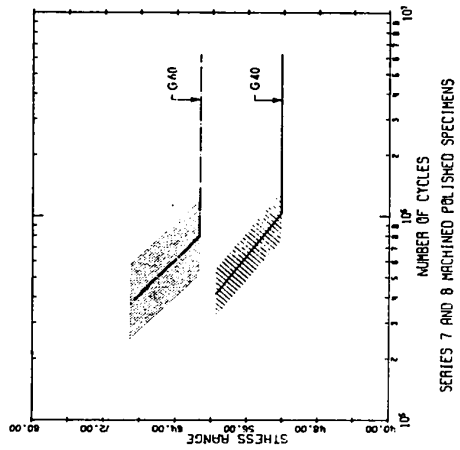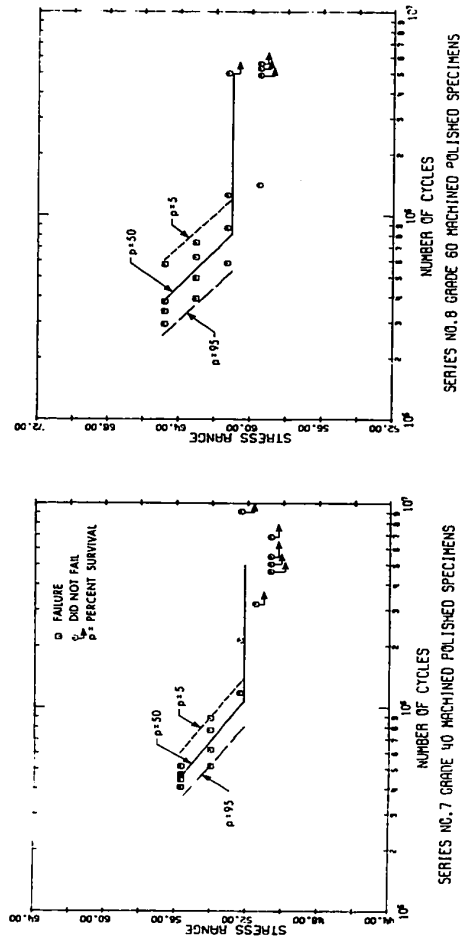
FIGURE 6-9   S-N-P CURVES FOR MACHINED POLISHED SPECIMENS
MINIMUM STRESS = 0.1 f_y

in Table E-1 in Appendix E for groups in which all specimens failed.
A Chi-Square goodness of fit analysis (46) was performed on this data
to test the hypothesis that the sequence of specimen failures was in-
dependent of their location in the test set-up. The value of Chi-
Square obtained from the observations was 3.25, which was less than
3.32, the critical value with 9 degrees of freedom at 95 percent level
of confidence. Thus, the hypothesis of independence was accepted
in the subsequent analysis it was assumed that the scatter in the
fatigue lives of the specimens was not caused by the testing machine.

6.3.2 Analysis of Long Life Data

The fatigue test data presented in Table D-2 in Appendix D
and FIGURES 6.6 to 6.9, show that the reinforcing bars exhibited a
practical fatigue limit and the scatter in the fatigue limit was con-
siderably lower than in fatigue life. These two observations agree
with previous findings (2,16).

The mean fatigue limit and its lower tolerance limit were ob-
tained by a sensitivity analysis (33), the results of which are pre-
sented in columns 8 and 9 of Table 6.1. The mean fatigue limits from
this analysis are plotted in FIGURES 6.7 to 6.9.

Referring to the fatigue test data given in these figures,
it may be noted, in general, that none of the four specimens tested at
the lowest stress level in each series failed, whereas at a stress 4 ksi
above the lowest level all the specimens failed. Thus, within a 4 ksi
stress range the response of the tests changed from non-failure to complete

TABLE 6.1

FATIGUE STRENGTH PROPERTIES OF FATIGUE SPECIMENS TESTED IN AIR

Series No.	Bar Grade	Fatigue Specimen Type	Minimum Stress ksi	Finite Life (Regression Coefficients)			Fatigue Limit at	
				Intercept A	Slope B	Residual Standard Deviation, s	50 Percent Survival ksi	95 Percent Survival ksi
(1)	(2)	(3)	(4)	(5)	(6)	(7)	(8)	(9)
1	G40	Deformed	5.0	8.546	-.0928	0.1136	25.7	24.1
2	G60	Deformed	6.7	9.007	-.1084	0.1268	26.0	24.4
3	G40	Plain as Rolled	5.0	10.306	-.1095	0.1176	37.6	34.8
4	G60	Plain as Rolled	6.7	10.804	-.1094	0.1202	42.0	38.8
5	G40	Plain (*)	5.0	10.306	-0.1095	0.1176	37.6	34.8
6	G60	Plain (*)	6.7	10.804	-.1094	0.1202	42.0	38.8
7**	G40	Machined, Polished	5.0	10.530	-.1050	0.0810	52.2	49.9
8**	G60	Machined, Polished	6.7	10.783	-.0860	0.1216	61.0	58.4

*Bars without rust and mill scale

**Date for series 7 and 8 has been corrected using a Goodman Diagram to 5.0 ksi and 6.7 ksi minimum stresses, respectively.

failure. These two bounds along with the results of the intermediate stress level provided information on the mean fatigue limit. Because this data was not sufficient to determine the fatigue limit distribution, a normal distribution was assumed in a sensitivity analysis of the data (33). This assumption is justified because the distribution of the fatigue strengths has been found to be a normal distribution in the entire range of the S-N curve (52).

The observed scatter in the fatigue limit was smaller than reported in the literature (2,28). This may be due to the simultaneous testing of four specimens under an identical stress cycle.

An analysis of variance (32) was performed on the mean fatigue limits obtained from the sensitivity analysis to investigate the effects of the surface conditions on the fatigue strength, the grade of steel and the interaction of these variables. The details of the analysis are presented in Table E-2 in Appendix E. The homogeneity of the variance of the mean fatigue limit was checked by Bartlett's test (33). The observed F statistic was 2.02, which was less than 2.06, the critical value of $F(7,5217)$ at the 5 percent level of significance. Thus the hypothesis of homogeneity of variance was accepted, the variances were pooled, and the pooled variance was used in the analysis of variance. The observed F values related to the bar surface characteristics, grade and the interaction of these variables were found to be significant to a one percent level of significance.

The results of the analysis of variance are presented in Table 6.2. From this table, it may be noted that there was no difference

108

TABLE 6.2

RESULTS FROM ANALYSIS OF VARIANCE OF FATIGUE LIMIT DATA

Grade	Bar Surface	Difference at significant level** of		
		5%	2.5%	1%
G40 and G60	Deformed vs As-rolled	Yes	Yes	Yes
	As-rolled vs Bars WRM*	No		
	As-rolled vs Machined, Polished	Yes	Yes	Yes
G40 vs G60	Deformed	No		
	As-rolled	Yes	Yes	
	Bars WRM*	Yes	Yes	
	Machined, Polished	Yes	Yes	Yes

*WRM - Bars without rust and mill scale
**The level of significance is the risk of rejecting the null hypothesis, i.e. no
difference exists, when it is true.

between the mean fatigue limits of plain bars with and without rust and mill scale and between deformed bars of Grades 40 and 60, at the 5 percent level of significance. All remaining specified variables were highly significant at the level of significance shown in this table.

6.3.3 Analysis of Finite Life Data

The regression model given by Equation (6.1) was fitted to the finite life data from each series.

$$\log N = A + B \, S_r \qquad\qquad (6.1)$$

This equation was chosen because statistical analyses presented in Appendix E showed that log N was normally distributed and because this equation gave a better fit (31) than several other S-N equations (47).

FIGURES 6.7 to 6.9 are S-N-P (stress-number of cycles-probability) diagrams showing the test data, a mean S-N curve for 50 percent survival, and 5 and 95 percent survival limits of the population. The determination of these curves for the finite life region involved two analytical expressions: the mean S-N equation given by Equation 6.1 and a life distribution function. The regression coefficients A and B and the residual standard deviation (s) of each series are given in Table 6.1. The replicate observations at each stress level provided the data on the life distribution. This data was used to determine the 5 and 95 percent survival lives plotted in

FIGURES 6.7 to 6.9. In each of these figures the S-N curves given in parts (a) and (b) are compared in (c). The data from series 5 and 6 is plotted along with that of series 3 and 4, respectively. It may be seen that the data of series 5 and 6 falls within the survival bands of series 3 and 4. Visual examination of these figures provides some idea of the differences in fatigue limits and lives due to the specified variables.

The test data in the finite life region was analysed to find the influence of the specified variables. An analysis of covariance (48,49) and Hald's method (50) were used to determine the significant variables. The assumptions in this analysis are discussed in section E.2 of Appendix E. The results from these analyses are presented in Table 6.3. Comparing Tables 6.2 and 6.3, it may be noted that the variables which influenced the fatigue limit, also influenced the fatigue life in the finite life region at the same level of significance. These observations support Weibull's concept that life and strength are both inter-related stochastic functions (51).

The effect of various specified variables on fatigue life was systematically studied by a multiple regression analysis (33). All the data in the finite life region were used in this analysis. A stepwise multiple linear regression procedure was used becuase of its versatility. A linear additive model in which log N was the dependent variable and S_r, K_T, f_u and R* were independent variables was used.

---

*R - surface roughness, CLA values (40).

TABLE 6.3

RESULTS FROM ANALYSIS OF COVARIANCE OF SPECIFIED VARIABLES

(FINITE LIFE DATA)

Grade	Bar Surface Characteristics	Difference at significant level of		
		5%	2.5%	1%
G40 and G60	Deformed vs As-rolled	Yes	Yes	
	As-rolled vs Plain WRM*	No	Yes	Yes
	As-rolled vs Machined, Polished	Yes	Yes	Yes
G40 vs G60	Deformed	No		
	As-rolled	Yes	Yes	
	Plain WRM*	Yes	Yes	
	Machined, Polished	Yes	Yes	Yes

*WRM – Bars without rust and mill scale.

The model, given in Equation (6.2) explained 82.7 percent of the variation in the test results. The order of significance of variables is the same as the order of the terms in Equation (6.2).

$$\log N = 0.4397 - 0.1075 \, S_r - K_T \, (0.0296 \, f_u - 1.4662)$$

$$+ \, 0.1310 \, f_u - R \, (0.0002 \, f_u - 0.0164) \tag{6.2}$$

where K_T = theoretical stress concentration factor. In the analysis K_T for plain as-rolled bars and machined polished specimen was assumed equal to 1*.

R = Surface roughness, CLA values (40)

f_u = Tensile strength of specimen, ksi.

The standard deviation of all the residuals of equation (6.2) was 0.110. The multiple regression analysis confirmed the results of the analysis of covariance regarding the signficance of the interaction between the grade and surface characteristics. The interaction terms in equation (6.2) are $K_T f_u$ and $R f_u$; each of which were found to be significant.

The inability of the multiple regression model to completely explain the variability in the fatigue data may have been due to the

---

*K_T = 1 for as-rolled bars is not strictly correct due to surface roughness. The error was partially compensated by inclusion of the R term in the equation.

absence of parameters defining the decarburized surface of reinforcing bar specimens, the absence of an approximate value of K_T for plain as-rolled bars and the assumptions inherent in the linear additive model. The derivation and assumptions in the multiple linear regression analysis are given in section E.3 of Appendix E.

6.4 Statistical Analysis of Fatigue Data from Concrete Beams

The data from the concrete beam, tested in Phase I was also divided into finite life and long life data for analysis. In order to obtain an expression for an average S-N relationship, equation (6.1) was fitted to the finite life beam data by a regression analysis. This analysis required no other assumption other than a linear relationship between dependent variable log N and independent variable S_r. This assumption is justified from fatigue tests. Test results having lives greater than one million cycles were used to estimate the mean fatigue limit at five million cycles.

Table 6.4 contains the regression coefficients A and B, the residual standard error of regression and the approximate mean fatigue limit for each test series. The slopes (B) and the residual standard errors (s) of the regression equations varied considerably among the twelve beam series. The fatigue lives at a stress range of 32 ksi predicted from regression equations are presented in column 8 of Table 6.4. In this table, the fatigue life and fatigue limit of the No. 5 Grade 75 bar (series 9) are considerably higher than those for the rest of the bars.

TABLE 6.4

FATIGUE STRENGTH PROPERTIES OF REINFORCING BARS IN BEAM TESTS

Beam Series No.	Bar Type		Minimum Stress ksi	Finite Life (Regression Coefficients)				Approximate Fatigue Limit at 5 Million Cycles
	Size No.	Grade		Intercept A	Slope B	Standard Deviation Regression (S)	Preidcted Value of Log N at 32 ksi	
(1)	(2)	(3)	(4)	(5)	(6)	(7)	(8)	(9)
1	8	G40	5.2	8.737	-0.0818	0.3172	6.1194	30.2
2	8	G60	6.9	8.175	-0.0678	0.1803	6.0054	30.5
3	8	G75	7.4	7.433	-0.0410	0.3741	6.1210	31.7
4	8	G40	21.2	9.068	-0.1126	0.0798	5.4648	26.1
5	8	G60	28.0	9.253	-0.1166	0.0276	5.5218	26.4
6	8	G75	34.1	9.620	-0.1142	0.0891	5.9656	26.4
7	5	G40	5.4	8.338	-0.0733	0.0798	5.9924	31.5
8	5	G60	6.3	8.282	-0.0732	0.0820	5.9406	31.3
9	5	G75	8.9	10.756	-0.1171	0.1555	>6.8970	36.5
10	10	G40	5.0	7.633	-0.0509	0.1684	6.0042	30.0
11	10	G60	6.4	7.315	-0.0448	0.2333	5.8814	28.8
12	10	G75	8.7	8.679	-0.0880	0.2320	5.8630	29.3
13*	8	G40	5.2	10.223	-0.1416	0.1534	5.6918	28.0

*Bar tested in Air

The average S-N equations for the twelve beam series presented in Table 6.4 are plotted in FIGURES 6.10 to 6.13. Each of these figures contains data from the three test series having the same bar diameter and minimum stress ratio (0.1 f_y or 0.4 f_y) but different grades of steel. The fourth plot in each of these figures compares the S-N curves of the three grades of steels. These plots show considerable deviation of the test data from the regression lines. This may be partly due to difficulties in precisely controlling the bar stresses in the beams since a small error in the applied stress results in a considerable variation in the fatigue life of a specimen or it may be due in part to the variations in the material properties. These two factors were properly accounted for in the phase II tests.

FIGURE 6.14 compares the fatigue strength of similar bars in air and in concrete beams. It may be seen that the finite as well as the long life sections of S-N lines for beams are higher than those for tests in air. The fatigue limit of the bars in air was 2 ksi lower than their counterparts in a beam.

Since the tests in the first phase were not planned in a manner that permitted statistical predictions, they might have been influenced by procedural testing bias. If, however, the variation in the test results due to procedural bias is considered to be smaller than the influence of the specified variables, it is possible to analyse this data statistically.

The finite life data of twelve beam series were analysed by a multiple regression analysis to study the variation in the test data
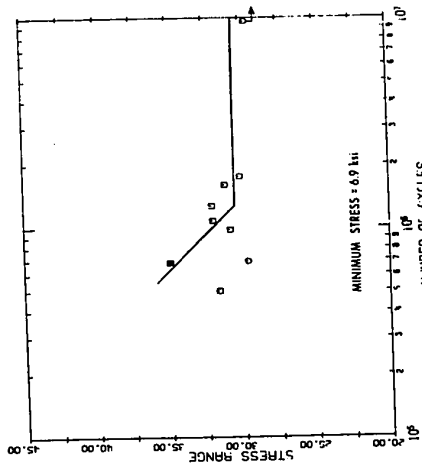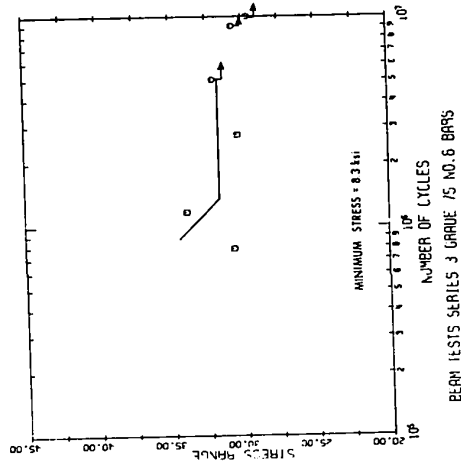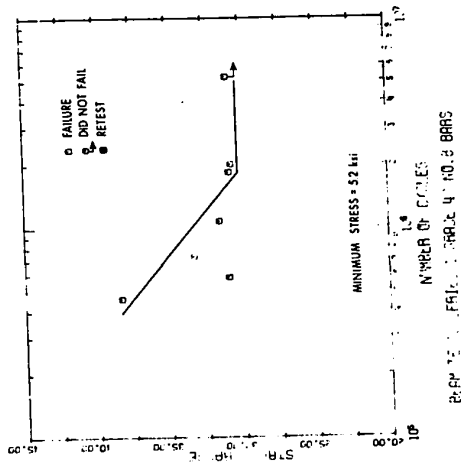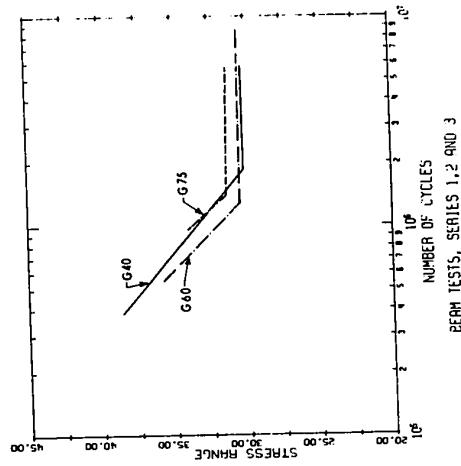
FIGURE 6-10   S-N CURVES FOR BEAM SPECIMEN, MINIMUM STRESS = 0.1 f_y
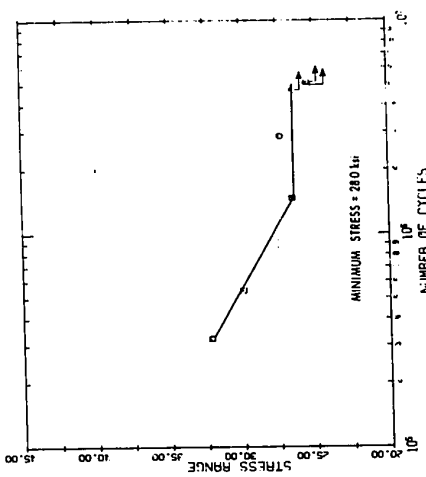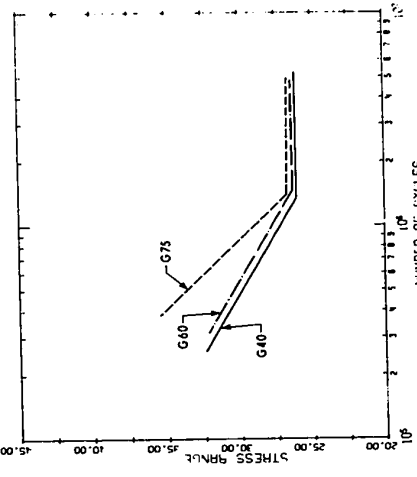
117
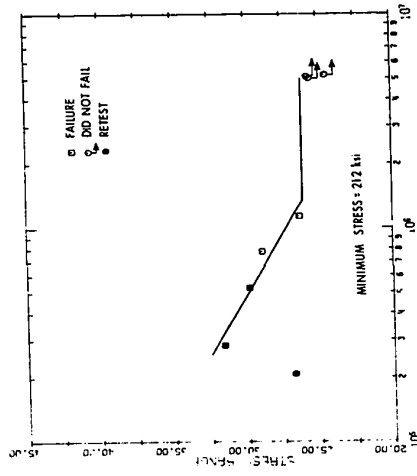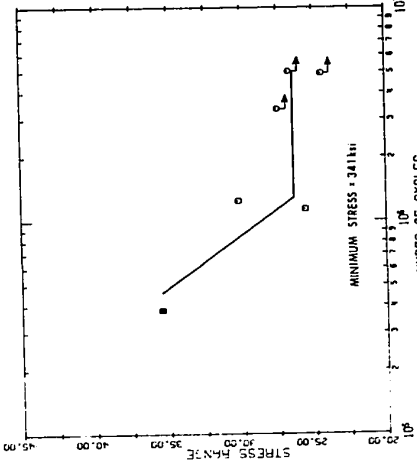
FIGURE 6-11 S-N CURVES FOR BEAM SPECIMENS, MINIMUM STRESS = 0.4f$_y$
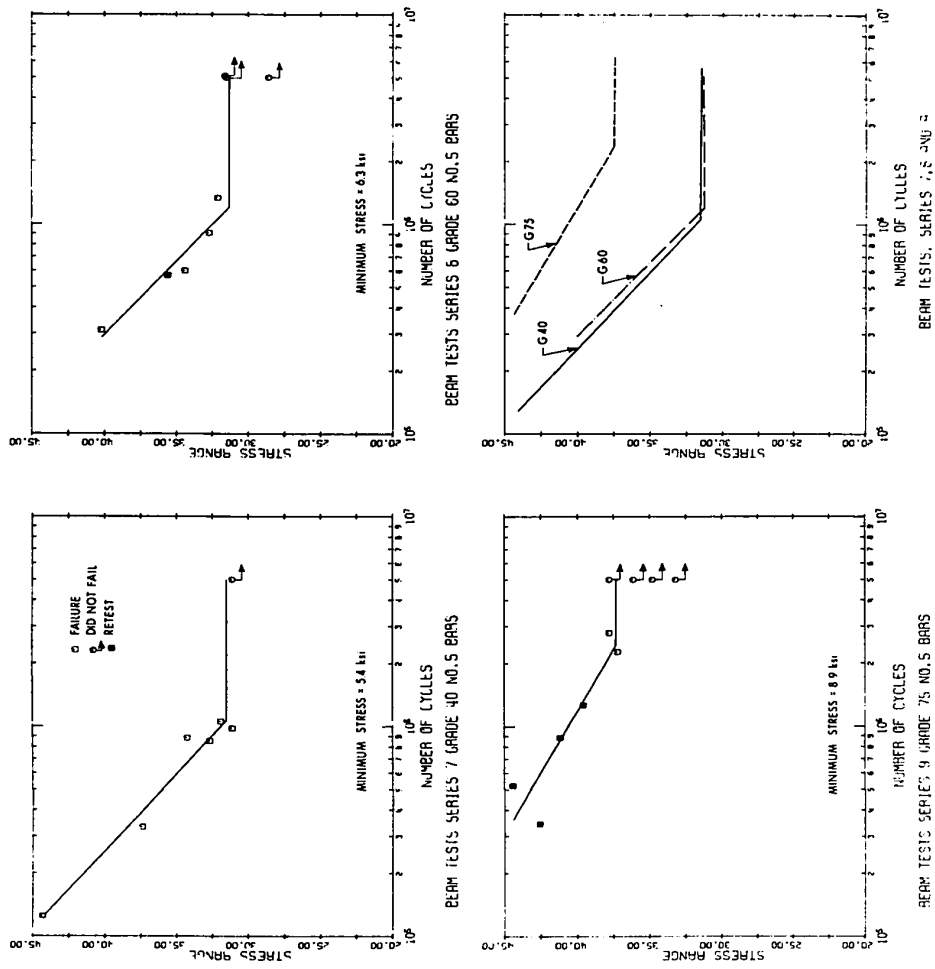
FIGURE 6-12   S-N CURVES FOR BEAM SPECIMENS MINIMUM STRESS = 0.1 f$_y$
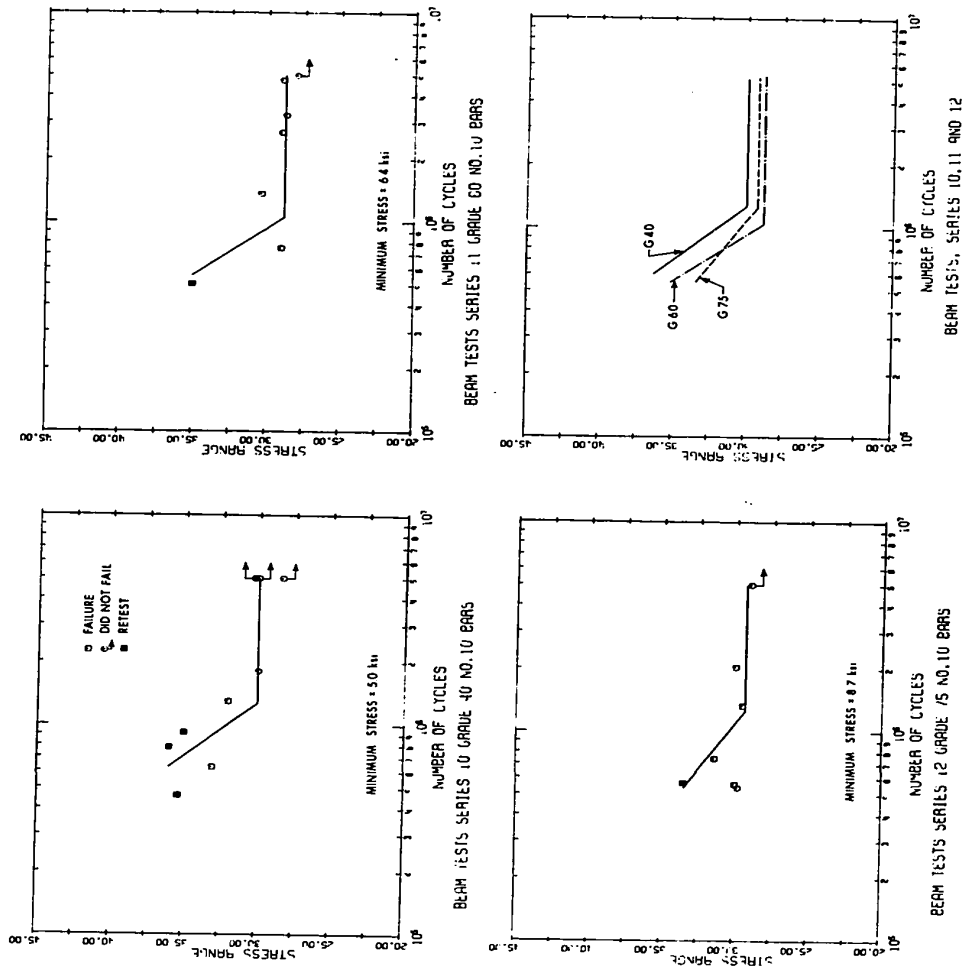
FIGURE 6-13   S-N CURVES FOR BEAM SPECIMENS, MINIMUM STRESS = 0.1 f_y
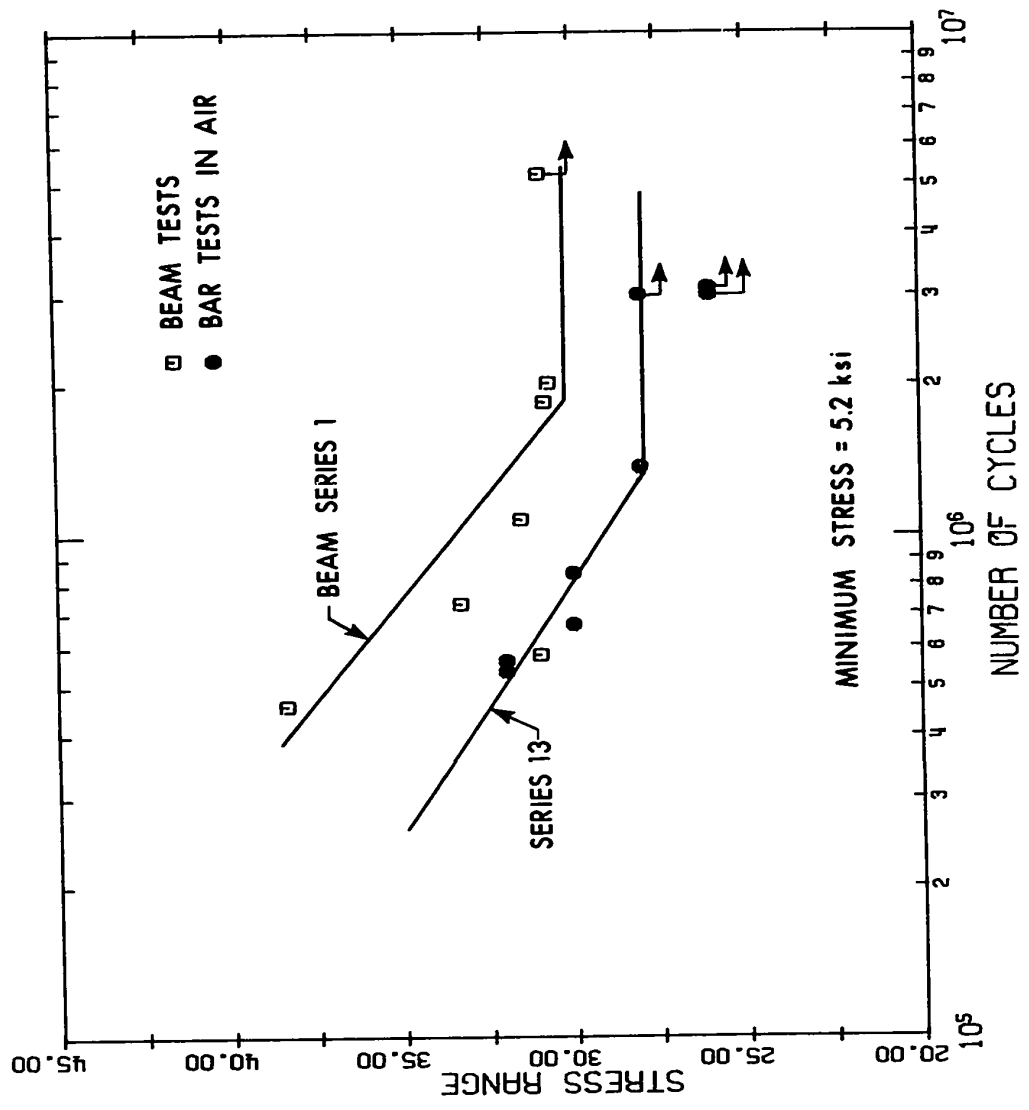
FIGURE 6-14 COMPARISON OF S-N CURVES OF GRADE 40 NO. 8 BARS IN BEAMS AND IN AIR

due to the specified and other variables. In this analysis the statistical conclusions on the tests in air were believed to be applicable for the beams.

A multiple linear regression model given in Equation (6.3), statistically explained 78.9 percent of the variation in the data and had a standard deviation of residuals equal to 0.168. The stress range, S_r, was again found to be the most significant variable followed by S_{min}, f_u and K_T in that order. In this analysis the data of beam series 9 was not included since this data was significantly different from the remaining test series with respect to fatigue strength as discussed in section E.3 of Appendix E. The details of the calculation of equation (6.3) are also given in the same appendix.

$$\log N = 9.5894 - 0.0633\ S_r - 0.0147\ S_{min} + .0033\ f_u - 0.8663\ K_T \quad (6.3)$$

where S_{min} = Minimum stress, ksi.

For the above regression model several other independent variables; D_{nom}, grain size and yield strength were tested and were found not significant.

The deformed bars in the first and second phases of tests were of similar deformation pattern and were made by the same manu-facturer. The test data in two phases differed only in the type of fatigue specimens. In order to analyse the data together, the fatigue strength of bar specimens was increased by 2 ksi to account for the concrete encasement. This data was also analysed by a multiple linear

regression analysis and Equation (6.4) was obtained. This model accounted for 77.8 percent of the variation in the data and had a standard deviation of residual equal to 0.161.

$$\log N = 10.9397 - 0.06648\, S_r - 0.0146\, S_{min}$$
$$- 1.5138\, K_T + .0042\, f_u \tag{6.4}$$

The significant variables in the above equation are same as that of Equation (6.3) except the order of significance of K_T was interchanged with f_u. It may also be noted that the regression coefficients in Equation (6.3) and (6.4) are different.

The combined deformed bar data analysed above is plotted in FIGURE 6.15. Two S-N curves are shown in this figure; one for Series 9 and other for the remaining tests. The S-N curve of the Series 9 is considerably above the other S-N curve falling outside the 95 percent tolerance limits of the remaining data, indicating that the fatigue strengths of the Series 9 specimens were significantly different from the rest of bars. The higher fatigue strength of the No. 5 Grade 75 bars was probably due to their relatively lower deformation K_T values and the fact that they had the finest grain structure among all the bars investigated.

6.5 Interpretation of Results of Statistical Analyses

It is not always necessary that a statistically significant variable should also be of engineering significance. The statistical analyses presented in sections 6.3 and 6.4 eliminated the non-significant
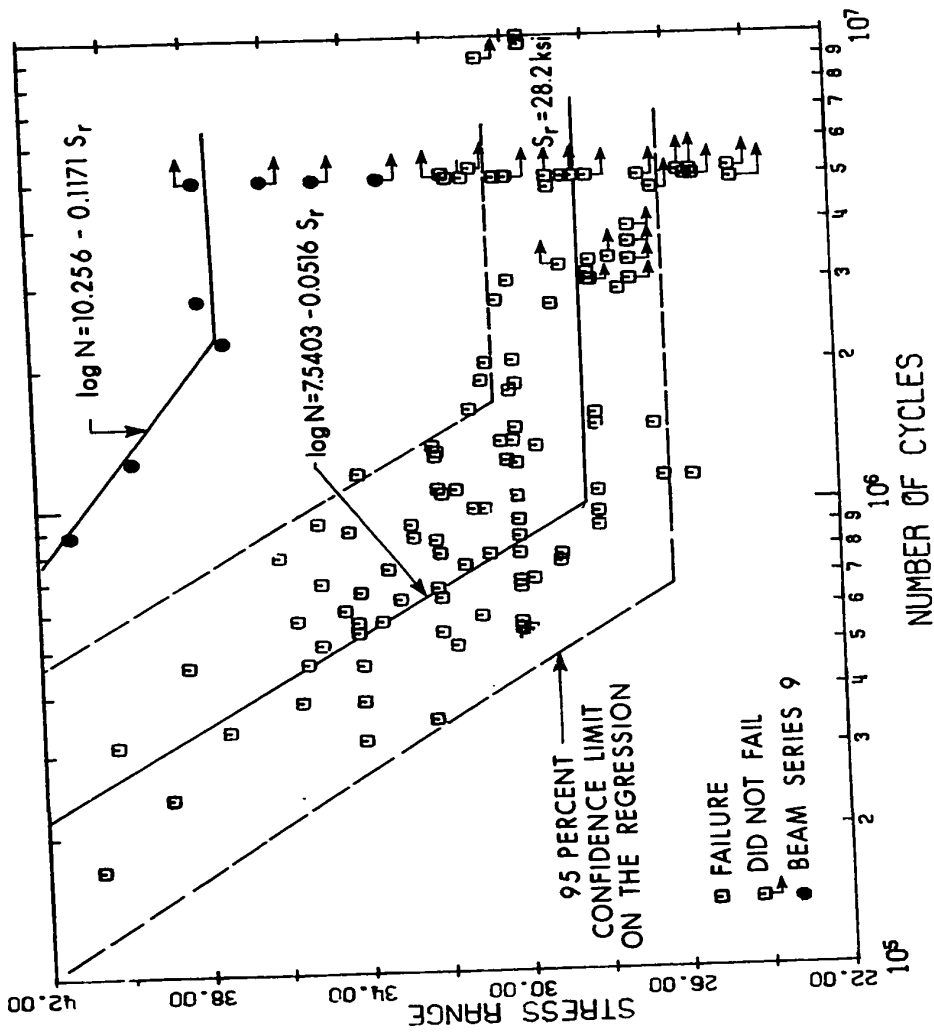
FIGURE 6-15   ALL DEFORMED BARS TEST DATA WITH TOLERANCE LIMITS

variables and selected the significant variables. In this section, the relative engineering importance of the specified variables will be presented. This material will be discussed more fully in Chapter VII with the published data.

Unlike aircraft structures, civil engineering structures are generally designed for a long life and their factors of safety are based on the fatigue strength rather than fatigue life. Thus, in comparing the influence of the various specified or other variables, fatigue limits will be compared in this section. In addition, it will be demonstrated that fatigue life comparisons may sometimes result in misleading conclusions.

The influences of the bar surface characteristics and grade on the fatigue limit and fatigue life are presented in Table 6.5. The fatigue limit ratios and fatigue life ratios were calculated from the data given in Table 6.1. The fatigue lives of two types of specimens were compared for an arbitrarily selected common stress level on the common range of each of their S-N curves.

The influence of bar surface characteristics on the fatigue limit is compared in section A of Table 6.5. For comparison purposes, the fatigue limit of deformed bars of Grade 40 and 60 were assumed unity and the fatigue limit ratios for other types of fatigue specimens are reported. These ratios are higher for Grade 60 than Grade 40 specimens indicating that the effect of stress concentration was higher on Grade 60 than Grade 40 specimens.

The influence of bar grade is compared in part B of Table

TABLE 6.5

INFLUENCE OF SURFACE CHARACTERISTICS AND
GRADE ON FATIGUE LIMIT AND FATIGUE LIFE

A. Influence of Bar Surface Characteristics

	Fatigue Limit Ratio		
	Deformed	Plain As-Rolled	Machined Polished
G40	1.00	1.48	2.03
G60	1.00	1.62	2.35

B. Influence of Bar Grade

	Fatigue Limit Ratio		Fatigue Life Ratio		
	G40	G60	S_r, ksi	G40	G60
Deformed	1.00	1.01	28	1.00	1.06
Plain As-Rolled	1.00	1.11	44	1.00	3.17
Machined Polished	1.00	1.31	58	1.00	22.65

Note: The fatigue limit ratios and life ratios were obtained from data given in Table 6.1.

6.5. The fatigue limit and life of the specimens of Grade 40 were considered unity and the corresponding ratios for Grade 60 are presented in this table. The ratio between the fatigue limits of Grade 40 and 60 deformed bars is 1.01 where as that of fatigue life is 1.06. These two ratios are not very far apart. When the fatigue limit and fatigue life ratios for Grade 40 and 60 for machined polished specimens are compared, however, the ratio in the former case is 1.31 whereas in the latter case it is 22.65. This demonstrates that the fatigue limit is increased by 31 percent by the increase in grade where as the fatigue life increased by 2265 percent. This probably presents a misleading conclusion though as FIGURE 6.9 will suggest the calculated ratio of lives is correct. Thus, only fatigue limit ratios will be presented for the beam tests.

The influence of grade, bar diameter and minimum stress on the fatigue limit for the beam tests is compared in Table 6.6. The influence of grade was almost negligible except for the No. 5 Grade 75 bars, which had a 16 percent higher fatigue limit than the remaining bars. The reduction in the fatigue limit due to increase in the minimum stress level varied between 23 to 27 percent. The influence of bar diameter corresponded to about a 5 percent decrease in fatigue limit with an increase in bar sizes from No. 5 to No. 8 and from No. 8 to No. 10. The fatigue limit of bars in the beam specimens was 8 percent higher than for those tested in air.

The above comparisons show that for the deformed bars the surface characteristics have the highest influence on fatigue limit

followed by minimum stress level and the bar diameter. The influence
of grade will only be significant when the stress concentrations are
reduced.

TABLE 6.6

INFLUENCE OF GRADE, DIAMETER AND MINIMUM STRESS ON FATIGUE LIMIT

A. Influence of Grade

Bar Size	Fatigue Limit Ratio		
	G40	G60	G75
No. 5	1.00	0.99	1.16
No. 8	1.00	1.01	1.05
No. 10	1.00	0.96	0.98

B. Influence of Minimum Stress

Grade	Fatigue Limit Ratio	
	0.1fy	0.3fy
G40	1.00	0.86
G60	1.00	0.87
G75	1.00	0.83

C. Influence of Bar Diameter

Grade	Fatigue Limit Ratio		
	No. 5	No. 8	No. 10
G40	1.04	1.00	0.95
G60	1.03	1.00	0.96
G75	1.15	1.00	0.93

D. Influence of Concrete Encasement

Grade	Fatigue Limit Ratio	
	Bar in Air	Bar in Beam
G40	1.00	1.08

Note: Fatigue limit ratios calculated from TABLE 6.4, Column 9.

CHAPTER VII

COMPARISON OF ALBERTA RESULTS WITH

PUBLISHED FATIGUE DATA

7.1 Introduction

The published fatigue tests on bars in concrete beams and those tested in air were briefly described in Chapter I. Because the majority of these tests were planned on a deterministic experimental design, it frequently is not possible to separate the variation in fatigue strength due to the specified variables and the scatter* in the test results. In one project (16), the tests were planned to permit evaluation of the influence of several specified variables statistically, but their scope was limited to the finite life region of the S-N curve. In comparing previous test results, it will be assumed that the scatter in the fatigue strength was smaller than the influence of the specified variables.

In this chapter, the findings from the fatigue tests, stress concentration analyses and metallurgical tests are used to explain the fatigue behavior of the bars tested in this project and those reported in the literature.

In section 7.2, several variables which may affect the fatigue

_____

*Scatter is the variation in fatigue data due to non-specified variables.

129

strength of bars are discussed. Empirical equations are developed to quantify the influences of the specified variables. These equations are used in section 7.3 to develop an engineering method to estimate the fatigue strength at two million cycles. This method is used to analyse the data from this and other projects.

7.2 Factors Affecting Fatigue Strength of Bars

7.2.1 Type of Fatigue Specimen

The selection of a proper fatigue specimen to simulate the fatigue behavior of bars in concrete structures is important. Most of the previous investigators tested bars embedded in concrete beams, since this type of fatigue specimen has been considered necessary to represent the most critical of field conditions. Some researchers have tested bar specimens in air, under pulsating tension. In the following paragraphs, the adequacy of the latter type of fatigue specimen to represent the fatigue behavior of bars in concrete structures is examined.

Rehm (9,56) conducted fatigue tests on smooth and deformed bars using both of the above described specimens. The test results showed that the fatigue strength of an embedded bar in a beam test was 20 percent lower than that of the same bar tested in air. Similar test results have been reported by Meyer (25). Contrary to these findings, however, tests on ribbed TOR-STAHL bars reported by Soretz (10), showed that embedded bars in beam tests had a fatigue strength at least 10 percent higher than similar bars tested in air.

The influence of concrete encasement on the fatigue strength of bars was extensively studied by Waseheidt (11). He tested plain bars and a variety of deformed bars in air and embedded in concrete prisms and beams. The test results are shown in FIGURE 7.1. The relative rib area (f_R), of the bars was found to be a significant variable in these tests. This parameter is defined as:

$$f_R = \frac{\text{lug area projected on a cross-section of bar}}{\overline{\Lambda}\text{(bar diameter)(rib spacing)}}$$

FIGURE 7.1 shows that as the f_R is reduced below .05 the fatigue strength of bars in beams decreases probably because the bond resistance is lower. Bars having f_R greater than .05 had no loss of fatigue strength due to embedment.

Wascheidt's beam tests showed an increase of 6 percent in fatigue strength due to concrete encasement for a bar having relative rib area f_R equal to .069. Alberta tests supported Wascheidt's and Soretz's test results. The fatigue strength of No. 8 bars, having f_R equal to .071, embedded in a beam was 8 percent higher than those tested in air. A similar result was found for Soretz's tests. Since the f_R values for tests reported by Rehm and Meyer could not be obtained, it is not possible to compare their results with the others.

The higher fatigue strength observed for bars embedded in beams than for bars tested in air could be explained by the following factors (10):

132
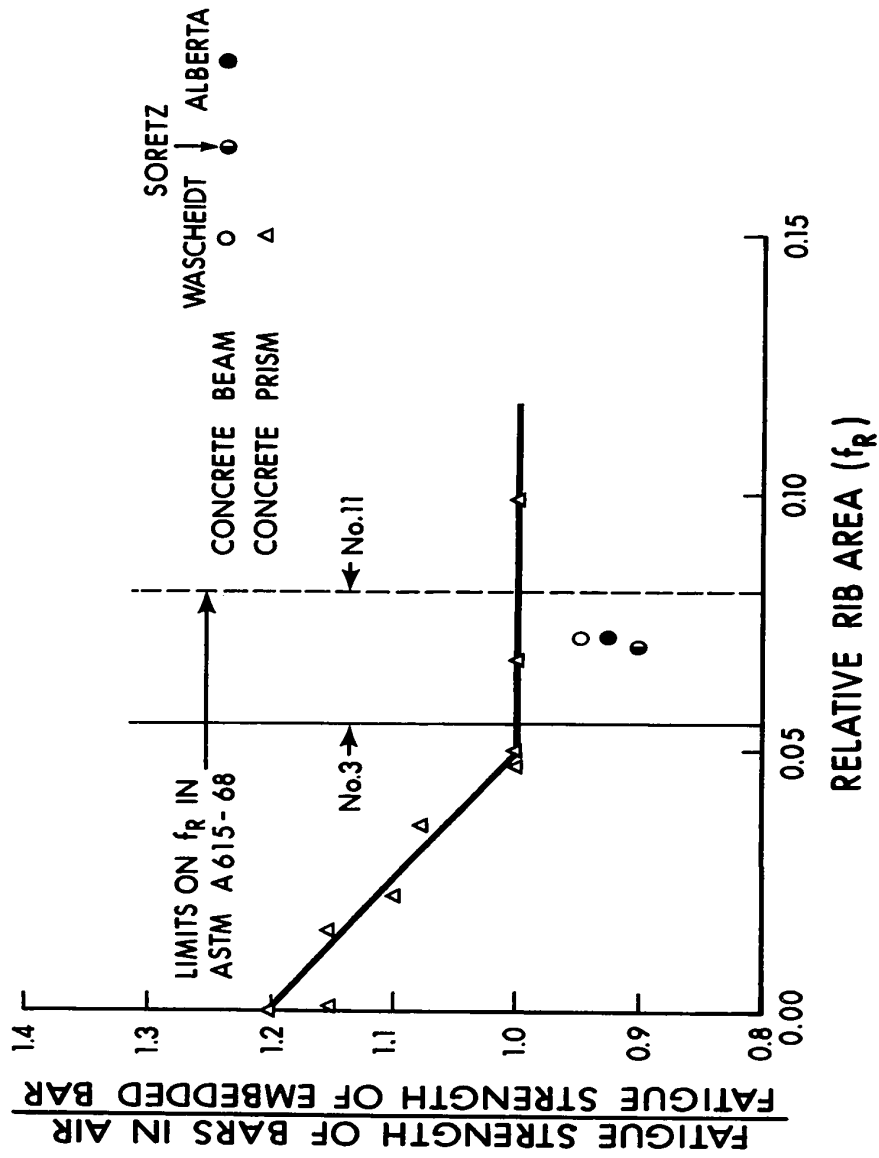
FIGURE 7-1   THE EFFECT OF CONCRETE ENCASEMENT ON FATIGUE STRENGTH

1. The calculation of steel stresses is made assuming the fully cracked state. The actual bar stresses are usually a little lower, as observed in tests (16) due to tension in the concrete. This difference increases with increasing efficiency of bond.

2. The cracks do not close after removal of the load, because small grains of material lodge between the faces of cracks. Hence the minimum stress in the bar may be higher than that calculated from the minimum load, leading to a higher apparent fatigue strength.

3. In a bar tested in air, the weakest section in the bar fails whereas in a beam, failure always occurs at or close to a crack. The probability is low that a crack and the weakest part of the bar will coincide, and failure therefore occurs at a higher stress.

4. On the other hand, a factor which may tend to reduce the fatigue strength of bars in beams, is the difference in the stress gradient in the bars in the beam and in tension specimens. The bars in the tension specimens have no stress gradient other than that due to stress concentrations, whereas the bars embedded in beams have an additional stress gradient due to the flexural loading. This factor would reduce the fatigue strength of bars in the beams.

Though the individual contributions of the above parameters

are not known, their net effect is about 5 to 10 percent higher
fatigue strength for bars tested in a beam than for the same bars
tested in air.

The minimum values of f_R allowed by the ASTM specification
for deformations (3) ranges from .058 for No. 3 bars to .077 for No.
11 bars. The test results plotted in FIGURE 7.1 suggest that the
fatigue strength of American bars tested in concrete beams of the
type tested should be about 5 percent higher than for those tested
in air.

Since it is easier and more economical to test individual
bars in air than it is to test them in beams, it is recommended that
bar specimens be used for future testing. The results obtained from
such tests would tend to be on the safe side and with this type of
specimen the investigator has a better idea of the bar stresses.

7.2.2 Bar Surface Characteristics

The four types of fatigue specimens; machined polished, as-
rolled plain bars, bars without rust and mill scale differed only in
their surface characteristics. They had the same chemical composition
and were produced by identical manufacturing processes.

The discussion in the following sections shows the influence
of the four above mentioned bar surface characteristics and their inter-
action with the two grades of reinforcing bars.

7.2.2.1 Machined Polished Surface

Fatigue tests on standard polished specimens, machined from
the center of reinforcing bars, were carried out to find the fatigue

strength of the bar steel. The results of these tests were intended to serve as a basis for finding the detrimental influences of the as-rolled surface and the deformations on the fatigue strength of the bar steel.

The metallographical observations revealed that the grain structure was uniform across the cross-section of the bar except close to the surface. The machined polished specimens came from the center of the reinforcing bars and had no decarburization, mill scale or rust, since these were concentrated within 1/30 inch from the surface of the reinforcing bar.

The statistical analysis of the fatigue data on machined polished specimens showed that the fatigue strength of the Grade 60 specimens was significantly higher than that of Grade 40 specimens and the fatigue strength of the machined polished specimens were considerably higher than those of as-rolled plain and deformed reinforcing bars. These observations indicate that the fatigue strength of the steel itself increases with an increase in grade and the rolled surface and deformations reduce the fatigue strength.

The fatigue strength of machined polished specimens has been more closely related to the tensile strength than any other mechanical properties (57). The following empirical relationship between the fatigue limit of machined polished specimens and tensile strength of the bar was derived from the test results:

$$S_{mf} = 0.649 \ f_u + 2.14 \tag{7.1}$$

where S_{mf} = fatigue strength at 2 million cycles of machined
polished specimens at S_{min} = 0 .

7.2.2.2 As-rolled Surface

Metallographical observations showed that an as-rolled bar surface consisted of rust and mill scale and a decarburized steel. These were present in all the reinforcing steel tested as shown in FIGURES C.1 to C.11 in Appendix C. In these figures and in TABLE 4.1, it may be noted that the thickness of decarburized layer and mill scale were almost constant in all cases.

The influence of rust and mill scale on fatigue strength was studied by testing plain as-rolled bars and bars with the rust and mill scale removed. The statistical analysis of the finite and long life fatigue data showed no significant difference between the two types of specimens*.

In contrast to the above finding the fatigue strength of plain as-rolled bars and bars without mill scale were significantly lower than those of machined polished specimens. This conclusion was reached from statistical analysis of finite life and long life fatigue data. These analyses also showed that Grade 60 bars with or without rust and mill scale had a significantly higher fatigue strength than those of Grade 40.

The surfaces of plain bars without rust and mill scale and the machined polished specimens differed with respect to decarburization and surface roughness. Several reports (36-39) conclude that the fatigue

---

*This conclusion may not be valid for severely rusted bars.

strength of steel is considerably reduced by decarburization. As shown in FIGURES 4.3 and 4.4 the decarburized surface had a lower carbon content than the interior of the bar which made the surface relatively weaker than the core. The fatigue cracks initiate and grow in this weaker region as shown in FIGURE 6.5, probably at a lower stress than would be required in the base metal leading to a lower fatigue strength.

The as-rolled bar surface was rougher than that of machined polished specimen as shown in FIGURE 4.9. The multiple regression analysis of the fatigue data showed that the surface roughness was a significant variable: the rougher the bar surface, the lower the fatigue strength (see Equation 6.2). The analysis also showed that the influence or surface roughness on fatigue strength, like that of stress concentrations was more detrimental in the higher grade steels.

No analytical procedure could be found to quantify the effect of decarburization and roughness on fatigue strength largely due to the absence of parameters defining the decarburization and surface roughness. In order to obtain an empirical expression for the influences of these parameters their effect was assumed to be the same as a stress concentration. An equivalent hypothetical value of K_T associated with their effect was obtained indirectly by the procedure described in the following paragraph.

The theoretical stress concentration caused due to the rolled surface was assumed to be the same for Grade 40 and 60 bars, because micro-hardness tests showed that the strength of decarburized layers were about 80 ksi for both grades (Table 4.1). The equivalent K_T value

of 2.92 was obtained from the experimental K_f values and the Neubers

constant obtained from Reference (57) for each grade of steel.

7.2.2.3 Deformation Details

Although most research reports on fatigue of deformed bars

suggest that the deformations have a pronounced influence on fatigue

strength, few systematic studies of this subject have been reported.

In Chapter V, it was seen that the deformations cause stress concentra-

tions in the bar and that the theoretical stress concentration factor

K_T is a function of the geometry of the deformation. It has been well

established that fatigue failures tend to occur at locations of high

stress concentrations and the damaging influence of a notch is a

function of K_T.

In these tests and most published tests, deformed bars tested

in air and in beam tests, failed at the bases of transverse lugs as

expected due to high stress concentration present at this section.

Some reports (10-13,19,23) have suggested that the inter-

section of the longitudinal and transverse lugs is a critical location

for fatigue crack initiation. In Europe this was considered so critical

that some bar producers there have manufactured bars in which the trans-

verse lugs are discontinued prior to reaching the longitudinal lugs.

It is also claimed (9-11) that these bars have higher fatigue strength

than the typical American bar.

The stress concentration measurements reported in Chapter V

do not support the above idea and the deformed bars tested in air did

not show any tendency to fail at the intersection of the lugs. The analysis of failure surfaces described in section 6.2, revealed that the fatigue failures were initiated by several independent cracks at the bases of transverse lugs. These cracks were found to be randomly distributed along the lug base. These observations contradict the idea that the intersection of the lugs is more critical than the bases of transverse lugs. This conclusion is strongly supported by the tests conducted by Hanson, et.al.(15) on hot rolled deformed bars in which the longitudinal and transverse lugs did not intersect. In these tests, no improvement in the fatigue strength was obtained by terminating the transverse lugs before they reached the longitudinal lugs.

The bars tested in the beam tests had the longitudinal lugs aligned in the horizontal plane. All the bars failed at the bases of transverse lugs towards the bottom side of beams. This failure location was expected due to the stress gradient across the depth of the bar in the beam, the stresses in the bottom halves of the bars being slightly higher than those at the upper halves.

To determine whether the bar orientation in a concrete beam had a significant influence on the fatigue strength, Burton (13) tested one series of beams with the longitudinal lugs placed in the horizontal plane and another series with them in the vertical plane. The test results showed that the bars had 5 to 7 percent less fatigue strength when the lugs were in a vertical plane than when the lugs were in the horizontal plane. This reduction in fatigue strength can be explained

by the stress gradient across the depth of the bar in the beam. The bars oriented with their lugs in the vertical plane have a larger stress at their extreme fibre than if the lugs were horizontal. As a result they would be expected to show a slight reduction in fatigue strength.

From the above discussion, it may be concluded that the bases of the transverse lugs are the most critical sections for fatigue failure. The theoretical stress concentration (K_T) in this region was found to be a statistically significant variable for the fatigue data of the Phase I and II tests. Equations (6.2) to (6.4) show that an increase in K_T is accompanied by a decrease in the fatigue life. This decrease is greater for higher grade steels. It is desirable, therefore, to reduce the K_T value of the deformations, especially for higher grade steels.

The theoretical stress concentration factor (K_T) can be minimized by efficiently proportioning the lug base radius (r), lug height (h), lug half width (w) and lug face angle (θ), as explained in section 5.4. Out of these variables, the r/h ratio was found to be the most significant variable affecting K_T as shown in FIGURE 5.8. The typical North American bars have r/h ratios ranging between 0.2 to 0.4, which are significantly lower than the optimum r/h ratio of 1.25 obtained in section 5.4.

The influence of r/h ratio on fatigue strength of bars is examined in FIGURE 7.2. This figure contains data from this and several other projects (15,18,26). To put this data on a comparable basis,
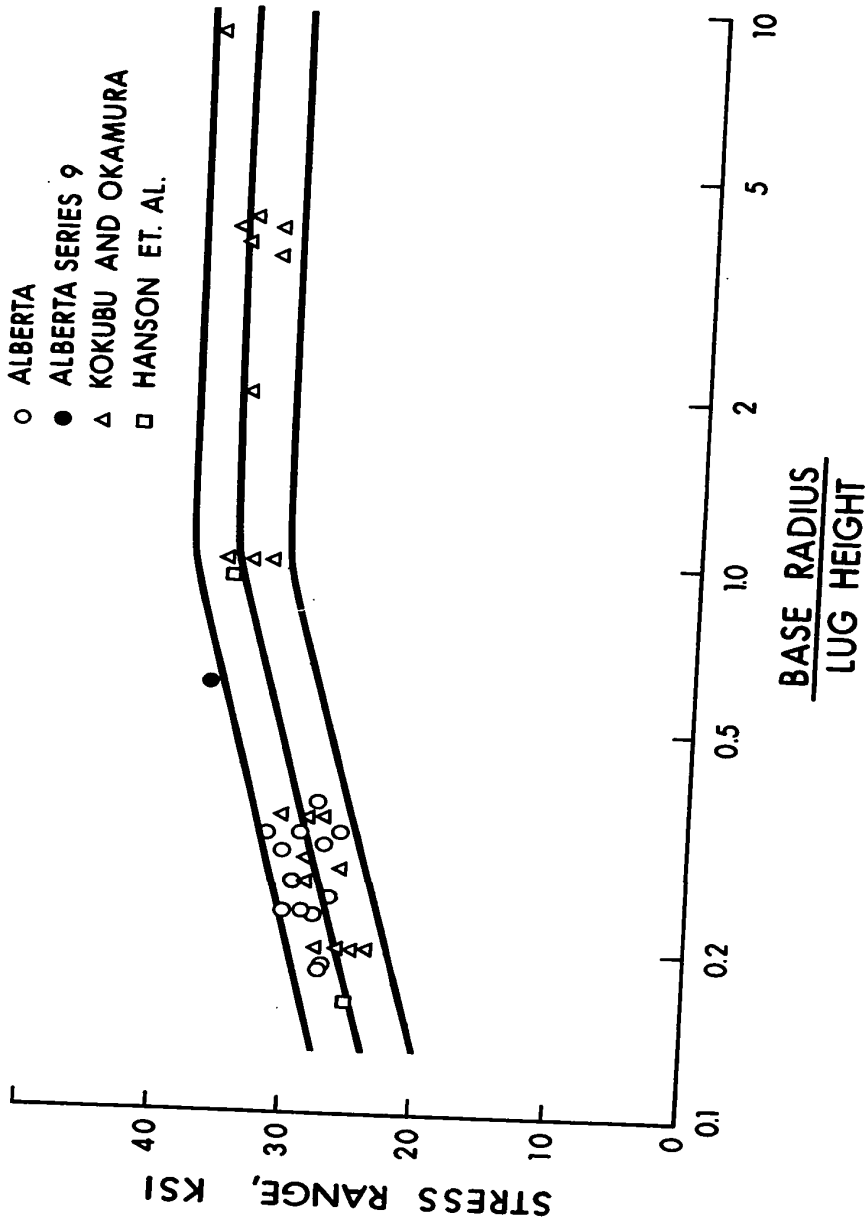
FIGURE 7-2   EFFECT OF r/h ON FATIGUE STRENGTH, $S_{min} = 0.1 f_y$

141

all the fatigue strengths were corrected to correspond to 0.1 f_y minimum
stress level using Modified Goodman Diagrams (see 7.2.3). Kokubu and
Okamura (26) mention "some bars were without arcs at their lug bases".
The data for these bars were plotted assuming the bars had a very small
lug base radius equal to one fifth of the lug height (16). In the case
of bars with the transverse lugs inclined to the bar axis at angles
other than 90 degrees, the radii were corrected to correspond to those
measured in the direction of the bar axis.

The test data in FIGURE 7.2, indicates that the fatigue strength
of the deformed bars is reduced when the ratio of radius to lug height
is less than about 1. It is interesting to note that the fatigue
strength is almost constant for r/h ratios greater than 1. These re-
sults again confirm stress concentration results presented in FIGURE
5.8.

It has been observed that the geometry of the deformations
varies with the condition of rolls. Thus, from the above discussion,
it may be expected that the fatigue strengths of bars rolled from fresh,
partially worn and fully worn rolls should differ.

Burton (13) tested bars produced using fresh, partially
worn and fully worn rolls. He found that the condition or folls had
minor influence on the fatigue strength.

Grönqvist (19) also studied the influence of the condition
of the rolls. His tests included bars rolled from fresh and fully
worn rolls for two deformation types. In one deformation type, there
was no appreciable difference due to the condition of rolls, but in the

other group, the fatigue strength of bars rolled from fully worn rolls was 39 percent higher than those of bars rolled from fresh rolls.

The fatigue data and the deformation geometry obtained from the above two investigations (13,19) is presented in Table 7.1. In this table, the data of the Alberta bars is also presented.

TABLE 7.1

INFLUENCE OF CONDITION OF ROLLS ON FATIGUE STRENGTH*

Data Source	Condition of Rolls	r in	h in	r/h	Fatigue Strength ksi
Burton (13)	Fresh Rolls	.015	.063	0.24	31.6
	Partially Worn Rolls	.018	.059	0.30	31.0
	Fully Worn Rolls	.020	.051	0.39	30.6
Grönqvist (19)	Fresh Rolls (Def. Type I)	.031	.051	0.61	33.0
	Fully Worn Rolls (Def. Type I)	.134	.024	5.6	46.8
	Fresh Rolls (Def. Type II)	.028	.040	0.7	40.0
	Fully Worn Rolls (Def. Type II)	.035	.035	1.0	41.2
Alberta	Fresh Rolls	.014	.076	0.19	28.0
	Fully Worn Rolls	.023	.071	0.32	31.2**

*At 2 million cycles

**This value was calculated from the analysis presented in section 7.3.

It may be noted in Table 7.1 that there was not appreciable variation in the fatigue strength due to the condition of the rolls except in one group of bars tested by Grönqvist. In this group of the r/h ratio increased from 0.61 to 5.6 for the two conditions of the rolls. This increase in r/h ratios is considerably larger than other tests reported in this table.

Although no bars rolled from fully worn rolls were tested in this project, the analysis presented in section 7.3 showed an increase of 3.2 ksi in the fatigue strength of these bars. This variation in the fatigue strength is of the same order as reported by others. From the above discussion it may be concluded that the influence of the condition of the rolls would largely depend on the extent of change in the geometry of the deformations. The fatigue strength of the bars rolled from fresh rolls in most cases would represent a lower bound of the fatigue strength of the bars.

7.2.3 Minimum Stress Level

The fatigue strength at various minimum stress levels is related to the type of steel and the applied stress function (2). In general, for hot rolled steels the stress range corresponding to any given fatigue life decreases with an increase in the minimum stress of the cycle.

Several investigators (9,11,12,23) have suggested that the fatigue strength is relatively insensitive to the minimum stress level. However, the statistical analysis of the beam data presented in section

6.4 found that S_{min} was a more significant variable than K_T and f_u. The fatigue strengths of bars at 0.4 f_y minimum stress level were significantly lower than those at 0.1 f_y minimum stress.

The fatigue limits of No. 8 bars of three grades at minimum stress levels of 0.1 and 0.4 f_y are compared using the Modified Goodman Diagrams shown in FIGURE 7.3. These figures were plotted for stress cycles corresponding to the fatigue strength at five million cycles. In a Goodman Diagram the average stresses in the cycles are plotted horizontally and the maximum and minimum stresses in the cycles are plotted vertically. It may be noted in this figure that straight line envelopes adequately represent the test data.

The straight line envelope to the Goodman diagram can be represented by Equation (7.1):

$$S_{max} = S_{f\ell} + S_{min} \left(\frac{f_u - S_{f\ell}}{f_u}\right) \qquad (7.2)$$

where S_{max} = maximum stress in a given cycle

S_{min} = minimum stress in the cycle

$S_{f\ell}$ = stress range in a cycle having minimum stress
            equal to zero

f_u = tensile strength of material

Although this conclusion differs from that reached by other investigators (9,11,12), it is supported by Goodman diagrams (29) for data from other investigations of hot rolled reinforcing bars (11,12).
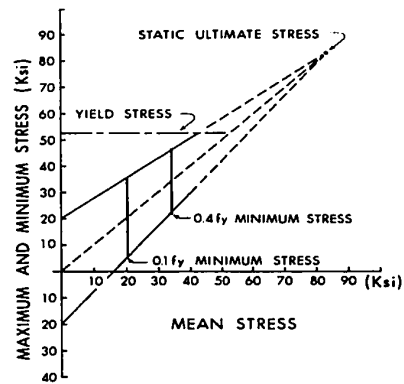
(a) GRADE 40
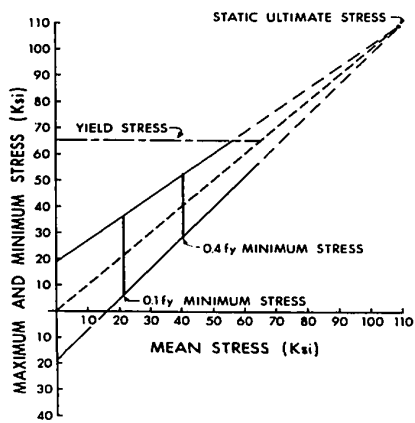
(b) GRADE 60
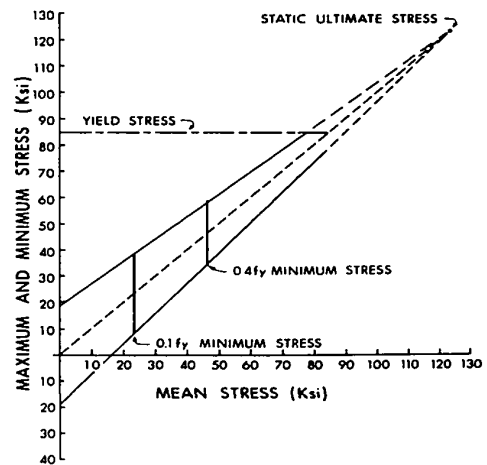
(c) GRADE 75

FIGURE 7-3 MODIFIED GOODMAN DIAGRAMS FOR
NO. 8 BARS (BEAM TESTS)

In a recently reported investigation, Hanson, et.al. (16), also support the above conclusion in the finite life region of the S-N curve. Their test program included Nos. 5, 8 and 11 bars of Grade 60 steel, and minimum stress levels of -0.1 f_y, 0.1 f_y and 0.3 f_y. The statistical analysis of their test data in the finite life region showed that the minimum stress level was a more significant variable than bar grade and bar diameter.

The Alberta tests and the other investigations suggest that the minimum stress level should be taken into account in design specifications.

7.2.4 Bar Diameter

In metal fatigue literature, it is generally concluded that the fatigue strength of small specimens with significant stress gradients due to notching or flexural loading is affected by size (2). Thus, the fatigue strength of machined specimens tends to increase as the specimen diameter is reduced below about 3/8 in. The size effect tends to disappear, however, in specimens comparable in size to most reinforcing bars.

For hot rolled reinforcing bars of identical manufacturing process and geometrically similar deformations, Wascheidt (11) reports that bars equivalent to No. 8 bars had 5 to 10 percent lower fatigue strength than those equivalent to No. 5 bars. These tests were in agreement with the observations made on multi-rib TOR-STAHL by several investigators in Germany.

Kokubu and Okamura (18) also observed a small decrease in fatigue strength with an increase in bar size for both plain and deformed bars. The tests included bars having diameters equivalent to No. 6 and No. 8 bars. The bars of both sizes were manufactured using the same manufacturing process and had similar deformation patterns.

Recent tests results reported by Hanson et.al (16) partly support the above results. Their tests included five bar sizes; Nos. 5, 6, 8, 10 and 11. The experimental observations and statistical analyses showed that No. 6 bars had the highest fatigue strength, followed by No. 5, No. 8, No. 11 and No. 10. The authors suggest that the irregular ranking of fatigue strength was due to the differences at the base of the deformations. These tests, however, suggest an overall trend similar to reported by Wascheidt and Kokubu, et.al.

Alberta tests included Nos. 5, 8 and 10 bars of Grade 40, 60 and 75 steels. The statistical analysis of all the beam tests having finite life suggested that the nominal diameter and the grain size were both significant variables, the grain size being more significant than the nominal bar diameter (see Appendix E.3). The fatigue strength decreased with an increase in the bar nominal diameter or an increase in the grain size of steel. The grain size of the steel was included in the multiple regression analysis as a non-specified variable because metallographical observations indicated that grain size increased with an increase in the bar diameter as shown in FIGURES 4.5 to 4.8.

The fatigue strengths of deformed bars at 5 million cycles reported in TABLE 6.4, also suggest a trend similar to that reported by other investigators (11,16,18). In general, fatigue strength of bars decreased about 5 percent from No. 5 bars to No. 8 and about 5 percent from No. 8 bars to No. 10 bars with the exception of No. 5 Grade 75 bars.

The No. 5 Grade 75 bars (Series 9) had an extremely fine grain structure as shown in FIGURE 4.7(c) and they had a r/h ratio of 0.74 as compared to an average value of 0.32 for the remaining eight types of bars in Phase I. The fatigue strength of the Series 9 bars was 28 percent higher than the remaining No. 5, 8 and 10 bars. Although a correction was made in the fatigue strength, by an analysis presented in section 7.3, to account for their higher r/h ratio, their measured fatigue strength was still 15 percent higher than the computed value. As a result, it may be concluded that the exceptionally high fatigue strength obtained for No. 5 Grade 75 bars was partly due to their extremely small grain size. From the steel chemistry of these bars (Appendix A), it was noted that these bars had a higher vanadium content than the other No. 5 bars. This alloying agent was probably responsible for the fine grain structure of these bars.

Due to the different fatigue strength and grain size of the No. 5 Grade 75 bars (see FIGURE 6.15 and FIGURES 4.5 to 4.8), the test data of these bars was excluded from the beam test data, and the multiple regression analysis was again performed on the remaining data. This analysis rejected both the bar diameter and grain size as signifi-

cant variables.

The above discussion suggests that although an increase in the grain size reduces the fatigue strength, the variation in the grain sizes of all but No. 5 Grade 75 bars was not large enough to cause a significant variation in the fatigue strengths. Hence, the influence of bar diameter or grain size in most of the reinforcing bars is small and should not be included in the design.

7.2.5 Grade of Steel

The influence of no other variable on fatigue strength has been more extensively investigated than the grade of reinforcing bars. In six major projects (11,12,16-19), grade of steel was selected as one of the specified variables in the tests. Three grade of steels; Grade 40, 60 and 75 in North America and equivalent grades in other parts of the world have been commonly used.

Findings from several projects (11,12,16,18,19) suggest that the fatigue strength of deformed reinforcing bars is insensitive to the grade of steel. These tests included reinforcing bars of numerous deformation types, bar sizes varying from No. 5 to No. 11 and tensile strengths ranging from 75 to 130 ksi.

Contrary to the above conclusion, Grade 75 bars showed much higher fatigue strength than Grade 40 and 60 bars of similar deformation type in tests at Queens University, Ontario (17). Twenty beams containing No. 5 bars were tested at 0.25 f_y minimum stress level. The fatigue strengths of Grade 40, 60 and 75 bars at 2 million cycles were observed to be 29.3, 32.7 and 39.3 ksi, respectively.

The beam tests in Phase I of the present test program included bars of three grades and three bar sizes. The fatigue strengths of bars at 5 million cycles for all but one test series, were 28.8 to 31.7 ksi at 0.1 f_y minimum stress level. The exception as mentioned earlier was series 9 (Grade 75 No. 5) which had a fatigue strength of 36.5 ksi.

The Grade 75 bars used in this project and at Queen's University had similar deformations and in fact, came from the same rolling plant. In sections 7.2.2.3 and 7.2.5, it was explained that the higher fatigue strength obtained for the Series 9 bars was due their higher r/h ratio and finer grain size than remaining bars. It is quite possible that both the bars had similar grain sizes and similar deformation geometry.

Because the deformation geometry, grain size and fatigue strength of the No. 5 Grade 75 bars discussed above are not common among the most of the American bars the results of these bars have limited applicability and were excluded from the analyses of the data. On the other hand, the reasons for enhanced fatigue strength of these particular bars should be studied more fully in future test series.

The tests in Phase II consisted of deformed bars of two grades. These bars were rolled in two successive passes through the same rolls. The geometrical dimensions of the deformations were measured to be the same. The statistical analysis of finite and long life data showed no significant difference between the fatigue strengths of Grade 40 and 60 bars (see Tables 6.2 and 6.3 and FIGURE 6.7). This supports

the beam test results and the conclusions arrived by previous researchers.

As mentioned earlier, however, the fatigue strength of machined polished specimens was a linear function of the tensile strength as shown in FIGURES 6.8 and 6.9.

The inconsistency in the effect of grade on fatigue strength on deformed bars, as-rolled bars and machined polished specimens is due to the interaction of the effects of stress concentrations and the grade of steel. The multiple regression analysis of the test data showed that the reduction in fatigue strength due to stress concentrations was higher for higher grade of bars. Thus, although the fatigue strength of the bar metal improves with an increase in grade, this is offset by a greater susceptability to stress concentrations.

7.2.6 Miscellaneous Factors

(a) Manufacturing Process

The details of manufacturing process of the deformed bars were discussed in section 2.2.2. There are two important aspects of this process; the chemistry of the steel and the rolling process.

A direct correlation between the fatigue strength and the chemical composition of steel has not been found. The chemistry of steel influences the tensile strength, grain size and the ductility, which in turn influence the fatigue properties. The observations made in this project suggest that steels having finer grain structure show a higher fatigue strength.

Two major factors; the decarburization of the billet surface

and the shape of rolling pass seem to have a pronounced influence on fatigue strength. Both these variables have been discussed previously.

(b) Bar Bends, Tack Welding or Stirrups and Welded Joints

Rehm (10,56) and Pfister and Hognestad (12) have reported tests on bar bends in concrete beams. In both projects a severe reduction in fatigue strength was observed due to bends. The fatigue strength of deformed bars bent through an angle of 45 degrees around a mandrel having diameters ranging from 6 to 8 times the nominal bar diameter were found to be about 50 percent of that of straight bars.

The fatigue strength of reinforcing bars was considerably lower for bars to which stirrups had been welded rather than tied (14). In these tests the stirrups were welded to the main reinforcement in a manner to simulate careless field practice.

The bars of both Grade 40 and 60 showed fatigue strengths of about 20 ksi as compared to 31 ksi for unwelded bars. A similar reduction in the fatigue strength was observed by Sanders, et.al. (21) and Walls, et.al. (22) when deformed bars were joined by welding.

7.3 An Engineering Method of Estimating Fatigue Strength

7.3.1 Approach

The empirical equations developed in section 7.2 and the method suggested by Kuhn and Hardrath (57) are used to estimate the fatigue strength of deformed reinforcing bars in concrete beams. The proposed method gives a reasonably good estimate of the fatigue strength at long life of deformed bars in concrete beams.

As explained earlier in section 7.2, the fatigue strength of the steel in the bar is reduced by two factors; the deformations and the decarburization of the bar surface. Both these variables were assumed to cause stress concentrations. The theoretical stress concentration factor K_T caused by the deformations is determined from FIGURE 5.8 and that due to decarburization from section 7.2.2.2. The fatigue strength reduction factor K_f is obtained from reference (57) for a given value of K_T, f_u and notch base radius.

The fatigue strength of the steel in the bar (S_{mf}) is calculated from equation (7.1). By applying the fatigue strength reduction factor K_f due to decarburization the fatigue strength of plain as-rolled bars is obtained. Using this strength and the K_f due to deformations the fatigue strength of deformed bars (S_{Df}) is calculated. It is assumed in this calculation that the two stress concentrations are cumulative. Thus, it is assumed that the amplified stresses due to the decarburization and surface roughness occur in the layer immediately adjacent to the surface and these high stresses are, in turn, amplified by the stress concentrations due to deformations.

The fatigue strength values calculated in this way are for a cycle having a minimum stress equal to zero. Therefore, a correction is made using Equation (7.2) for the appropriate minimum stress level corresponding to the actual tests.

Finally, the fatigue strength of bars is increased by 2 ksi to account for the influence of concrete encasement as described in section 7.2.1.

The above method indirectly accounts for the effect of bar size because of the relationship between K_T and K_f is a function of the absolute radius at the base of lug.

7.3.2 Application to the Analysis of Fatigue Data

The method outlined in section 7.3.1 could only be applied to the published tests which provided adequate data for the deformation geometry. Thus, the calculations presented in Table 7.2 include the fatigue tests of this project and those of references (12,15).

It may be noted from Table 7.2 that average difference between the calculated and observed fatigue strengths was 00.45 ksi with a standard deviation of 1.93 ksi.

TABLE 7.2

STRESS CONCENTRATION FACTORS AND COMPUTED FATIGUE STRENGTH

Data Source (1)	Bar Size (2)	f_u (3)	S_{min} (4)	K_T (5)	K_f (6)	Calculated S_f (S_{min} = 0)			Calc. $S_{CR}*$ (10)	Test S_R (11)	$S_{CR} - S_R$ (12)
						Machined Polished (7)	As-rolled (8)	Deformed Bars (9)			
	No.	ksi	ksi			ksi	ksi	ksi	ksi	ksi	
ALBERTA TESTS (Phase I) Beam Tests											
Series 1	8	83.1	5.2	2.06	1.55	56.1	40.4	26.1	27.1	30.2	- 3.1
2	8	109.0	6.8	2.14	1.68	72.8	47.26	28.1	29.0	30.5	- 1.5
3	8	123.5	8.3	2.05	1.72	82.2	51.1	29.7	29.3	30.7	+ 1.4
4	8	83.1	21.2	2.06	1.55	56.1	40.4	26.1	23.3	25.6	- 2.3
5	8	109.0	28.2	2.14	1.68	72.8	47.3	28.1	24.9	25.5	- 0.6
6	8	123.5	34.4	2.05	1.72	82.2	51.1	29.7	25.7	24.9	+ 0.8
7	5	76.3	5.0	2.08	1.52	51.6	40.6	26.7	27.5	30.5	- 3.0
8	5	109.2	6.6	2.03	1.60	73.0	47.3	29.6	30.4	31.3	- 0.9
9	5	122.1	8.9	1.81	1.56	81.4	50.7	32.5	33.2	38.3	- 5.1**
10	10	83.1	5.0	2.09	1.57	56.1	40.4	25.7	26.8	30.0	- 3.2
11	10	110.5	6.4	2.10	1.68	73.8	47.7	28.4	29.3	28.8	+ 0.5
12	10	109.5	8.3	2.12	1.69	73.2	47.4	28.0	28.9	29.3	- 0.4
13 (bar in air)	8	83.1	5.2	2.06	1.55	56.1	40.4	26.1	24.6	28.0	- 3.4

157

TABLE 7.2 (continued)

Data Source	Bar Size	f_u	S_{min}	K_T	K_f	Calculated $S_f(S_{min}=0)$			Calc. $S_{CR}*$	Test S_R	$S_{CR}-S_R$
(1)	(2)	(3)	(4)	(5)	(6)	Machined Polished (7)	As-rolled (8)	Deformed Bars (9)	(10)	(11)	(12)
ALBERTA TESTS (Phase II) Tests in Air											
Series 1	8	81.5	5.0	2.16	1.59	55.1	39.9	25.1	23.9	25.7	-1.8
2	8	98.8	6.7	2.16	1.66	66.3	44.5	26.8	25.4	26.0	-0.6
3	8	86.3	5.0	--	--	58.2	41.2	--	38.9	37.6	+1.3
4	8	100.1	6.7	--	--	67.1	44.9	--	42.3	42.0	+0.3
5	8	86.3	5.0	--	--	58.1	41.2	--	39.9	37.6	+1.3
6	8	100.1	6.7	--	--	67.1	44.9	--	42.3	42.0	+0.3
7	-	81.5	5.0	--	--	55.0	--	--	--	55.0	0.0
8	-	98.8	6.7	--	--	66.2	--	--	--	65.2	+1.0
PCA Tests (1964) Beam Tests											
Deformation Type A-G40	8	76.2	4.3	1.52	1.30	51.6	38.6	29.7	30.8	35.2	-4.4
A-G40	8	76.2	12.9	1.52	1.30	51.6	38.6	29.7	29.1	33.3	-4.2
A-G60	8	117.5	6.0	1.52	1.36	78.4	49.5	36.1	36.5	34.4	+2.1
A-G60	8	117.5	19.0	1.52	1.36	78.4	49.5	36.1	33.6	31.5	+2.1

TABLE 7.2 (continued)

158

Data Source (1)	Bar. Size (2)	f_u (3)	S_{min} (4)	K_T (5)	K_f (6)	Calculated $S_f(S_{min} = 0)$			Calc. S_{CR}* (10)	Test S_R (11)	$S_{CR} - S_R$ (12)
						Machined Polished (7)	As-rolled (8)	Deformed Bars (9)			
A-G75	8	127.5	9.0	1.52	1.37	84.8	52.2	38.1	38.1	39.1	- 1.0
A-G75	8	127.5	27.0	1.52	1.37	84.8	52.2	38.1	34.0	33.0	+ 1.0
B-G40	8	82.4	4.9	1.62	1.32	55.6	40.2	30.5	31.5	34.7	- 3.2
B-G40	8	82.4	14.5	1.62	1.32	55.6	40.2	30.5	28.6	30.3	- 1.7
B-G75	8	126.8	8.1	1.62	1.40	84.4	52.0	37.1	37.9	37.6	+ 0.3
B-G75	8	126.8	24.4	1.62	1.40	84.4	52.0	37.1	33.5	32.3	+ 1.2
C-G75	8	122.5	9.3	1.84	1.50	81.6	50.8	33.8	33.7	32.2	+ 1.5
C-G75	8	122.5	29.1	1.84	1.50	81.6	50.8	33.8	29.7	27.1	+ 2.6
PCA Tests (1967)											
Lugs Horizontal	8	74.7	4.7	2.02	1.44	50.6	38.1	26.5	28.2	28.3	- 0.1
Lugs Vertical	8	74.7	4.7	2.02	1.44	50.6	38.1	26.5	28.2	26.7	+ 1.5
Lugs Horizontal	8	108.4	5.1	2.02	1.49	72.5	47.1	31.6	32.8	32.5	+ 0.3
Lugs Vertical	8	108.4	5.1	2.02	1.49	72.5	47.1	31.6	32.8	31.0	+ 1.8

*Corrected for S_{min} and concrete encasement
**Bar with exceptionally fine grain

CHAPTER VIII

DESIGN SPECIFICATIONS

In this chapter, the current specifications for deformed bars which influence the fatigue strength are examined. A proposal is made for the inclusion of an additional clause in the deformation specifications to improve the fatigue strength of deformed bars.

A specification for permissible stresses under repeated loading for commercially available deformed bars is developed from the findings of this project and the published North American test data. This specification is compared with the one recently proposed by Hanson, et.al. (16).

8.1 Comparison of Specifications from Various Codes

As previously explained, two parameters of the deformed bar surface; the decarburization and the deformations significantly reduce the fatigue strength of reinforcing bars. Of these two variables, only the deformation details are controlled by the code requirements for practical reasons.

In Table 8.1, the deformation and fatigue strength requirements from various codes are compared. Only those deformation requirements which are relevant to the fatigue strength are given in this table. It is interesting to note that the Swiss code (5) has no requirements for the deformations, whereas the remaining codes essentially

159

CHAPTER VIII

DESIGN SPECIFICATIONS

In this chapter, the current specifications for deformed bars which influence the fatigue strength are examined. A proposal is made for the inclusion of an additional clause in the deformation specifications to improve the fatigue strength of deformed bars.

A specification for permissible stresses under repeated loading for commercially available deformed bars is developed from the findings of this project and the published North American test data. This specification is compared with the one recently proposed by Hanson, et.al. (16).

8.1 Comparison of Specifications from Various Codes

As previously explained, two parameters of the deformed bar surface; the decarburization and the deformations significantly reduce the fatigue strength of reinforcing bars. Of these two variables, only the deformation details are controlled by the code requirements for practical reasons.

In Table 8.1, the deformation and fatigue strength requirements from various codes are compared. Only those deformation requirements which are relevant to the fatigue strength are given in this table. It is interesting to note that the Swiss code (5) has no requirements for the deformations, whereas the remaining codes essentially

159

TABLE 8.1

COMPARISON OF FATIGUE STRENGTH AND DEFORMATION

SPECIFICATIONS FROM VARIOUS CODE

Code	Deformation Specification*					Fatigue Strength Specification
	Minimum Lug Height (h)	Minimum Lug Width (2w)	Maximum Lug Spacing (ℓ)	Minimum Lug face Angle, degrees (θ)	Remarks	
ASTM (3)	$.05\ D_{nom}$	---	$0.7\ D_{nom}$	45	---	No clause on fatigue strength
Swiss (5)	---	---	---	---	No specifications on deformations	Stress range at 2×10^6 cycles, ksi <table><tr><td>Rating</td><td>$S_{min}=0$</td><td>$S_{min} = \frac{1}{2} S_{max}$</td></tr><tr><td>Bad</td><td>28.1</td><td>23.9</td></tr><tr><td>Good</td><td>35.2</td><td>28.1</td></tr><tr><td>Very Good</td><td>42.2</td><td>--</td></tr></table>Fatigue strength data to be supplied by producer
German (4)	$.05\ D_{nom}$	$0.1\ D_{nom}$	$0.8\ D_{nom}$	45	Minimum relative rib area (f_R) specified	Fatigue strength of bars to be supplied by manufacturer
Japanese (6)	$.05\ D_{nom}$	---	$0.7\ D_{nom}$	45	$h \leq 0.1\ D_{nom}$	No clause on fatigue strength
Canadian (7)	$0.05 D_{nom}$	---	$0.7\ D_{nom}$	45		No clause on fatigue strength

*For No. 5 or higher size bars

have similar requirements for deformations. The German code provides elaborate details of the deformation lug parameters (4). The minimum relative rib area (f_R) requirement of the German code is intended to control the bond properties. This requirement although not specified in other codes is actually satisfied indirectly. As discussed earlier in section 7.2.1, this requirement would lead to a higher fatigue strength for bars in concrete beams than in air.

The German and Swiss codes (4,5) require the bar manufacturer to furnish fatigue strength data if the bars are to be used for structures predominantly under repeated loads. The Swiss code gives guidelines to distinguish between bars of good and bad fatigue strengths. This code also takes into account the influence of minimum stress level. The North American and Japanese codes have no specifications or guidelines for the fatigue strength.

Two approaches can be used to improving the fatigue strength of reinforcing bars. Either the producer can be required to provide fatigue data as required in some European codes (4,5) or a clause could be introduced in the deformation specifications to insure an improved fatigue strength.

The findings of this project and previous fatigue test data suggest that an additional clause specifying minimum lug base radius to lug height (r/h) equal to 1.25 should be included into the ASMT (A615-68) specifications. It should be noted that this additional clause does not violate any of the current ASTM specifications on deformed bars.

8.2 Proposed Specifications

Although the test data from this project by itself is not sufficiently broad to allow the development of fatigue strength design specifications, the large number of published tests on North American bars makes this objective possible.

FIGURE 8.1 shows all the tests reported on North American bars and the Alberta results. The test specimens plotted included three grades; G40, 60 and 75 steels, bar sizes ranging from No. 5 to No. 11 and minimum stress levels from -0.1 f_y to 0.3 f_y.

Two tolerance limits are shown in FIGURE 8.1, the tolerance limit on the Alberta tests is higher than that proposed by Hanson, et.al. indicating that bars tested in this project had better fatigue strengths than those tested in some of the other projects.

The tolerance limit obtained by Hanson, et.al. on the fatigue test results of 236 beams is also a lower limit for all the North American test data as may be seen in FIGURE 8.1. On the basis of this conclusion Hanson, et.al. (16) proposed the following design equation:

$$S_r = [40 - 19(\log N-5)](1.13 - 0.67 \frac{S_{min}}{f_y}) \qquad (8.1)$$

The above relationship was obtained by assuming linear relationship between stress range and design life for design life less than one million cycles and constant stress range for life greater than one million cycles.

From FIGURE 8.1, it may be noted that the fatigue life of
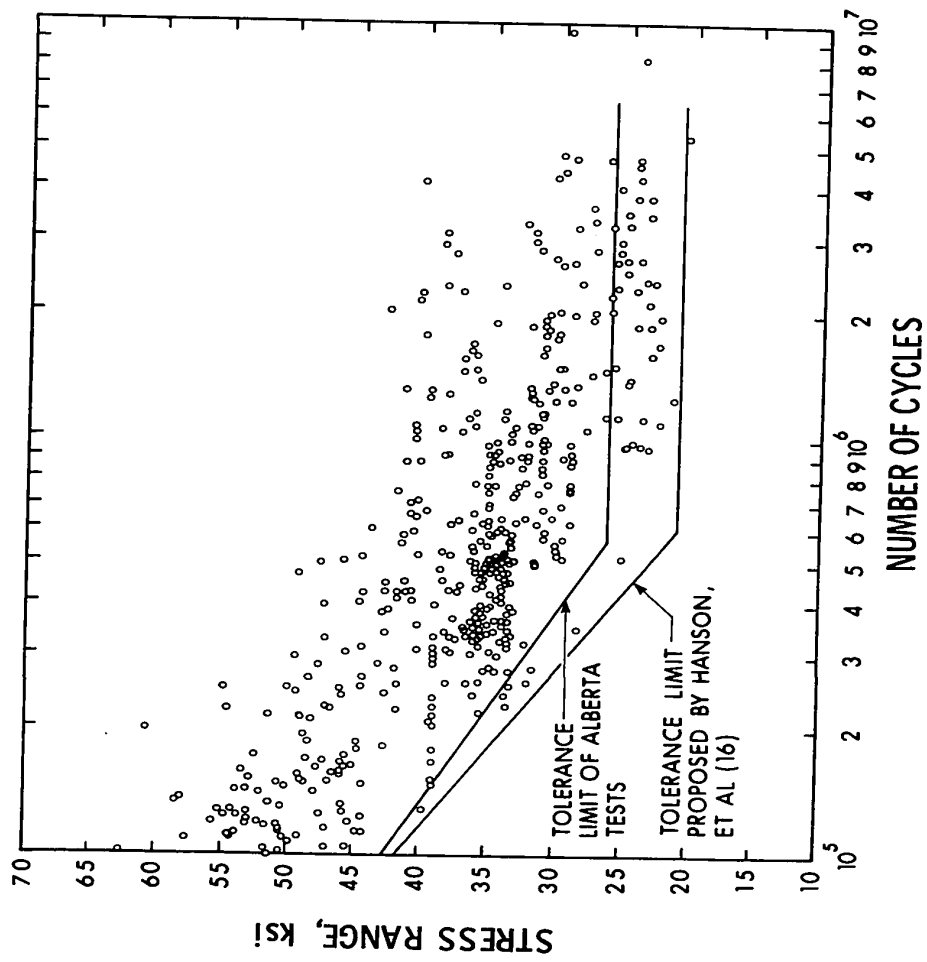
FIGURE 8-1 COMPARISON OF TOLERANCE LIMITS WITH PUBLISHED FATIGUE DATA

all reported tests is greater than 100,000 cycles at 40 ksi stress range and at stress range equal to 21 ksi the fatigue life of specimens was greater than one million cycles. Based on these observations and assuming a linear relationship between stress range (S_r) and design life (N) equation (8.2) was obtained.

$$S_r = 40 - 19(\log N-5) \qquad (8.2)$$

The minimum stress levels of specimens reported in FIGURE 8.1 varied between $-0.1 \ f_y$ to $0.3 \ f_y$. Assuming conservatively that the lower limit of the test data corresponded to a minimum stress level of $0.2 \ f_y$, Equation (8.3) is obtained by using the Modified Goodman equation (7.1).

$$S_r = [40 - 19(\log N-5)] \ \frac{(1 + \frac{0.2 \ f_y}{f_u})}{(1 + \frac{S_{min}}{f_u})} \qquad (8.3)$$

The ratio f_y to f_u of reinforcing bar reported in FIGURE 8.1 ranged from 0.58 to 0.76. Using the average value of 0.67 in the equation (8.3), equation (8.4) is obtained:

$$S_r = \frac{[45.5 - 21.5(\log N-5)]}{(1 + \frac{2}{3} \ \frac{S_{min}}{f_y})} \qquad (8.4)$$

The calculated values of stress range obtained from equation

(8.4) are given in Table 8.2 for given design life and minimum stress levels.

TABLE 8.2

PERMISSIBLE STRESS RANGE IN DEFORMED

BARS UNDER REPEATED LOADS, ksi

Minimum Stress	Design Life (Cycles)		
	100,000	500,000	1,000,000 and over
0.0	45	30	24
0.2 f_y	40	28	21
0.4 f_y	36	24	19

The design relationship given by Equation (8.4) and Table 8.2 has slightly less variation due to minimum stress levels than the relationship proposed by Hanson et.al. (Equation (8.1)).

Proposed Specification

The stress range in a deformed reinforcing bar meeting ASTM (A615-68) specification, under repeated application of service loads, shall not exceed

$$S_r = [45.5 - 21.5(\log N{-}5)]/(1 + \frac{2}{3}\frac{S_{min}}{f_y})$$

where

S_r = stress range, in ksi

N = design fatigue life

S_{min} = minimum stress level, considering tensile stress positive and compressive stress negative

f_y = specified yield strength of bar

The value of S_r at N equal to 1 million cycles may be used for all greater values of N.

Higher stress ranges may be permitted if guaranteed by the manufacturer based on fatigue tests on similar bars.

CHAPTER IX
CONCLUSIONS

9.1 Summary .

An investigation of the fatigue behavior of reinforcing bars has been presented. The investigation included fatigue tests, metallographical observations and stress concentration analyses. In all, thirteen types of plain and deformed bars were tested. Fatigue tests were made on concrete beams, reinforcing bar specimens and machined polished specimens.

The fatigue test results were analysed statistically and the findings were compared with previous results. The fatigue behavior of bars in concrete beams and in air were explained on the basis of metallographical observations and stress concentration analyses.

A number of specifications and codes dealing with the details of reinforcing bar deformations were compared and discussed. An additional clause has been proposed which would alter the shape of deformations in order to improve the fatigue strength of reinforcing bars. A design relationship between the fatigue strength of bars, design life and minimum stress level was also proposed.

167

9.2 Conclusions

The principal conclusions from this project are as follows:

A. **Effect of Bar Surface Characteristics on Fatigue Strength**

1. The fatigue strength of deformed bars is considerably reduced by deformations, surface decarburization and roughness. Ordinary and mill scale did not influence the fatigue strength of the bars for the cases investigated.

2. The detrimental influences of the deformations, decarburization and surface roughness may be estimated by the stress concentration theory. The average value of the fatigue strength reduction factor, K_f, due to deformations was 1.60 and that due to decarburization and roughness was 1.41 in these tests. These were found to be cumulative in effect.

3. The influence of the theoretical stress concentration factor, K_T, was more severe on higher grade steels.

4. The effect of the ratio of the lug base radius to lug height (r/h) on the value of K_T was more pronounced than the effects of all other parameters defining the shape of the deformations. The value of K_T decreased with an increase in the r/h ratio. However, for values of r/h greater than 1, this decrease was not appreciable.

5. A ratio of r/h equal to 1.25 was found to be optimum for good fatigue strength.

6. Fatigue failures always initiated at the bases of transverse lugs. The suggestion made by several previous investigators

that the intersections of lugs are a more critical stress
concentration than the lug bases was not supported by the
strain measurements or the crack initiation and growth
studies conducted on the failure surfaces. The latter
studies indicated that several independent cracks
initiated in the weak decarburized layer at the bases
of lugs and that these cracks were responsible for the
fatigue failure.

7.   The influence of the wearing of rolls on the fatigue
strength of bars depended on the extent of the change of
the deformation geometry. The computed fatigue strength
of the bars rolled from fully worn rolls was about 3.2 ksi
higher than that observed for bars produced from new
rolls.

B.   Effect of Minimum Stress Level on Fatigue Strength

The fatigue strength of the bars decreased with an increase
in the minimum stress level from 0.1 f_y to 0.4 f_y of No. 8
Grade 75 bars. Statistically the minimum stress level was
a more significant variable than grade of steel and nominal
diameter of the bar. Consequently, the minimum stress level
was included in the proposed allowable fatigue strength
formula given in Chapter VIII. This recommendation is not
in agreement with several previous proposals to exclude the
minimum stress level from the design relationship. The
test data at various minimum stress levels of this and other

projects may be represented by a Modified Goodman Law.

C. **Effect of Bar Size on Fatigue Strength**

Although there was a decrease of about 5 percent in the average fatigue limits of bars with an increase in the bar size from No. 5 to No. 8 and No. 8 to No. 10 bars, this decrease was not found to be statistically significant in the data having fatigue lives less than one million cycles.

An exceptionally high fatigue strength was obtained for the No. 5 Grade 75 bars. The fatigue strength of these bars at 5 million cycles was 36.5 ksi as compared to an average of 30.0 ksi for the remaining bars. This difference was attributed to their relatively higher r/h ratio and finer grain size. Further research is warranted to study the cause of this favorable behavior.

D. **Effect of Bar Grade on Fatigue Strength**

The fatigue strength of deformed bars was found to be insensitive to the grade of steel (G40, 60 and 75). This conclusion is in agreement with previous findings.

In contrast to the above, the fatigue strength of the bar steel increased linearly with the grade of the bar and was about 2.19 times greater than that of deformed bars.

The fatigue strength of the plain as-rolled bars also increased with the bar grade, however, this increase was not as marked as that of bar steel. On an average, the fatigue strength of the plain as-rolled bars was 1.55 times greater

than that of the deformed bars.

The reduced fatigue strength of the plain as-rolled bars as
compared to that of the bar metal was attributed to the
decarburization and roughness of the as-rolled surface.

The further reduction in fatigue strength occurred between
the plain as-rolled bars and deformed bars due to the de-
formations.

9.3 Recommendations

A. Proposed Specification

The proposed specification on the fatigue strength of de-
formed bars outlined in Chapter VIII was based on the all
existing test data on North American deformed bars. Though
the fatigue strengths of the bars investigated in this project
were considerably higher than those obtained from the pro-
posed permissible stresses, the higher strength can not be
counted on unless a change is made in the deformation clause
of the ASTM Standard.

B. Suggestions for Future Research

Since it is easier and more economical to test deformed bars
in air than to test them in concrete beams, it is recommended
that future tests should be performed on deformed bar speci-
mens in air. The existing test data indicates that the fatigue
strengths of the bars in air should be about 2 to 2.5 ksi less
than that in the beam tests.

Future research should be oriented towards improving the fatigue strength of deformed bars. The first step in this direction would be to improve deformation details. The findings of this project strongly suggest that bars having a lug base radius to lug height equal to 1.25 should exhibit optimum fatigue strength. This aspect of the problem needs further investigation. Suitable field techniques should be developed to measure the lug base radius.

The reasons for the desirable behavior of the No. 5 Grade 75 bars in this test series also warrant more study.

LIST OF REFERENCES

1. Hognestad, Eivind, "Trend in Consumer Demands for New Grades of Reinforcing Steel", Proceedings Fall Business Meeting, Concrete Reinforcing Steel Institute, 1967, pp. 22-32, PCA Development Department Bulletin D130.

2. Forrest, P.G., Fatigue of Metals, Pergamon Press, 1962.

3. "Standard Specification for Deformed Billet-Steel Bars for Concrete Reinforcement, A615-68", American Society for Testing and Materials, Philadelphia, 1968.

4. Technische Baubestimmungen DIN 488 (1968) Beuth-Vertrieb, Berlin, Germany.

5. Schweizericher Inginier-Und Architektenverein (SIA), "Norm für die Berechnung, konstruktion und Ausführung von Bauwerken ans Beton, Stahlbeton und spannbeton", Norm Nr. 162, SIA, Zurich, 1968, 88 pp.

6. Japanese Industrial Standards G3112, Japanese Society of Civil Engineers, Tokyo.

7. "Specifications for Deformed Billet-Steel Bars for Concrete Reinforcement with 60,000 psi Minimum Yield Point", G30.10-1964, Canadian Standards Association, Ottawa.

8. "Standard Specification for Highway Bridges", American Association of State Highway Officials, 1961, Washington, D.C.

9. Rehm, Gallus, "Contribution to the Problem of Fatigue Strength of Steel Bars for Concrete Reinforcement", (In German with English and French Summaries), 6th Congress Preliminary Publication, International Association for Bridge and Structural Engineers, Stockholm, 1960, pp. 35-46.

10. Soretz, S., "Fatigue Behavior of High Yield Stress Reinforcement", Concrete and Constructional Engineering, Vol. 60, No. 7, July 1965, pp. 272-280.

11. Wascheidt, M., "Zur Frage der Duerschwingfestigkeit von Befonstählen in einbetonierten Zustand (On the Fatigue Strength of Embedded Concrete Reinforcing Steels)", Doctoral Thesis, Technical University of Achen, Germany, 1965, also abbreviated version, Technische Mutteilungen Krupp-Forschungsberichte, Vol. 24, No. 4, 1966, pp. 173-196.

12. Pfister, J.F., and Hognestad, E., "High Strength Bars as Concrete Reinforcement, Part 6, Fatigue Tests", Journal of the PCA Research and Development Laboratories, Vol. 6, No. 1, January 1964, pp. 65-84; PCA Development Department Bulletin D74.

13. Burton, K.T., "Fatigue Tests of Reinforcing Bars", Journal of the PCA Research and Development Laboratories, Vol. 7, No. 3, September 1965, pp. 13-23; PCA Development Bulletin D93.

14. Burton, K.T., and Hognestad, E., "Fatigue Tests of Reinforcing Bars - Tack Welding of Stirrups", Journal of American Concrete Institute, Proceedings, Vol. 64, No. 5, May 1967, pp. 244-252, PCA Development Bulletin D116.

15. Hanson, J.M., Burton, K.T. and Hognestad, E., "Fatigue Tests of Reinforcing Bars - Effect of Deformation Pattern", Journal of the PCA Research and Development Laboratories, Vol. 10, No. 3, September 1968, pp. 2-13; PCA Development Bulletin D145.

16. Hanson, J.M., Somes, N.F., Helgason, , Coorley, W.G., and Hognestad, E., "Fatigue Strength of High Yield Reinforcing Bars", Interim Report, National Cooperative Highway Research Program, Project No. 4-7, Highway Research Board, Feb. 1970. 45 pp.

17. Lash, S.D., "Can High-Strength Reinforcement be Used for Highway Bridges", First International Symposium - Concrete Bridge Design, ACI Publication SP-23, American Concrete Institute, Detroit, 1969, pp. 283-299.

18. Kokubu, M., and Okamura, H., "Fatigue Behavior of High Strength Deformed Bars in Reinforced Concrete Bridges", First International Symposium - Concrete Bridge Design, ACI Publication SP-23, American Concrete Institute, Detroit, 1969, pp. 301-316.

19. Grönqvist, Nils-Ove, "Fatigue Strength of Reinforcing Bars", Second International Symposium - Concrete Bridge Design, ACI Publication SP-26, American Concrete Institute, Detroit, 1969, pp. 1011-1059.

20. Grönqvist, Nils-Ove, "Static Strength of Reinforcing Bars Formerly Subjected to Pulsating Load", Second International Symposium - Concrete Bridge Design, ACI Publication SP-26, American Concrete Institute, Detroit, 1969, pp. 1060-1099.

21. Sanders, W.W., Jr., Hoadley, P.G., and Munse, W.H., "Fatigue Behavior of Welded Joints in Reinforcing Bars of Concrete", Welding Journal, Vol. 40, No. 12, Research Supplement, 1961, pp. 529-s to 535-s.

22. Walls, J.C., Sanders, W.W., Jr. and Munse, W.H., "Fatigue Behavior of Butt-Welded Reinforcing Bars in Reinforced Concrete Beams", Journal of the American Concrete Institute, Proceedings, Vol. 62, No. 2, February 1965, pp. 1969-192.

23. Fisher, J.W., and Viest, I.M., "Fatigue Tests Bridge Materials of AASHO Road Test", Highway Research Board, Special Report 66, 1961, pp. 132-147.

24. The AASHO Road Test, Report 4, Bridge Research, Highway Research Board, Special Report 61D, National Academy of Sciences National Research Council, Washington, D.C., 1962, 217pp.

25. Mayer, M., "Duerfestigkeit von Spannbetonbauteilen (Fatigue Strength of Prestressed Concrete Structural Elements)", Deutscher Ausschus für Stahlbeton, Vol. 176, Berlin, 1966, 69 pp.

26. Kokubu, M., Okamura, H., "Fatigue Behavior of High Strength Deformed Bars in Reinforced Concrete Bridges", Journal of the Faculty of Engineering, University of Tokyo, Vol. 29, 1968.

27. Menzies, J.B., "The Fatigue Strength of Steel Reinforcement in Concrete", Building Research Station Publication, Garston, U.K., Paper No. 16/71.

28. Committee E-9 on Fatigue, A Guide for Fatigue Testing and Statistical Analysis of Fatigue Data, ASTM Special Technical Publication No. 91-A, American Society of Testing and Materials, Philadelphia, 1963, 83 pp.

29. Jhamb, I.C., and MacGregor, J.G., "Fatigue Strength of Deformed Reinforcing Bars", Structural Engineering Report No. 17, University of Alberta, Edmonton, Canada.

30. The Making Shaping and Treating of Steel, Edited by McGannon, H.E., United States Steel, 1964.

31. Reemsnyder, H.S., "Procurement and Analysis of Structural Fatigue Data", Journal of the Structural Division, ASCE, Vol. 95, No. ST7, 1969, pp. 1533-1551.

32. Anderson, R.L., and Bancroft, T.A., Statistical Theory in Research, McGraw-Hill, 1952.

33. Dixon, W.J., and Massey, F.J., Jr., "Introduction to Statistical Analysis, Third Edition, McGraw-Hill, 1969.

34. Cotton, F.A., and Wilkinson, G., Advances in Inorganic Chemistry, John Wiley and Sons, New York, 1966, pp. 847.

35. Amsler Manual, Instruction No. 122/10, Alfred J. Amsler and Company, Schaffhausen, Switzerland.

36. Metal Handbook, 8th Edition, Vol. 1, Properties and Selection of Materials, American Society of Metals, Metal Park, Novelty, Ohio, 1965.

37. Metals Engineering-Design, American Society of Mechanical Engineers Handbook, Second Edition, McGraw-Hill, 1965 (Chapter 8.4, "Decarburization").

28. Committee E-9 on Fatigue, A Guide for Fatigue Testing and Statistical Analysis of Fatigue Data, ASTM Special Technical Publication No. 91-A, American Society of Testing and Materials, Philadelphia, 1963, 83 pp.

29. Jhamb, I.C., and MacGregor, J.G., "Fatigue Strength of Deformed Reinforcing Bars", Structural Engineering Report No. 17, University of Alberta, Edmonton, Canada.

30. The Making Shaping and Treating of Steel, Edited by McGannon, H.E., United States Steel, 1964.

31. Reemsnyder, H.S., "Procurement and Analysis of Structural Fatigue Data", Journal of the Structural Division, ASCE, Vol. 95, No. ST7, 1969, pp. 1533-1551.

32. Anderson, R.L., and Bancroft, T.A., Statistical Theory in Research, McGraw-Hill, 1952.

33. Dixon, W.J., and Massey, F.J., Jr., "Introduction to Statistical Analysis, Third Edition, McGraw-Hill, 1969.

34. Cotton, F.A., and Wilkinson, G., Advances in Inorganic Chemistry, John Wiley and Sons, New York, 1966, pp. 847.

35. Amsler Manual, Instruction No. 122/10, Alfred J. Amsler and Company, Schaffhausen, Switzerland.

36. Metal Handbook, 8th Edition, Vol. 1, Properties and Selection of Materials, American Society of Metals, Metal Park, Novelty, Ohio, 1965.

37. Metals Engineering-Design, American Society of Mechanical Engineers Handbook, Second Edition, McGraw-Hill, 1965 (Chapter 8.4, "Decarburization").

38. Lipsitt, H.A., and Horne, G.T., "The Fatigue Strength of De-
    carburized Steel", American Society of Testing and Materials,
    Proceedings, Vol. 57, 1957, pp. 587-599.

39. Jackson, L.R. and Pochapsky, T.E., "Effect of Composition on the
    Fatigue Strength of Decarburized Steel", Transactions of
    American Society of Metals, Vol. 39, 1949, pp. 45-60.

40. Pritchard, R.T., T4 Workshop Technology, English Universities
    Press, London, pp. 168-173.

41. Peterson, R.E., Stress Concentration Design Factors, John Wiley
    and Sons, New York, 1956.

42. Derecho, A.T., Munse, W.H., "Stress Concentration at External
    Notches in Members Subjected to Axial Bending", Engineering
    Experimental Station Bulletin No. 494, University of
    Illinois, Urbana, 1968.

43. Wilson, E.L., "A Digital Computer Program for the Finite Element
    Analysis of Solids with Non-Linear Material Properties",
    University of California, Berkeley, 1965.

44. Building Code Requirements for Reinforced Concrete, ACI 318-63,
    American Concrete Institute, Detroit, 1963, 144pp.

45. Tetelman, A.S., and McEvily, Jr., A.J., Fracture of Structural
    Materials, John Wiley and Sons, 1967.

46. Guttman, I., and Wilks, S.S., Introductory Engineering Statistics,
    John Wiley, 1967, pp. 197.

47. Weibull, W., Fatigue Testing and Analysis of Results, Pergamon
    Press, 1961.

48. Reemsnyder, H.S., "Some Significant Parameters in Fatigue Properties of Weld Joints", Welding Journal, Vol. 48, May 1969, pp. 213-s to 220-s.

49. Li, C.C., Introduction to Experimental Statistics, McGraw-Hill, New York, 1964, pp. 142.

50. Hald, Abraham, Statistical Theory with Engineering Applications, John Wiley and Sons, New York, 1952.

51. Weibull, W., "Analysis of Fatigue Test Results", First Seminar on Fatigue and Fatigue Design, Department of Civil Engineering and Engineering Mechanics, Columbia University, New York, 1963.

52. Baistenaire, F., "A Study of the Scatter of Fatigue Test Results of Statistical and Physical Methods", Fatigue of Aircraft Structures, Pergamon Press, New York, 1963, pp. 53-85.

53. Blom, G., Statistical Estimates and Transformed Beta-Variables, John Wiley and Sons, 1958.

54. Kimball, B.F., "On the Choice of Plotting Positions on Probability Paper", Journal of the American Statistical Association, Vol. 55, 1960, pp. 546-560.

55. Groben, G., Stepwise Multiple Regression Computer Program, CS:101, University of Alberta Computing Center, Edmonton.

56. Rehm, Gallus, "Kriterien zur Beuteilung von Bewehrungsstaben mit hochwertigan Verbund", Stahlbetonbau Festschrift Rüsch , W. Ernst und Sohn, München, 1969.

57. Kuhn, Paul, and Hardrath, H.F., "An Engineering Method for Esti-
    mating Notch-Size Effect in Fatigue Tests on Steel",
    Technical Note 2805, National Advisory Committee for
    Aeronautics, Washington, October 1952.

58. MacGregor, J.G., Jhamb, I.C., and Nuttall, N., "Fatigue Strength
    of Hot Rolled Deformed Reinforcing Bars", American Concrete
    Institute, Proceedings, Vol. 68, No. 3, March 1971, pp.
    1969-179.

57. Kuhn, Paul, and Hardrath, H.F., "An Engineering Method for Esti-
    mating Notch-Size Effect in Fatigue Tests on Steel",
    Technical Note 2805, National Advisory Committee for
    Aeronautics, Washington, October 1952.

58. MacGregor, J.G., Jhamb, I.C., and Nuttall, N., "Fatigue Strength
    of Hot Rolled Deformed Reinforcing Bars", American Concrete
    Institute, Proceedings, Vol. 68, No. 3, March 1971, pp.
    1969-179.

APPENDIX A

CHEMICAL ANALYSIS OF REINFORCING BARS

TABLE A-1

CHEMICAL ANALYSIS OF REINFORCING BARS - PHASE I

BAR SIZE	No. 10			No. 8			No. 5		
GRADE OF STEEL	G40	G60	G75	G40	G60	G75	G40	G60	G75
Content in percent:									
Carbon	0.36	0.42	0.42	0.36	0.47	0.42	0.34	0.52	0.43
Manganese	0.73	1.38	1.52	0.64	1.29	1.12	0.51	0.77	1.19
Sulphur	0.036	0.041	0.025	0.038	0.043	0.029	0.04	0.044	0.030
Phosphorus	0.018	.03	*	.032	.034	*	.017	.041	*
Copper	0.14	0.28	.04	0.35	0.30	0.12	0.27	0.27	.05
Nickel	.08	0.11	.04	0.10	0.13	.05	0.14	0.11	.05
Chromium	0.16	0.12	.05	0.14	0.13	0.15	.09	0.14	0.25
Molybdenum	<.05	<.05	<.05	<.05	<.05	<.05	<.05	<.05	<.05
Silicon	0.23	0.27	0.29	0.24	0.21	0.25	0.21	0.25	0.29
Vanadium	**	*	0.125	*	*	.097	*	*	.09
Tin	<.05	<.05	<.05	<.05	<.05	<.05	<.05	<.05	<.05
Niobium	*	*	*	*	*	*	*	*	*
Aluminium	*	*	<.05	*	*	<.05	*	*	<.05

* Trace, <.01
** Not detected

TABLE A-2

CHEMICAL ANALYSIS OF REINFORCING BARS - PHASE II

BAR SIZE	No. 8			
BAR TYPE	PLAIN		DEFORMED	
GRADE OF STEEL	G40	G60	G40	G60
Content in percent:				
Carbon (C)	0.33	0.34	0.34	0.34
Manganese (Mn)	0.64	0.99	0.61	1.00
Sulphur (S)	0.039	.036	0.036	0.034
Phosphorus (P)	0.026	0.024	.024	0.024
Copper (Cu)	0.41	0.29	0.41	0.29
Nickel (Ni)	0.10	0.12	0.11	0.12
Cromium (Cr)	0.16	0.11	0.15	0.11
Molybdenum (Mo)	<.05	<.05	<.05	<.05
Silicon (Si)	0.28	0.23	0.28	0.23
Vanadium (V)	*	*	*	*
Tin (Sn)	<.05	<.05	<.05	<.05
Niobium (Cb)	*	<.05	*	<.05
Aluminium (Al)	*	*	*	**

*Trace, <.01
**Not detected

APPENDIX B

TEST SET-UP DRAWINGS

B2
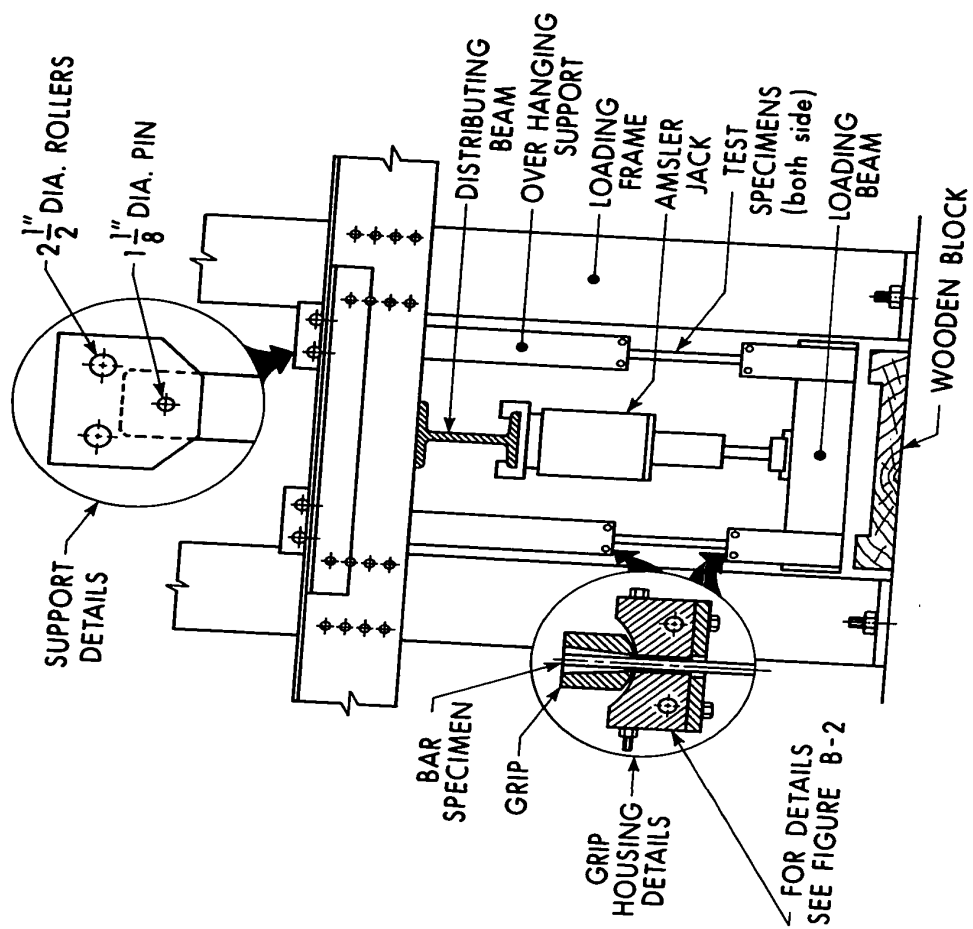
FIGURE B-1 DETAILS OF TEST SET-UP

SECTION B - B

SECTION A - A

SCALE IN INCHES
0 1 2 3 4
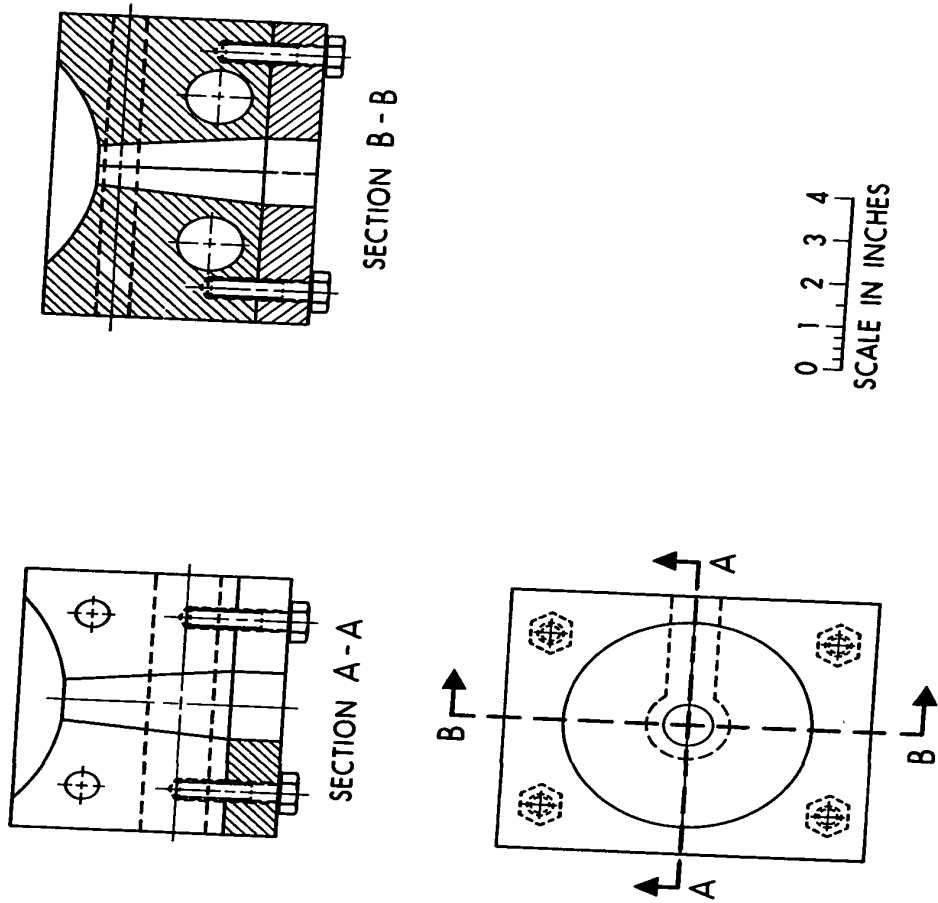
FIGURE B-2 DETAILS OF GRIP HOUSING

APPENDIX C

GRAIN STRUCTURE AND MICRO-HARDNESS

CHARTS FOR REINFORCING BARS

TABLE C.1

RELATIONSHIP BETWEEN KNOOP HARDNESS

NUMBER AND TENSILE STRENGTH

Knoop Hardness Number	Approximate Tensile Strength ksi
164	72
167	74
170	75
173	71
176	78
180	80
184	81
188	83
192	85
196	87
201	89
206	91
211	93
216	96
221	98
226	101
231	103
236	106
241	109
246	108
251	112
261	117
272	123
284	129
297	136

(a) GRAIN STRUCTURE   0 ⌊ INCHES ⌋ 0.01

(b) KNOOP HARDNESS GRADIENTS THROUGH
DECARBURIZED SURFACE (1 kg LOAD)

FIGURE C-1   GRAIN STRUCTURE AND MICRO-HARDNESS
DATA FOR GRADE 40 NO. 5 BARS

(a) GRAIN STRUCTURE 0 INCHES 0.01

(b) KNOOP HARDNESS GRADIENTS THROUGH
DECARBURIZED SURFACE (1 kg LOAD)

FIGURE C-1   GRAIN STRUCTURE AND MICRO-HARDNESS
DATA FOR GRADE 40 NO. 5 BARS

(a) GRAIN STRUCTURE   0 | INCHES | 0.01

(b) KNOOP HARDNESS GRADIENTS THROUGH
DECARBURIZED SURFACE (1 kg LOAD)

FIGURE C-2   GRAIN STRUCTURE AND MICRO-HARDNESS
DATA FOR GRADE 60 NO. 5 BARS

(a) GRAIN STRUCTURE 0 |___|___| INCHES |___| 0.01

(b) KNOOP HARDNESS GRADIENTS THROUGH
DECARBURIZED SURFACE (1 kg LOAD)

FIGURE C-2   GRAIN STRUCTURE AND MICRO-HARDNESS
DATA FOR GRADE 60 NO. 5 BARS

(a) GRAIN STRUCTURE

0 ____ INCHES 0.01

(b) KNOOP HARDNESS GRADIENTS THROUGH
DECARBURIZED SURFACE (1 kg LOAD)

FIGURE C-3   GRAIN STRUCTURE AND MICRO-HARDNESS
DATA FOR GRADE 75 NO. 5 BARS

(a) GRAIN STRUCTURE   0 ⊢—INCHES—⊣ 0.01

(b) KNOOP HARDNESS GRADIENTS THROUGH
    DECARBURIZED   SURFACE (1 kg LOAD)

FIGURE C-3   GRAIN STRUCTURE AND MICRO-HARDNESS
                  DATA FOR GRADE 75 NO. 5 BARS

(a) GRAIN STRUCTURE   0 |__,__,__| INCHES |__,__| 0.01

(b) KNOOP HARDNESS GRADIENTS THROUGH
DECARBURIZED   SURFACE (1 kg LOAD)

FIGURE C-4   GRAIN STRUCTURE AND MICRO-HARDNESS
DATA FOR GRADE 40 NO. 8 BARS (PHASE I)

(a) GRAIN STRUCTURE

0 ___ INCHES ___ 0.01

(b) KNOOP HARDNESS GRADIENTS THROUGH
DECARBURIZED SURFACE (1 kg LOAD)

FIGURE C-4   GRAIN STRUCTURE AND MICRO-HARDNESS
DATA FOR GRADE 40 NO. 8 BARS (PHASE I)

(a) GRAIN STRUCTURE 0 ⊢⊢⊢⊢⊢ INCHES 0.01

(b) KNOOP HARDNESS GRADIENTS THROUGH
    DECARBURIZED SURFACE (1 kg LOAD)

FIGURE C-5   GRAIN STRUCTURE AND MICRO-HARDNESS
             DATA FOR GRADE 60 NO. 8 BARS (PHASE I)

(a) GRAIN STRUCTURE   0   INCHES   0.01

(b) KNOOP HARDNESS GRADIENTS THROUGH
    DECARBURIZED SURFACE (1 kg LOAD)

FIGURE C-5   GRAIN STRUCTURE AND MICRO-HARDNESS
                  DATA FOR GRADE 60 NO. 8 BARS (PHASE I)

(a) GRAIN STRUCTURE

(b) KNOOP HARDNESS GRADIENTS THROUGH
DECARBURIZED SURFACE (1 kg LOAD)

FIGURE C-6   GRAIN STRUCTURE AND MICRO-HARDNESS
DATA FOR GRADE 75 NO. 8 BARS

(a) GRAIN STRUCTURE

0 ___ INCHES ___ 0.01

(b) KNOOP HARDNESS GRADIENTS THROUGH
DECARBURIZED SURFACE (1 kg LOAD)

FIGURE C-6   GRAIN STRUCTURE AND MICRO-HARDNESS
DATA FOR GRADE 75 NO. 8 BARS

(a) GRAIN STRUCTURE   0   INCHES   0.01

(b) KNOOP HARDNESS GRADIENTS THROUGH
DECARBURIZED SURFACE (1 kg LOAD)

FIGURE C-7   GRAIN STRUCTURE AND MICRO-HARDNESS
DATA FOR GRADE 40 NO. 10 BARS

(a) GRAIN STRUCTURE 0 ⊢ INCHES ⊣ 0.01

(b) KNOOP HARDNESS GRADIENTS THROUGH DECARBURIZED SURFACE (1 kg LOAD)

FIGURE C-7   GRAIN STRUCTURE AND MICRO-HARDNESS DATA FOR GRADE 40 NO. 10 BARS

(a) GRAIN STRUCTURE

(b) KNOOP HARDNESS GRADIENTS THROUGH
DECARBURIZED SURFACE (1 kg LOAD)

FIGURE C-8   GRAIN STRUCTURE AND MICRO-HARDNESS
DATA FOR GRADE 60 NO. 10 BARS

(a) GRAIN STRUCTURE   0 ⊢ INCHES ⊣ 0.01

(b) KNOOP HARDNESS GRADIENTS THROUGH
DECARBURIZED SURFACE (1 kg LOAD)

FIGURE C-8   GRAIN STRUCTURE AND MICRO-HARDNESS
DATA FOR GRADE 60 NO. 10 BARS

(a) GRAIN STRUCTURE 0 INCHES 0.01

(b) KNOOP HARDNESS GRADIENTS THROUGH
DECARBURIZED SURFACE (1 kg LOAD)

FIGURE C-9   GRAIN STRUCTURE AND MICRO-HARDNESS
DATA FOR GRADE 75 NO. 10 BARS

(a) GRAIN STRUCTURE 0 INCHES 0.01

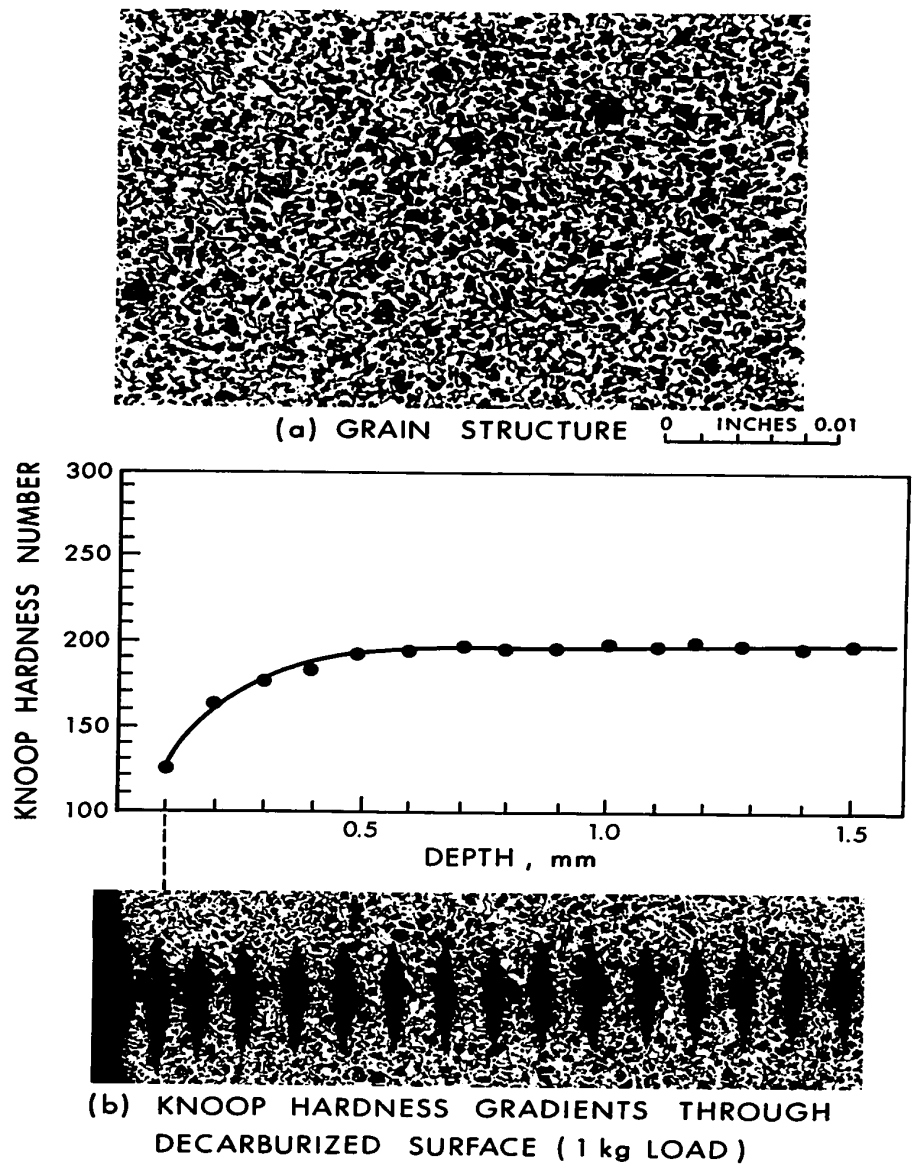(b) KNOOP HARDNESS GRADIENTS THROUGH
DECARBURIZED SURFACE (1 kg LOAD)

FIGURE C-9   GRAIN STRUCTURE AND MICRO-HARDNESS
DATA FOR GRADE 75 NO. 10 BARS

(a) GRAIN STRUCTURE   0 ⊢—INCHES—⊣ 0.01

(b) KNOOP HARDNESS GRADIENTS THROUGH
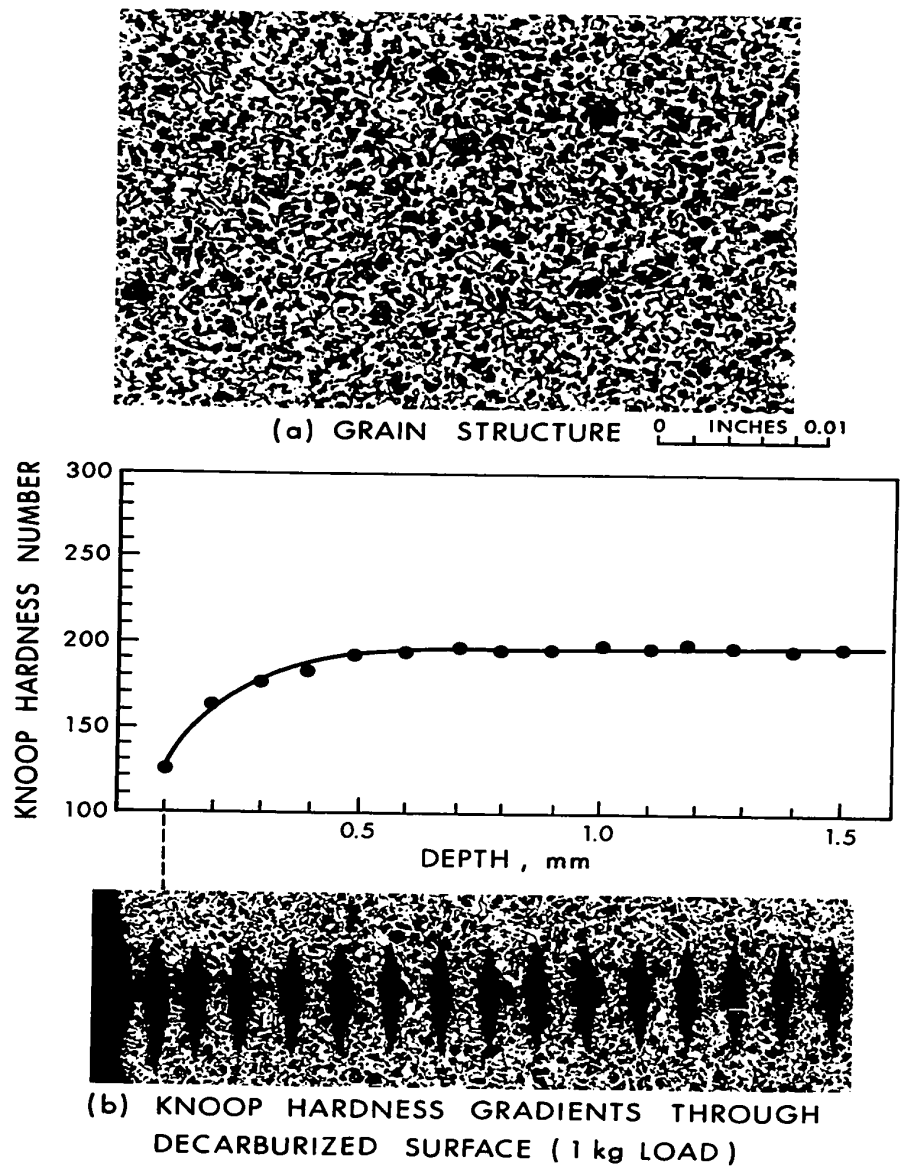   DECARBURIZED SURFACE (1 kg LOAD)

FIGURE C-10   GRAIN STRUCTURE AND MICRO-HARDNESS
               DATA FOR GRADE 40 NO. 8 BARS (PHASE II)

(a) GRAIN STRUCTURE   0 ⊢ INCHES ⊣ 0.01

(b) KNOOP HARDNESS GRADIENTS THROUGH
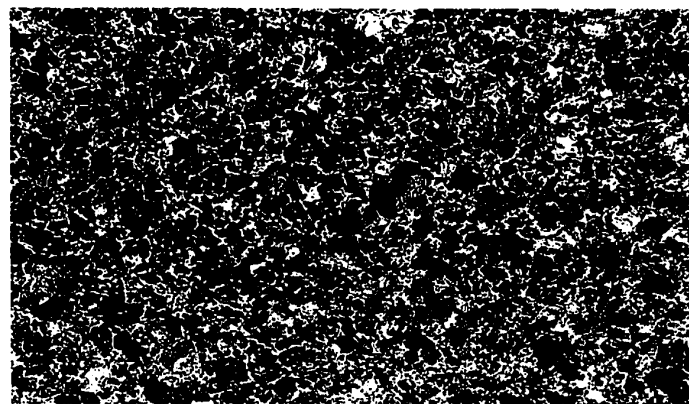   DECARBURIZED SURFACE (1 kg LOAD)

FIGURE C-10   GRAIN STRUCTURE AND MICRO-HARDNESS
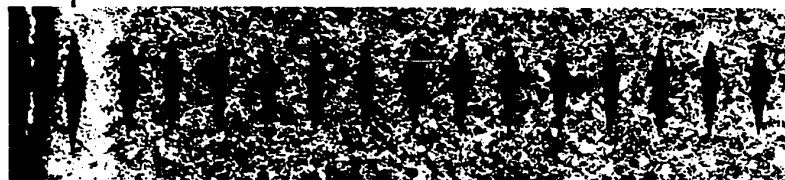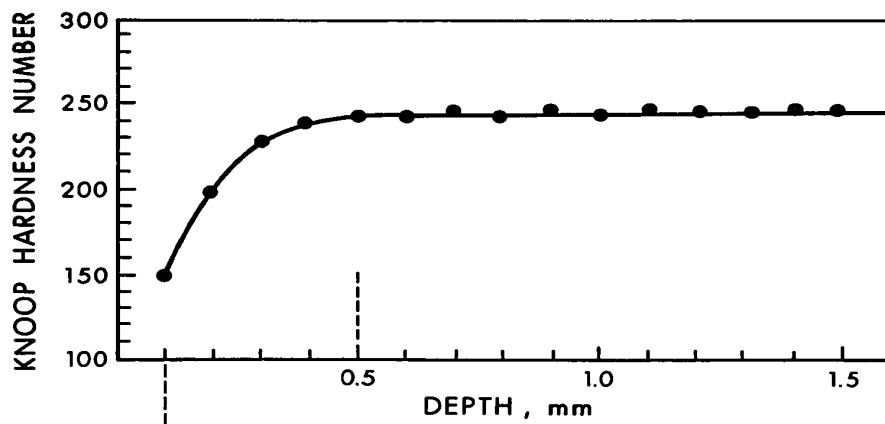   DATA FOR GRADE 40 NO. 8 BARS (PHASE II)
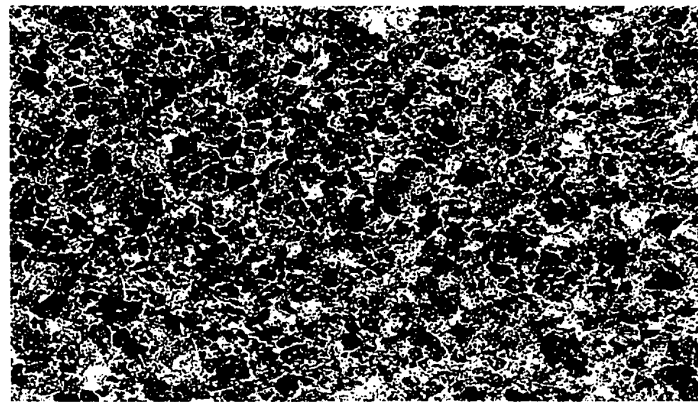
(a) GRAIN STRUCTURE

0   INCHES   0.01

(b) KNOOP HARDNESS GRADIENTS THROUGH
DECARBURIZED SURFACE (1 kg LOAD)

FIGURE C-11   GRAIN STRUCTURE AND MICRO-HARDNESS OF
GRADE 60 NO. 8 BARS (PHASE II)

(a) GRAIN STRUCTURE

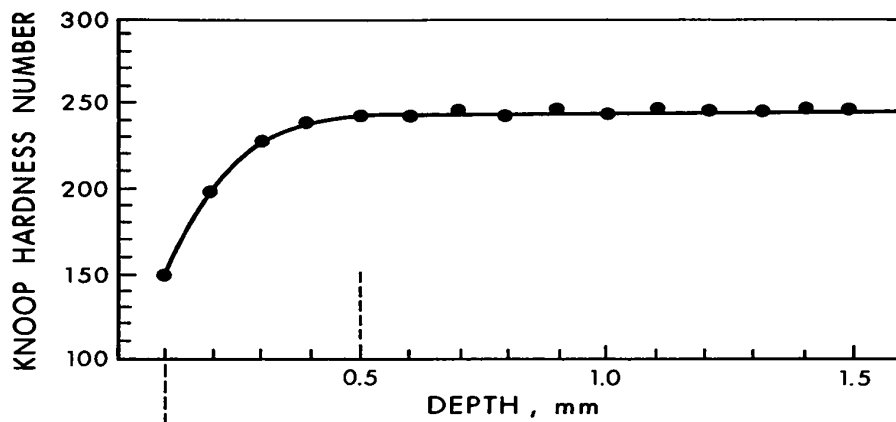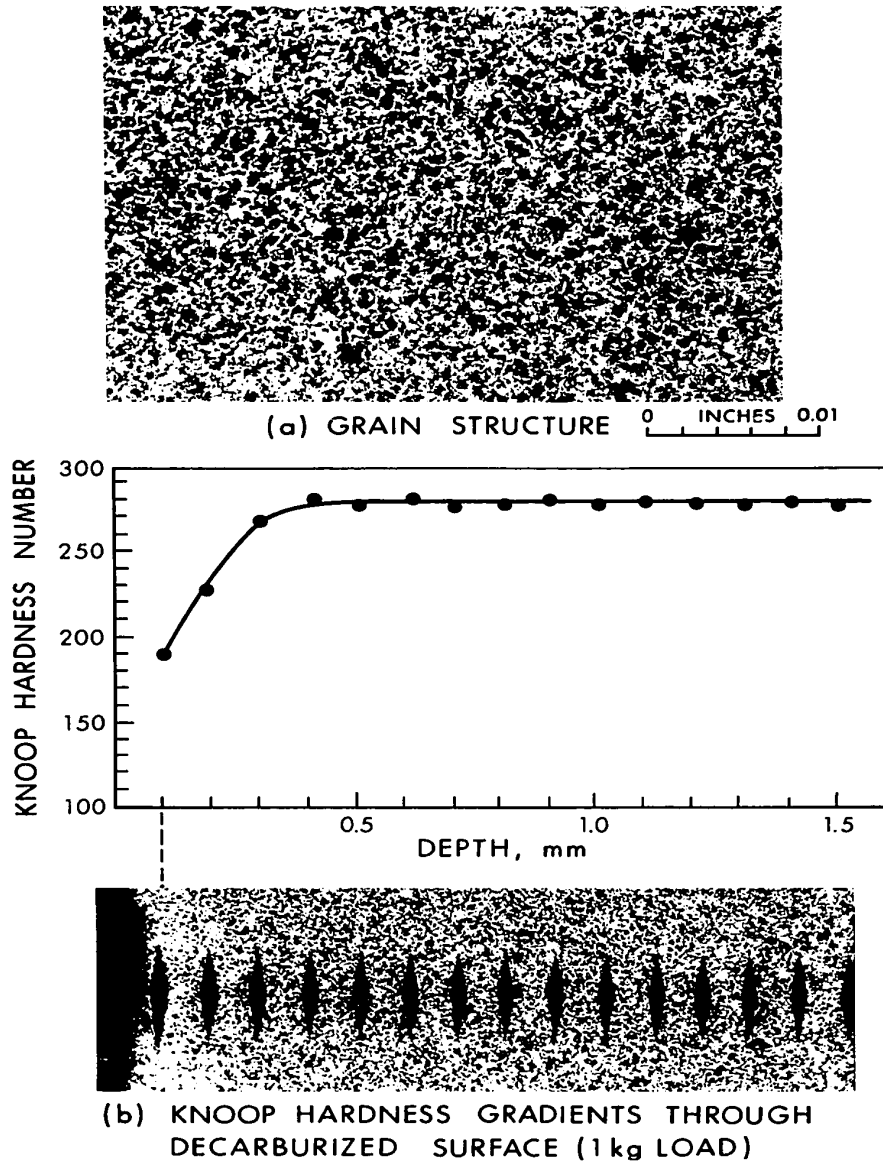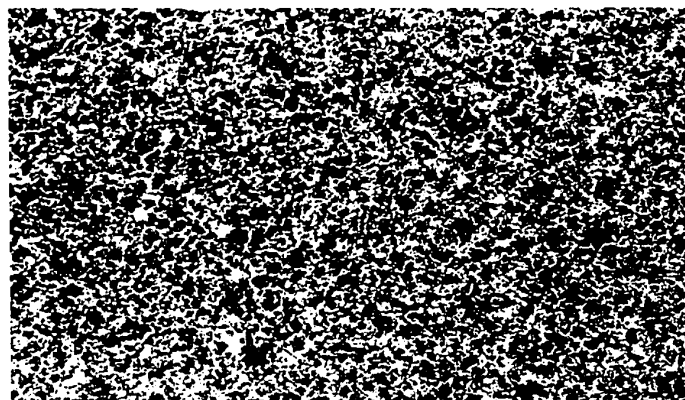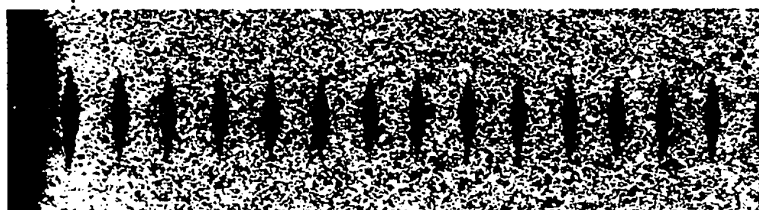

(b) KNOOP HARDNESS GRADIENTS THROUGH
DECARBURIZED SURFACE (1 kg LOAD)

FIGURE C-11   GRAIN STRUCTURE AND MICRO-HARDNESS OF
GRADE 60 NO. 8 BARS (PHASE II)
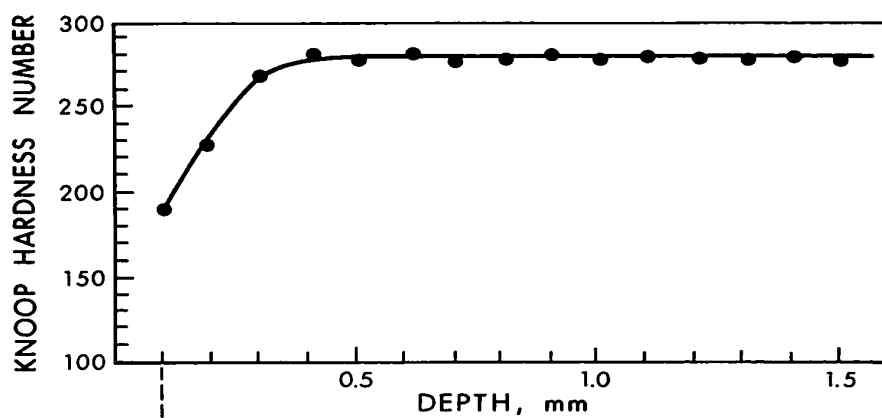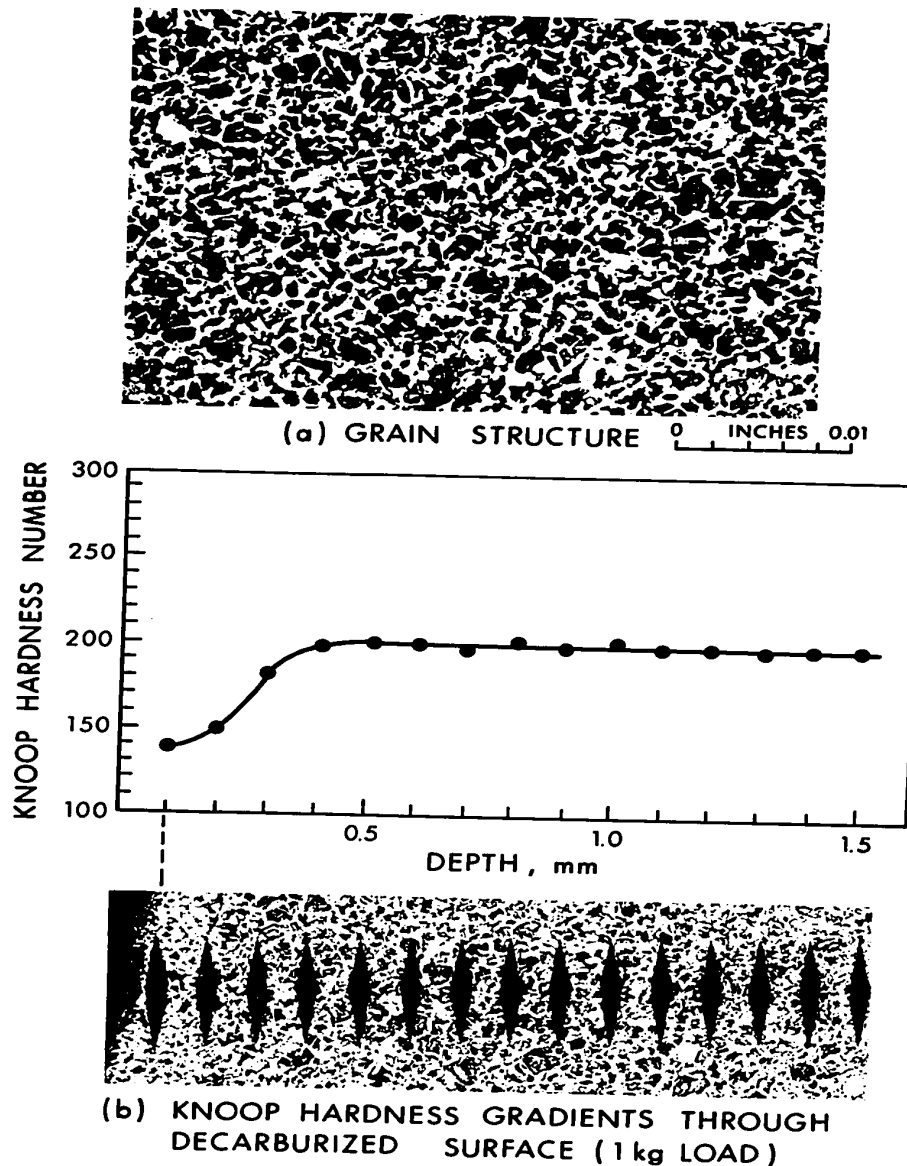
APPENDIX D

FATIGUE TEST DATA

TABLE D-1
FATIGUE TEST DATA ON REINFORCED CONCRETE BEAMS

SPECIMEN MARK	YIELD STRENGTH KSI	TENSILE STRENGTH KSI	MIN STRESS KSI	STRESS RANGE KSI	CYCLES TO FAILURE
BEAM TESTS SERIES 1 GRADE 40 NO.8 BARS					
8-G40-1	52.7	83.1	5.27	38.38	457700.
8-G40-2	52.7	83.1	5.16	33.31	730400.
8-G40-3	52.7	83.1	5.20	30.69	2005600.
8-G40-4	52.7	83.1	5.20	30.82	1837000.
8-G40-5	52.7	83.1	5.18	30.90	1023400.
8-G40-6	52.7	83.1	5.16	31.54	1074200. *
8-G40-11	52.7	83.1	5.21	31.00	577400.
BEAM TESTS SERIES 2 GRADE 60 NO.8 BARS					
8-G60-1	65.6	109.0	6.92	32.00	1078300.
8-G60-2	65.6	109.0	6.90	31.14	1595600.
8-G60-3	65.6	109.0	6.88	30.12	1745600.
8-G60-4	65.6	109.0	6.88	29.67	690600.
8-G60-5	65.6	109.0	6.86	29.56	9607000. *
8-G60-6	65.6	109.0	6.86	32.05	1270000.
8-G60-11	65.6	109.0	6.76	30.84	978000.
8-G60-12	65.6	109.0	6.76	31.64	499300.
8-G60-10R	65.6	109.0	6.95	34.97	684300.
BEAM TESTS SERIES 3 GRADE 75 NO.8 BARS					
8-G75-1	84.4	123.5	8.50	30.75	782300.
8-G75-2	84.4	123.5	8.31	29.59	10400900. *
8-G75-3	84.4	123.5	8.28	30.37	2725900.
8-G75-4	84.4	123.5	8.26	30.64	9000000.
8-G75-5	84.4	123.5	8.44	32.06	5000000. *
8-G75-6	84.4	123.5	8.24	33.96	1172500.
BEAM TESTS SERIES 4 GRADE 40 NO.8 BARS					
8-G40-7	52.7	83.1	21.25	26.32	1134600.
8-G40-8	52.7	83.1	21.10	28.95	777000.
8-G40-9	52.7	83.1	21.27	25.53	5000000. *
8-G40-10	52.7	83.1	21.40	24.45	5000000. *
8-G40-12	52.7	83.1	21.08	25.70	5000000. *
8-G40-9R	52.7	83.1	21.40	31.63	282200.
8-G40-10R	52.7	83.1	21.40	26.80	207300.
8-G40-12R	52.7	83.1	21.08	29.90	525600.

* BEAM DID NOT FAIL

R- RETEST

TABLE D-1 (CONTINUED)

SPECIMEN MARK	YIELD STRENGTH KSI	TENSILE STRENGTH KSI	MIN STRESS KSI	STRESS RANGE KSI	CYCLES TO FAILURE

BEAM TESTS SERIES 5 GRADE 60 NO.8 BARS

SPECIMEN MARK	YIELD STRENGTH KSI	TENSILE STRENGTH KSI	MIN STRESS KSI	STRESS RANGE KSI	CYCLES TO FAILURE
8-G60-7	65.6	109.0	27.80	27.30	2856400.
8-G60-8	65.6	109.0	28.00	30.00	541300.
8-G60-9	65.6	109.0	28.22	26.53	1463900.
8-G60-10	65.6	109.0	28.40	25.35	5000000.*
8-G60-13	65.6	109.0	28.60	26.33	4703700.*
8-G60-14	65.6	109.0	28.20	25.40	5000000.*
8-G60-14R	65.6	109.0	27.84	32.20	322400.

BEAM TESTS SERIES 6 GRADE 75 NO.8 BARS

SPECIMEN MARK	YIELD STRENGTH KSI	TENSILE STRENGTH KSI	MIN STRESS KSI	STRESS RANGE KSI	CYCLES TO FAILURE
8-G75-7	84.4	123.5	33.80	27.50	3341300.
8-G75-8	84.4	123.5	34.30	30.24	1240500.
8-G75-9	84.4	123.5	34.43	26.70	5000000.*
8-G75-10	84.4	123.5	34.55	25.60	1133700.
8-G75-11	84.4	123.5	34.65	25.65	234900.
8-G75-12	84.4	123.5	34.70	24.40	4903000.*
8-G75-9R	84.4	123.5	34.30	35.55	381400.*

BEAM TESTS SERIES 7 GRADE 40 NO.5 BARS

SPECIMEN MARK	YIELD STRENGTH KSI	TENSILE STRENGTH KSI	MIN STRESS KSI	STRESS RANGE KSI	CYCLES TO FAILURE
5-G40-1	50.0	76.3	6.08	37.40	331600.
5-G40-2	50.0	76.3	5.90	34.25	882100.
5-G40-3	50.0	76.3	5.72	31.10	5000000.*
5-G40-4	50.0	76.3	5.36	32.65	852800.
5-G40-5	50.0	76.3	5.18	31.90	1056000.*
5-G40-6	50.0	76.3	5.00	31.10	979200.
5-G40-3R	50.0	76.3	5.00	44.30	124400.

BEAM TESTS SERIES 8 GRADE 60 NO.5 BARS

SPECIMEN MARK	YIELD STRENGTH KSI	TENSILE STRENGTH KSI	MIN STRESS KSI	STRESS RANGE KSI	CYCLES TO FAILURE
5-G60-1	65.8	109.2	6.57	32.70	908300.
5-G60-2	65.8	109.2	6.57	28.60	5000000.*
5-G60-3	65.8	109.2	6.57	31.50	5000000.*
5-G60-4	65.8	109.2	6.57	34.40	598700.
5-G60-5	65.8	109.2	6.57	32.10	1335500.
5-G60-6	65.8	109.2	6.57	31.60	5000000.*
5-G60-3R	65.8	109.2	6.57	40.20	311500.
5-G60-6R	65.8	109.2	6.57	35.60	569500.

* BEAM DID NOT FAIL
R- RETEST

TABLE D -1 (CONTINUED)

SPECIMEN MARK	YIELD STRENGTH KSI	TENSILE STRENGTH KSI	MIN STRESS KSI	STRESS RANGE KSI	CYCLES TO FAILURE
BEAM TESTS SERIES 9 GRADE 75 NO.5 BARS					
5-G75-1	89.4	122.1	8.94	33.20	5000000.*
5-G75-2	89.4	122.1	8.94	34.80	5000000.*
5-G75-3	89.4	122.1	8.94	37.80	2788000.
5-G75-4	89.4	122.1	8.94	37.20	2263400.
5-G75-5	89.4	122.1	8.94	36.10	5000000.*
5-G75-6	89.4	122.1	8.94	37.80	5000000.*
5-G75-1R	89.4	122.1	8.90	44.40	521400.
5-G75-2R	89.4	122.1	8.90	41.20	882100.
5-G75-5R	89.4	122.1	8.94	42.60	342100.
5-G75-6R	89.4	122.1	8.94	39.60	1260300.
BEAM TESTS SERIES 10 GRADE 40 NO.10 BARS					
10-G40-1	49.7	83.1	4.97	33.03	630000.
10-G40-2	49.7	83.1	4.97	29.97	1803600.
10-G40-3	49.7	83.0	4.97	28.37	5000000.*
10-G75-4	49.7	83.1	4.97	30.00	5000000.*
10-G40-5	49.7	83.1	4.97	32.00	1296300.
10-G40-6	49.7	83.1	4.97	30.30	5000000.*
10-G40-3R	49.7	83.1	5.00	35.37	460900.
10-G40-4R	49.7	83.1	4.97	36.00	782000.
10-G40-6R	49.7	83.1	4.97	35.00	919700.
BEAM TESTS SERIES 11 GRADE 60 NO.10 BARS					
10-G60-1	64.2	110.5	6.42	30.38	1361700.
10-G60-2	64.2	110.5	6.42	28.98	4750000.
10-G60-3	64.2	110.5	6.42	28.98	750700.
10-G60-4	64.2	110.5	6.42	29.00	2669900.
10-G60-5	64.2	110.5	6.40	28.00	5000000.*
10-G60-6	64.2	110.5	6.42	28.75	3225900.
10-G60-5R	64.2	110.5	6.40	35.00	504200.
BEAM TESTS SERIES 12 GRADE 75 NO.10 BARS					
10-G75-1	83.0	109.5	8.30	31.38	742100.
10-G75-2	83.0	109.5	8.30	29.78	538100.
10-G75-3	83.0	109.5	8.30	29.00	5000000.*
10-G75-4	83.0	109.5	8.30	30.00	558900.
10-G75-5	83.0	109.5	8.30	30.00	2029400.
10-G75-6	83.0	109.5	8.30	29.50	1327300.
10-G75-3R	83.0	109.5	8.30	33.50	565800.

* BEAM DID NOT FAIL
R- RETEST

D5

TABLE D-1 (CONTINUED)

SPECIMEN MARK	YIELD STRENGTH KSI	TENSILE STRENGTH KSI	MIN STRESS KSI	STRESS RANGE KSI	CYCLES TO FAILURE
SERIES NO. 13,NO.8 GRADE 40 DEFORMED BARS IN AIR					
8-G40-1A	52.7	83.1	5.20	26.00	3000001. *
8-G40-3A	52.7	83.1	5.20	26.00	3000001. *
8-G40-4A	52.7	83.1	5.20	30.00	664100.
8-G40-2A	52.7	83.1	5.20	30.00	840100.
8-G40-5A	52.7	83.1	5.20	28.00	3000001. *
8-G40-6R	52.7	83.1	5.20	28.00	1363800.
8-G40-1AR	52.7	83.1	5.20	32.00	562100.
8-G40-3AR	52.7	83.1	.5.20	32.00	535200.

TABLE D-2
FATIGUE TEST DATA ON REINFORCING BAR SPECIMENS

SPECIMEN MARK	GROUP NO.	TEST SEQUENCE	YIELD STRENGTH KSI	TENSILE STRENGTH KSI	MIN STRESS KSI	STRESS RANGE KSI	CYCLES TO FAILURE
SERIES NO. 1, NO. 8 GRADE 40 DEFORMED BARS							
D-G40-2	1	4	50.6	81.5	5.0	30.0	412700.
D-G40-6	1	4	50.6	81.5	5.0	30.0	786200.
D-G40-10	1	4	50.6	81.5	5.0	30.0	534600.
D-G40-8	1	4	50.6	81.5	5.0	28.0	632700.
D-G40-3	2	6	50.6	81.5	5.0	28.0	1222100.
D-G40-5	2	6	50.6	81.5	5.0	28.0	685200.
D-G40-11	2	6	50.6	81.5	5.0	26.0	925200.
D-G40-15	2	6	50.6	81.5	5.0	26.0	785100.
D-G40-4	3	9	50.6	81.5	5.0	26.0	1554600.
D-G40-9	3	9	50.6	81.5	5.0	26.0	1060100.
D-G40-12	3	9	50.6	81.5	5.0	25.0	3000001.*
D-G40-13	3	9	50.6	81.5	5.0	25.0	892100.
D-G40-14	4	13	50.6	81.5	5.0	25.0	3000001.*
D-G40-17	4	13	50.6	81.5	5.0	25.0	3000001.*
D-G40-16	4	13	50.6	81.5	5.0	25.0	1423300.
D-G40-18	4	13	50.6	81.5	5.0	25.0	3000001.*
SERIES NO. 2, NO. 8 GRADE 60 DEFORMED BARS							
D-G60-2	5	1	61.4	96.8	6.7	32.0	254600.
D-G60-6	5	1	61.4	96.8	6.7	32.0	382800.
D-G60-14	5	1	61.4	96.8	6.7	32.0	315300.
D-G60-15	5	1	61.4	96.8	6.7	32.0	456300.
D-G60-3	6	3	61.4	96.8	6.7	28.0	854300.
D-G60-7	6	3	61.4	96.8	6.7	28.0	665300.
D-G60-9	6	3	61.4	96.8	6.7	28.0	923400.
D-G60-11	6	3	61.4	96.8	6.7	26.0	1453400.
D-G60-1	7	10	61.4	96.8	6.7	26.0	3000001.*
D-G60-4	7	10	61.4	96.8	6.7	26.0	956700.
D-G60-8	7	10	61.4	96.8	6.7	26.0	1468000.
D-G60-13	7	10	61.4	96.8	6.7	25.0	3000001.*
D-G60-5	8	16	61.4	96.8	6.7	25.0	3000001.*
D-G60-10	8	16	61.4	96.8	6.7	25.0	3000001.*
D-G60-12	8	16	61.4	96.8	6.7	25.0	3000001.*
D-G60-16	8	16	61.4	96.8	6.7	25.0	3000001.*
SERIES NO. 3, NO. 8 GRADE 40 PLAIN BARS							
P-G40-4	9	8	54.2	86.3	5.0	38.0	1324500.
P-G40-24	9	8	54.2	86.3	5.0	38.0	3000001.*
P-G40-17	9	8	54.2	86.3	5.0	38.0	962800.
P-G40-5	9	8	54.2	86.3	5.0	38.0	1044500.
P-G40-10	10	11	54.2	86.3	5.0	36.0	3000001.*
P-G40-14	10	11	54.2	86.3	5.0	36.0	3000001.*
P-G40-25	10	11	54.2	86.3	5.0	36.0	3000001.*
P-G40-9	10	11	54.2	86.3	5.0	36.0	3000001.*
P-G40-28	11	15	54.2	86.3	5.0	36.0	383200.
P-G40-11	11	15	54.2	86.3	5.0	42.0	721500.
P-G40-3	11	15	54.2	86.3	5.0	42.0	549500.
P-G40-2	11	15	54.2	86.3	5.0	42.0	446400.
P-G40-19	12	20	54.2	86.3	5.0	42.0	783200.
P-G40-6	12	20	54.2	86.3	5.0	40.0	1132200.
P-G40-23	12	20	54.2	86.3	5.0	40.0	683100.
P-G40-16	12	20	54.2	86.3	5.0	38.0	3000001.*

* BAR DID NOT FAIL

TABLE D-2 (CONTINUED)

SPECIMEN MARK	GROUP NO.	TEST SEQUENCE	YIELD STRENGTH KSI	TENSILE STRENGTH KSI	MIN STRESS KSI	STRESS RANGE KSI	CYCLES TO FAILURE
		SERIES NO.4,NO.8	GRADE 60 PLAIN BARS				
P-G60-20	13	2	67.0	100.1	6.7	40.0	3000001.*
P-G60-12	13	2	67.0	100.1	6.7	40.0	3000001.*
P-G60-5	13	2	67.0	100.1	6.7	40.0	1862300.
P-G60-7	13	2	67.0	100.1	6.7	40.0	3000001.*
P-G60-11	14	7	67.0	100.1	6.7	44.0	653500.
P-G60-30	14	7	67.0	100.1	6.7	44.0	1101300.
P-G60-32	14	7	67.0	100.1	6.7	44.0	927500.
P-G60-23	14	7	67.0	100.1	6.7	44.0	1321100.
P-G60-9	15	17	67.0	100.1	6.7	42.0	3000001.*
P-G60-27	15	17	67.0	100.1	6.7	42.0	1462300.
P-G60-10	15	17	67.0	100.1	6.7	42.0	1083100.
P-G60-28	15	17	67.0	100.1	6.7	42.0	3000001.*
P-G60-21	16	23	67.0	100.1	6.7	46.0	428000.
P-G60-16	16	23	67.0	100.1	6.7	46.0	775300.
P-G60-25	16	23	67.0·	100.1	6.7	46.0	625200.
P-G60-8	16	23	67.0	100.1	6.7	46.0	562400.
		SERIES NO. 5,NO.8,GRADE 40 PLAIN BARS(‡)					
W-G40-22	17	12	54.2	86.3	5.0	40.0	1080200.
W-G40-8	17	12	54.2	86.3	5.0	40.0	911700.
W-G40-20	17	12	54.2	86.3	5.0	40.0	1300300.
W-G40-15	17	12	54.2	86.3	5.0	40.0	572900.
W-G40-27	18	18	54.2	86.3	5.0	38.0	1209300.
W-G40-34	18	18	54.2	86.3	5.0	38.0	935200.
W-G40-18	18	18	54.2	86.3	5.0	38.0	1042100.
W-G40-30	18	18	54.2	86.3	5.0	38.0	3120001. *
		SERIES NO.6,NO.8, GRADE 60 PLAIN BARS(‡)					
W-G60-1	21	5	67.0	100.1	6.7	44.0	881300.
W-G60-29	21	5	67.0	100.1	6..7	44.0	1156200.
W-G60-14	21	5	67.0	100.1	6.7	44.0	727400.
W-G60-34	21	5	67.0	100.1	6.7	44.0	1387000.
W-G60-31	22	14	67.0	100.1	6.7	42.0	3000001. *
W-G60-3	22	14	67.0	100.1	6.7	42.0	3000001. *
W-G60-13	22	14	67.0	100.1	6.7	42.0	1374700.
W-G60-24	22	14	67.0	100.1	6.7	42.0	988400.

* BAR DID NOT FAIL
‡ BARS WITHOUT RUST AND MILLSCALE

TABLE D-2 (CONTINUED)

SPECIMEN MARK	GROUP NO.	TEST SEQUENCE	YIELD STRENGTH KSI	TENSILE STRENGTH KSI	MIN STRESS KSI	MAXIMUM STRESS KSI	CYCLES TO FAILURE
SERIES NO. 7, GRADE 40, MACHINED POLISHED SPECIMENS							
M-G40-3	25	25	54.2	86.3	-12.0	50.0	4658001. *
M-G40-1	25	25	54.2	86.3	-12.0	50.0	6870001. *
M-G40-7	25	25	54.2	86.3	-12.0	50.0	5056001. *
M-G40-2	25	25	54.2	86.3	-12.0	50.0	5000001. *
M-G40-10	26	26	54.2	86.3	-12.0	54.0	622000.
M-G40-14	26	26	54.2	86.3	-12.0	54.0	890000.
M-G40-15	26	26	54.2	86.3	-12.0	54.0	517000.
M-G40-8	26	26	54.2	86.3	-12.0	51.0	776000.
M-G40-12	27	27	54.2	86.3	-12.0	52.0	3219001. *
M-G40-16	27	27	54.2	86.3	-12.0	52.0	10145001. *
M-G40-6	27	27	54.2	86.3	-12.0	52.0	2142001.
M-G40-13	27	27	54.2	86.3	-12.0	56.0	1183001.
M-G40-9	28	30	54.2	86.3	-12.0	56.0	444000.
M-G40-4	28	30	54.2	86.3	-12.0	56.0	471000.
M-G40-11	28	30	54.2	86.3	-12.0	56.0	409000.
M-G40-5	28	30	54.2	86.3	-12.C		416000.
SERIES NO. 8, GRADE 60, MACHINED POLISHED SPECIMENS							
M-G60-4	29	28	67.0	100.1	-6.0	66.0	738000.
M-G60-7	29	28	67.0	100.1	-6.0	66.0	495000.
M-G60-3	29	28	67.0	100.1	-6.0	66.0	392000.
M-G60-16	29	28	67.0	100.1	-6.0	66.0	626000.
M-G60-5	30	29	67.0	100.1	-6.0	62.0	1422000.
M-G60-8	30	29	67.0	100.1	-6.0	62.0	5000001. *
M-G60-15	30	29	67.0	100.1	-6.0	62.0	5000001. *
M-G60-13	31	31	67.0	100.1	-6.0	62.0	4909001. *
M-G60-6	31	31	67.0	100.1	-6.0	64.0	586000.
M-G60-2	31	31	67.0	100.1	-6.0	64.0	1261000.
M-G60-9	31	31	67.0	100.1	-6.0	64.0	5000001. *
M-G60-11	32	32	67.0	100.1	-6.0	64.0	872000.
M-G60-13	32	32	67.0	100.1	-6.0	68.0	577000.
M-G60-1	32	32	67.0	100.1	-6.0	68.0	379000.
M-G60-14	32	32	67.0	100.1	-6.0	68.0	339000.
M-G60-10			67.0	100.-1	-6.0	68.0	294000.

* BAR DID NOT FAIL

APPENDIX E

STATISTICAL CONSIDERATIONS AND DATA USED

IN STATISTICAL ANALYSES

TABLE E-1

FREQUENCY OF ORDER OF FAILURE AND LOCATION

OF SPECIMEN IN THE TEST ASSEMBLY

Order of Failure	Specimen Location in the Test Assembly			
	NE	NW	SE	SW
First	7	9	13	11
Second	8	6	14	12
Third	10	8	7	7
Fourth	7	9	6	10

Notes: 1. Total number of test group analysed = 10.

2. Only SE and SW locations were used to test group no. 17 and 21.

TABLE E-2

ANALYSIS OF VARIANCE OF FATIGUE LIMIT DATA

Source	Degrees of Freedom DF	Mean Square MS	F Statistic
Surface characteristics	3	520.76	82.66
Grade	1	1651.23	262.1
Interaction	3	3094.23	491.15
Within cells	79	6.30	
Total	86		

E.1 Assumptions in Analysis of Finite Life Data

Because fatigue life (N) and strength (S) both are regarded as stochastic quantities (47), it is generally considered necessary to plot such data in the form of S-N-P curves. In order to plot these curves two analytical expressions are required; an average S-N curve and a life or strength distribution function. Since replicate tests were made at each stress level in each series, it was possible to estimate the parameters of life distribution function.

The regression model given Equation (6.1) was found to adequately represent the relationship between the dependent variable log N and independent variable S_r.

$$\log N = A + B\, S_r \qquad\qquad (6.1)$$

Since the same model was to be used for the computations of confidence intervals, percentiles of survival and statistical tests, the following three assumptions incumbent to the regression analysis (16) had to be examined:

1. The data observed during each test constitutes a random sample from a population of all possible test results.

2. The observed fatigue lives are a random sample from a log-normal population.

3. The observed fatigue lives have constancy of variance.

The first assumption of a random sample was satisfied to a large degree by the randomization of the sampling provedure, of the

samples assigned to various groups and of the test sequence as described in section 3.3.3.

The replicate observations at each stress level were used to check the second and third assumptions. The fatigue life data from series 1 to 8 has been plotted, on log-normal probability paper in FIGURES E-1 to E-3. The cumulative frequency (100-p) equal to $(i - 3/8)/(n + 1/4)$ suggested by Blom (53) and Kimball (54) was used for plotting these graphs. The observed log N values have been plotted on the abcissa. It may be noted that observed fatigue lives of test groups fell along the computed lines which were almost parallel indicating that the distribution is approximately normal and had consistency of variance (33). These plots also gave a preliminary indication that there was not much difference between the fatigue lives of series 3 and 5; and series 4 and 6.

A more accurate and familiar method to test normalcy is to plot cumulative observations against regression residuals on normal probability paper. The data in each series was analysed by the regression equation (6.1) and the residuals of the observations were calculated. This data has been plotted in FIGURES E-4 and E-5. Again the plotted position suggested by Blom (53,54) was used. The slope of the cumulative frequency distribution (CFD) was determined from the standard error of regression(s). Since the s values for series 1 to 4 were almost equal, only one CFD line is shown in FIGURE E-4. It may be noted that the residuals closely follow the CFD line. In FIGURE E-5, though the residuals from series 7 and 8 follow their respective

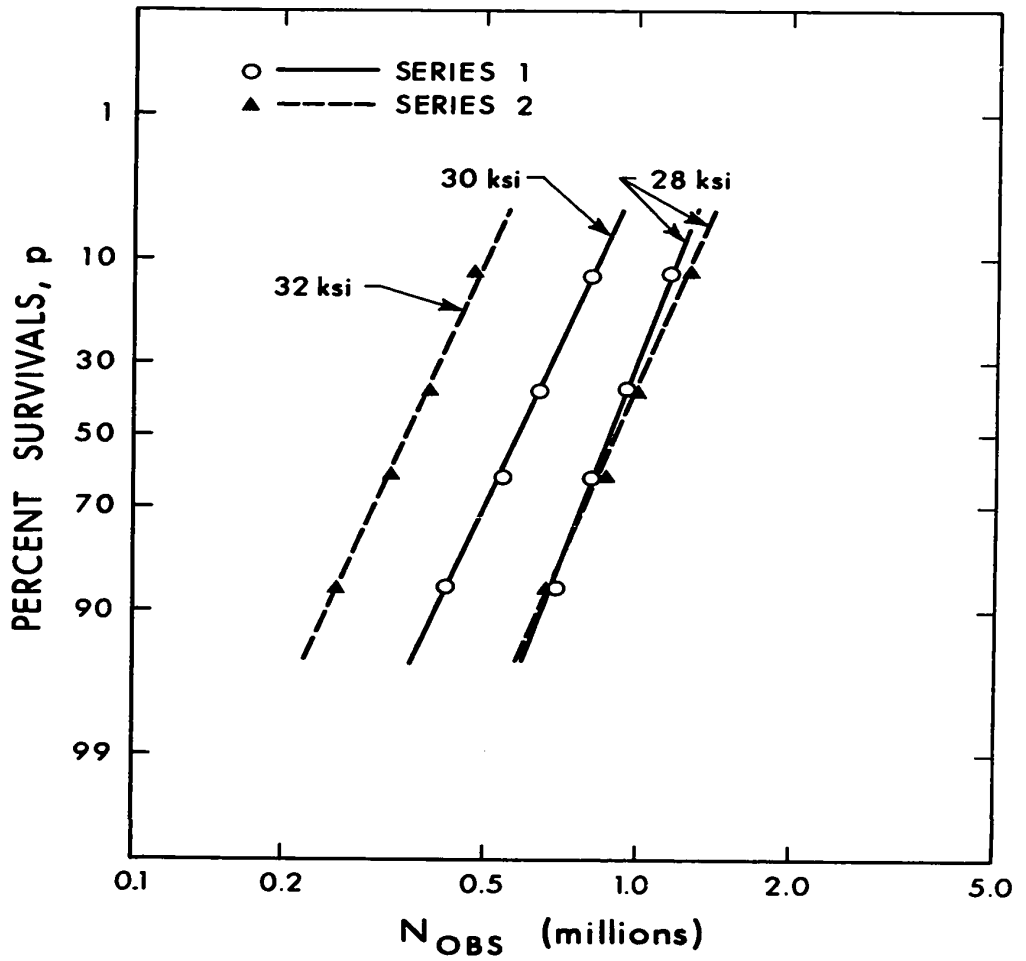FIGURE E-1   CUMULATIVE FREQUENCY DISTRIBUTION OF
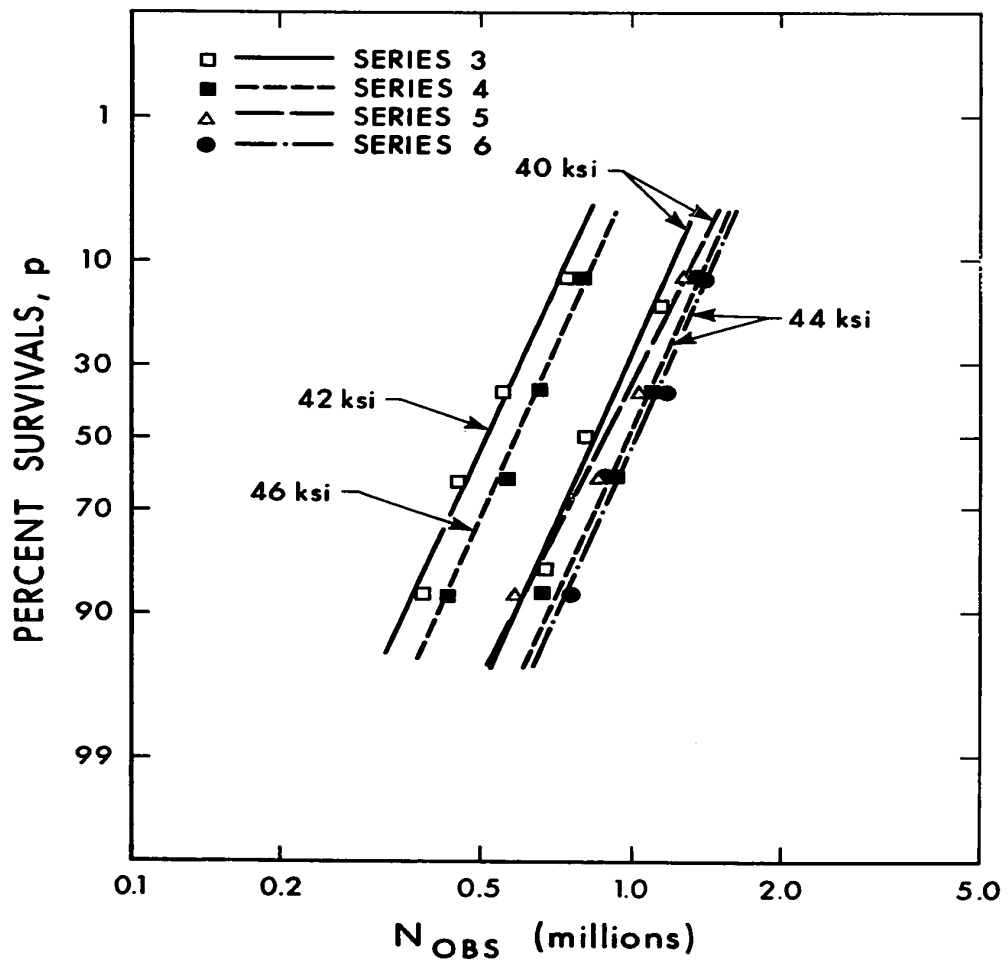TEST DATA FROM SERIES 1 AND 2

FIGURE E-2   CUMULATIVE FREQUENCY DISTRIBUTION OF
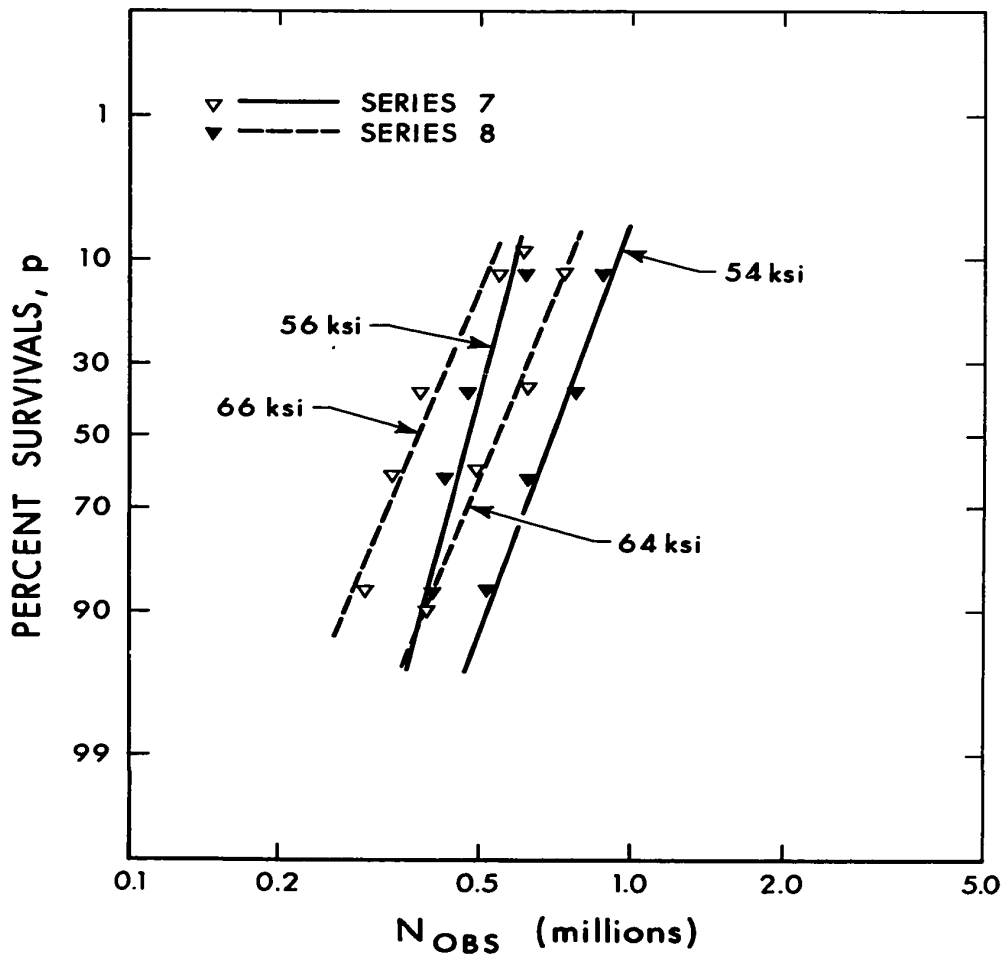TEST DATA FROM SERIES 3 TO 6

FIGURE E-3   CUMULATIVE FREQUENCY DISTRIBUTION OF
TEST DATA FROM SERIES 7 AND 8
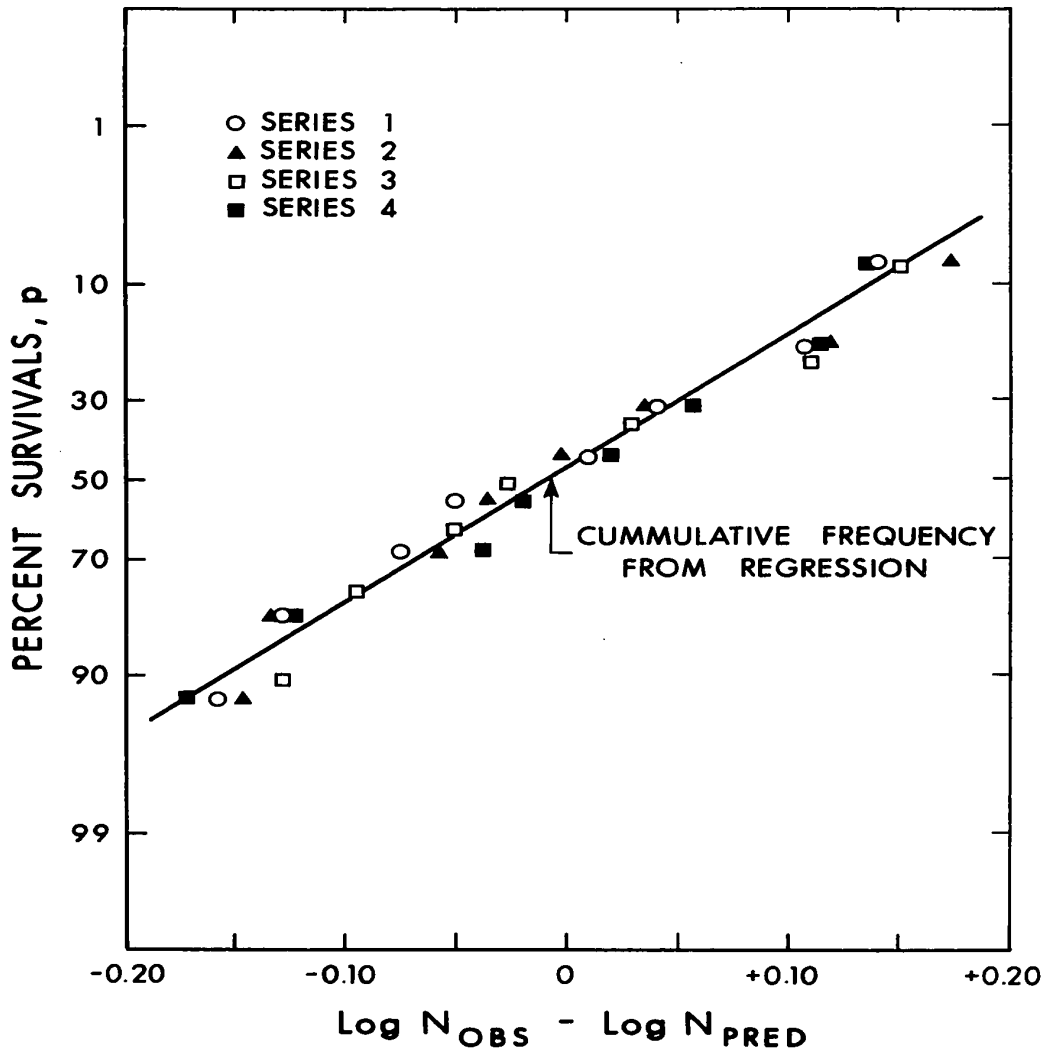
FIGURE E-4   CUMULATIVE FREQUENCY DISTRIBUTION OF
RESIDUALS FROM SERIES 1 TO 4
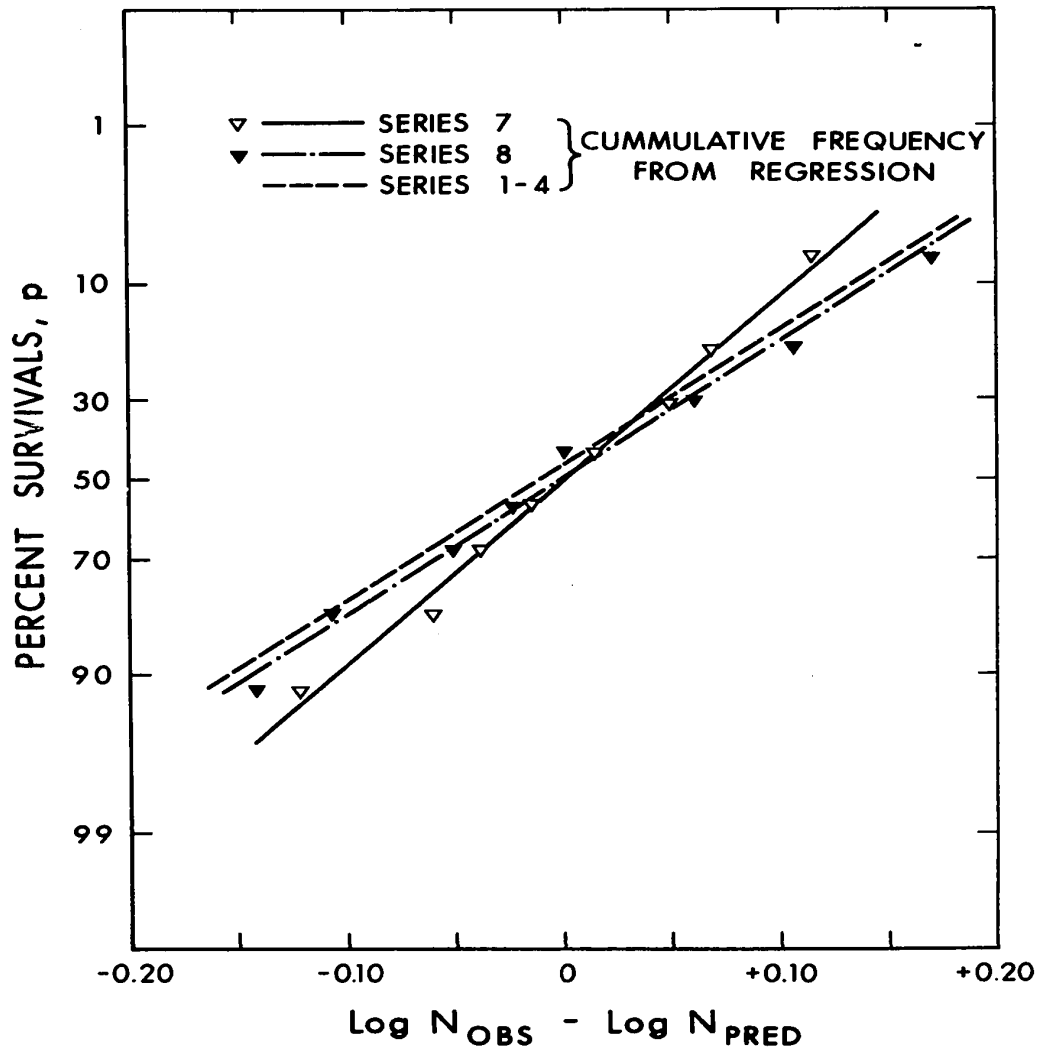
FIGURE E-5   CUMULATIVE FREQUENCY DISTRIBUTION OF
RESIDUALS FROM SERIES 7 AND 8

CFD lines obtained from regression, their slopes are slightly different. For comparison the slope of the CFD line shown in FIGURE E.4 is also shown in this figure. The overall homogeneity of variance of the regression residuals from all series was checked by Barlett's test (33). At 5 percent level of significance the observed F value of 1.92, was less than 2.06 for $F(5,18.67)$. Thus, the hypothesis of homogeneity of variance was accepted. From FIGURES E-4, E-5 and the Barlett's tests the assumption of normality of the log N population and consistency of variance were assumed to be satisfied.

The regression equations obtained for each series were plotted as the mean S-N curves ($p = 50\%$) and the tolerance limits ($p = 95\%$, $p = 5\%$) were obtained from the cumulative life distributions. The resulting S-N-P curves are plotted in FIGURES 6-7 to 6-9.

E.2 Analysis of Covariance (ANOCOVA)

The analysis of covariance (49) is a combined application of linear regression and the analysis of variance. The essential difference between the analysis of variance and ANOCOVA is that, in the latter case, the means squares must be partitioned into two components, regression and residual. The residual components which are freed from the effect of regression are used to calculate the F ratio. The ANOCOVA model given in equation (E.1) was used to investigate the influence of the specified variables.

$$y_{i\alpha} = \mu + \tau_i + \beta(x_{i\alpha} - \bar{x}) + \varepsilon_{i\alpha} \qquad (E.1)$$

where $y_{i\alpha}$ = observed log fatigue life

μ = constant to all observations

τ_i = effect of ith variable

$x_{i\alpha}$ = stress range (S_r)

$\varepsilon_{i\alpha}$ = error term

α = number of observations in a group

The assumptions (48) implicit in this model were same as outlined in Section E.1 for the regression analysis except that it was also assumed that the regression lines fitted to individual groups had a common slope and standard error estimate. In Section E.1 it was shown that the regression lines had common standard error estimate. The slopes of the regression equations were compared by Hald's method (50). The hypothesis that the slopes of the regression equations were different was rejected to 5 percent level of significance. Hence all the assumptions of the ANOCOVA were satisfied.

TABLE E-3, presents sample calculations of ANOCOVA analysis to investigate the treatment effect (grade) between series 3 and 4. The observed F statistic was 7.78 as compared to the values of the critical $F(1,13)$ equal to 4.67, 6.41 and 9.07 at 5, 2.5 and 1 percent levels of significances. Thus the hypothesis of significant difference is accepted at 5 and 2.5 percent level, but rejected at 1 percent level. The conclusions from similar analyses are presented in TABLE 6.3.

TABLE E-3

DETAILS OF CALCULATION FOR ANOCOVA ANALYSIS (50)

A. The sum of squares and products, regression, and residual sum of squares, based on finite life data from series 3 and 4.

Source	df	(yy)	(xy)	(xx)	b	(yy)'	(yy)''
Between series	1	2.5584	28.7942	324.0			0.6496
Within series	14	29.7890	207.2429	1496.0	0.1385	28.7031	1.0860
		32.3474	236.0371	1820.0	0.1296	30.6117	1.7356

B. The analysis of variance based on the original and residual sum of squares

Source	Original			Residual		
	df	(yy)	msq	df	(yy)''	msq
Between series	1	2.5584	2.5584	1	0.6496	0.6496
Within series	14	29.7890	2.1278	13	1.0860	0.0835
Total, T	15	32.3474	F = 1.20	14	1.7356	F = 7.78

Note: For symbols and details of calculations see Reference (50)

E.3 Multiple Linear Regression

Multiple linear regression allows the study of the influences
of several independent variables on a dependent variable. The step-
wise multiple regression (55) is preferred for its versatility. This
procedure allows one to systematically admit or expel an independent
variable under a given entrance criteria. The independent variables
are entered in the regression in steps, in order of their significance
depending upon the entrance criteria. No entry is possible if the
entrance criteria is not met.

The above method allowed the fatigue data from all test
series to be combined and analysed together. In the regression log N
was considered to be the dependent variable and several specified
and other variables were taken as independent variables. A linear
additive model was used in the regression and a partial F value of
2.0 was considered as an entrance criterion.

The results of the stepwise multiple regression over the
specified variables is given in TABLE E-4. All the finite life data
of the Phase II tests was used in the regression. The specified
variables S_r, K_T, f_u and R and the interaction terms $S_r K_T$ and R f_u
were found to be significant. The interaction terms S_r, K_T, $S_r f_u$
and S_r R were tested and rejected as not significant. The partial
F-ratios for the significant variables were much higher than the
entrance criteria. The regression model explained in statistical
terms 82.7 percent of the variation in the data. The inability of
the model to explain 100 percent variation in the data may be due to

TABLE E-4

MULTIPLE REGRESSION OVER SPECIFIED

VARIABLES (FINITE LIFE DATA - PHASE II)

Stepwise Results		Variables Entered					
		S_r	K_T	f_u	K_T-f_u	f_u-R	R*
Residual Standard Deviation, s		0.179	0.163	0.160	0.150	0.143	0.110
Multiple R^2		0.269	0.501	0.536	0.624	0.672	0.827
Regression F-Ratio		4.14	8.72	6.86	7.98	8.064	17.33
Degrees of Freedom, DF		1-53	2-52	3-51	4-50	5-49	6.48
Partial F-Ratio	S_r	4.14	17.38	20.05	30.08	21.52	69.34
	K_T		12.41	15.06	5.192	10.03	13.73
	f_u			2.60	11.053	16.74	62.92
	K_T-f_u				8.36	14.50	36.78
	f_u-R					5.51	38.24
	R						35.39
Regression Coefficient	Constant	6.0247	6.8243	6.4953	4.5774	3.9082	0.4397
	S_r	-0.0051	-0.0163	-0.0198	-0.0241	-0.0441	-0.1075
	K_T		-0.2506	-0.2824	1.1011	1.6312	1.4662
	f_u			0.0056	0.0294	0.0504	0.1310
	K_T-f_u				-0.0159	-0.0238	-0.0296
	f_u-R					-0.0001	-0.0002
	R						0.0164
Standard Error Estimate of Regression Coefficient	S_r	0.0025	0.0039	0.0044	0.0044	0.0095	0.0129
	K_T		0.0711	0.0727	0.4833	0.5150	0.3957
	f_u			0.0035	0.0088	0.0123	0.0165
	K_T-f_u				0.0055	0.0062	0.0049
	f_u-R					0.0000	0.0000
	R						0.0027

*Surface Roughness - CLA Values.

the absence of a parameter defining the decarburized surface of the reinforcing bar specimens, the absence of an approximate value of K_T for plain as-rolled bars and the assumptions inherent in the linear additive model.

The data from the fatigue tests on beams was also analysed by the stepwise multiple regression analysis, the results of the regression are presented in Table E-5. Though only four variables; S_r, S_{min}, f_u and D_{nom} were specified in the tests, K_T and grain size (g)* were also included in the regression. The test data was analysed in two stages. In the first stage, all the data was included, whereas in the second stage all the data except that of series 9 (G75 No. 5 bars) was included. The regression models obtained in the two cases are given in Equation (E.2) and (E.3), respectively.

$$\log N = 9.6285 - 0.0681\ S_r - 1.0081\ K_T - 0.0153\ S_{min}$$

$$+ 0.0049\ f_u + 0.0012\ g - 0.1529\ D_{nom} \qquad (E.2)$$

$$\log N = 9.5894 - 0.0633\ S_r - 0.0147\ S_{min} + 0.0033\ f_u - 0.8663\ K_T \qquad (E.3)$$

It is interesting to note that in Equation (E.2), S_r, K_T, S_{min}, f_u, g and D_{nom} are significant variables whereas in Equation

---

*g - Number of grains per square inch at 100 magnification.

TABLE E-5

MULTIPLE LINEAR REGRESSION OVER SPECIFIED AND OTHER VARIABLES (Finite Life Data - Phase I)*

Stepwise Results		Variable Entered			
		S_r	S_{min}	f_u	K_T
Residual Standard Deviation, s		0.199	0.175	0.171	0.168
Multiple R^2		0.641	0.747	0.765	0.789
Regression F-ratio		33.56	29.70	21.66	17.35
Degrees of Freedom, DF		1-48	2-47	3-46	4-45
Partial F-Ratio	S_r	33.56	58.41	56.42	60.47
	S_{min}		15.62	18.97	21.65
	f_u			3.02	4.20
	K_T				2.42
Regression Coefficient	Constant	7.0995	8.0405	7.7194	9.5894
	S_r	-0.0493	-0.0621	-0.0603	-0.0633
	S_{min}		-0.0122	-0.0136	-0.0147
	f_u			0.0028	0.0033
	K_T				-0.8663
Standard Error of Estimate of Regression Coefficient	S_r	00.0085	0.0081	0.0080	0.0081
	S_{min}		0.0030	0.0031	0.0031
	f_u			0.0016	0.0016
	K_T				0.5573

*Except Series 9

(E.3) only S_r, S_{min}, K_T and f_u are significant variables. This non-uniformity of significance of variables was caused due to relatively higher fatigue strength of series 9 bars having the finest grain structure and a relatively lower K_T value (1.81). Since these pro-perties were not common among other series, the model given in Equation (E.3) was considered to represent the entire test series except series 9. The details of calculations of this model are presented in Table E-5. In this analysis no attempt was made to test the interaction terms, since the significance of the specified or the other variables could not be checked individually.

The data from all the deformed bars tested in Phases I and II was combined by making a correction to the strengths of specimens tested in air to account for concrete encasement. The multiple linear regression results reported in Table E-6 confirmed the findings of the multiple linear regression analysis of beam tests alone. Again, in this analysis the data of series 9 was excluded. The multiple correlation coefficient obtained was 0.778 though the multiple cor-relation could have been improved by admitting interaction terms in the regression but this was not done for the reasons explained earlier.

The combined data from the deformed bars from Phase I and II has been plotted in FIGURE 6.15. The regression equation shown in this figure was obtained from the multiple regression model given in Table E-6. The tolerance limit on the test data was calculated at the mean S_r and was assumed constant for the range of S_r plotted in this figure.

TABLE E-6

MULTIPLE LINEAR REGRESSION OVER SPECIFIED AND OTHER
VARIABLES (FINITE LIFE DATA- PHASE I AND II)*

Stepwise Results		Variables Entered			
		S_r	S_{min}	K_T	f_u
Residual Standard Deviation, s		0.191	0.181	0.170	0.161
Multiple R^2		0.628	0.682	0.732	0.778
Regression F-Ratio		44.30	29.13	25.33	23.40
Degrees of Freedom, DF		1-68	2-67	3-66	4-65
Partial F-Ratio	S_r	44.30	57.99	75.39	84.20
	S_{min}		8.85	15.02	24.18
	K_T			9.95	13.01
	f_u				8.71
Regression Coefficient	Constant	7.5403	7.8634	11.0517	10.9397
	S_r	-0.0516	-0.5917	-0.0665	-0.0665
	S_{min}		-0.0088	-0.0112	-0.0146
	K_T			-1.3925	-1.5138
	f_u				0.0042
Standard Error of Estimate of Regression Coefficient	S_r	0.0078	0.0078	0.0077	0.0072
	S_{min}		0.0030	0.0029	0.0030
	K_T			0.4414	0.4197
	f_u				0.0014

*Except beam Series 9